Fall 2019

Molecular Modeling of Tethered Polyelectrolytes for Novel Biomedical Applications

Merina Jahan

Molecular Modeling of tethered polyelectrolytes for novel biomedical applications

by

Merina Jahan

Bachelor of Science
Bangladesh University of Engineering and Technology, 2013

Submitted in Partial Fulfillment of the Requirements

for the Degree of Doctor of Philosophy in

Chemical Engineering

College of Engineering and Computing

University of South Carolina

2019

Accepted by:

Mark J. Uline, Major Professor

Melissa A. Moss, Committee Member

Tarek Shazly, Committee Member

R. Michael Gower, Committee Member

Cheryl L. Addy, Vice Provost and Dean of the Graduate School

Acknowledgments

At first, I would like to express my sincere gratitude to my advisor Dr. Mark J. Uline for giving me the opportunity to work with him. He not only guided me to conduct research and present my work effectively to the greater scientific community, but also taught me humility and respectfulness to others. I am forever grateful to him for all his support and help throughout the years for both my academic and professional development.

I thank my respected committee members: Dr. Melissa A. Moss, Dr. Tarek Shazly and Dr. Robert Michael Gower for taking their time to be on my committee and provide constructive feedback to make my work better. Since my comprehensive exam, their suggestions and feedback helped me to address the right questions and finding the answers accordingly, to serve not only the small community of theoretical polymer researchers, but also to serve the broader audience in biomedical research.

I am thankful to my groupmates, Dr. Ebtisam Aldaais, Dr. Donya Ohadi, Shauna Celeste Kennard and Dr. Nick Vander Munnik for their help and support. I will forever cherish the fond memories of our time together in our small office cubicles.

I also thank Marcia Rowen, Vernon Dorrell and Loretta Hardcastle from the Department of Chemical Engineering for their help and support on numerous administrative and logistical matters. I will always remember their warm smile and greetings whenever we met in Swearingen corridor.

I thank my father, mother, my sisters Jhuma and Jerin for their unconditional love and support throughout my life. My father is not with us anymore, but it is his love and enthusiasm for my PhD that kept me going through the dark days after

losing him at the very early stage of my research career. Wherever I am today, I owe all of it to my mother. Being a girl from a small town in Bangladesh, I have achieved what many others can only dream of, only because of the courage and support she provided. My sisters are my biggest supporters and constant source of inspiration to overcome whatever comes in my way.

Last but not the least, I thank my wonderful husband Asif, for his love and support during my PhD journey. We shared our lives as graduate students, in failure and success. It is him who kept me motivated to keep going in all the depressing times and pushing boundaries to get out of my comfort zone. I can not wait to see what future holds for us.

Abstract

Current research trends throughout the world focus on designing intelligent materials and systems for diverse applications in all courses of life. Biomaterials research encompasses a major part in this revolution due to the increased effort in fulfilling unmet medical needs to treat complex physiological and neurodegenerative disorders. Polymers play inevitable roles in these research endeavors for their ubiquitous presence in biological systems. Therefore, it is crucial to understand how the polymeric molecules interact within diverse biological environments, to efficiently engineer them for various drug delivery and biosensing systems. The use of experimental design and selection of different polymers for diverse applications alone is an arduous task. Hence, theoretical studies on these biological systems become important starting points for projects that have previously been only studied with experimental techniques. Using theory can make the job easier for researchers in biomedical engineering by both coalescing large bodies of experimental data into conceptual frameworks and narrowing down a parameter search space.

Along this line, our research focuses on theoretical molecular level modeling of complex polymeric molecules, both biological and synthetic, for drug delivery and biosensing applications. The objective is to design new polymeric systems based on their structural, thermodynamic and physicochemical properties to help enhance the experimental design. This research work uses a Self Consistent Field Theory (SCFT) based approach for different applications involving polymers, that are tethered and electrolytic in nature. The molecular theory studies the thermodynamic and structural behavior of the polymers as a function of their molecular composition and

physicochemical environments. This theory is able to perform systematic thermodynamic calculations at low computational cost, while including a detailed molecular description of the molecules in the system. The competition of all relevant molecular interactions, such as electrostatics, van der Waals, thermodynamic and chemical equilibrium is described in this model.

The first study involves elucidating the behavior of ssDNA aptamers in different biological environments. Our study suggests that the structure of the aptamer chains varies significantly due to charge regulation effects, in response to changes in salt concentration, types and ionic strength of salt and density of the aptamer brush. The understanding gained from this study can help to facilitate aptamer selection process against specific target molecules.

Our second study inquires the property changes of ssDNA aptamers in presence of divalent metal cations and quantifies the number of metal ions bound to the aptamer chains. The results imply that the ion cloud around the oligomers is uniformly distributed in different sequences and reinforces the dominance of non-specific electrostatic attraction between the nucleobases and the cations as the driving force for cation-binding. Our results also show that the ionic strength has a more prominent effect on the structure and properties of the oligomer brushes when they are densely grafted, compared to their sparsely grafted counterparts. In its current state, this model can serve as a foundation for field theoric studies of more complex systems to dissect the ion binding scenario around aptamers and single stranded nucleic acids.

The third study in this dissertation analyses the behavior of a pH responsive polymer (PMAA), complexed with a small molecule drug (PD166793), and grafted to a nanoparticle surface, to design a controlled and sustained drug delivery system for enhanced cardiovascular repair. The molecular theory results elucidate the reasons for why the polymer shows poor drug binding at physiological pH and higher drug binding at acidic pH. Based on these findings, we present a proof of concept of how

the molecular level understanding of this system can be leveraged to increase drug binding at physiological pH by adding a strong polyelectrolyte to the system. This study can aid in designing new drug delivery systems with improved efficacy and sustainability, not only for cardiovascular diseases, but also for other critical and time-sensitive diseases.

Table of Contents

List of Figures

Chapter 1

Introduction

Macromolecules, generally known as polymers, are large molecules made up of single units called monomers. The major classes of molecules that are necessary for life on earth are biological macromolecules or biopolymers, such as, proteins, lipids, carbohydrates and nucleic acids. From lipid bilayers in our cell membrane to DNA in our hereditary genes, all are examples of polymers. All of these polymers show different level and nature of interactions with one another and also with other organic or inorganic substances in their surrounding environment. All the functions in a living body are governed by these interactions. Hence, it is of utmost importance to have a fundamental understanding of the interactions of different polymers with other organic or inorganic substances to leverage their capabilities in novel biomedical applications.

Polyelectrolytes are a class of polymers that are capable of protonating and deprotonating in aqueous solution environment. Their monomer units bear an electrolyte group that dissociates and makes the polymers charged in suitable polar solvent (mostly water). Polyelectrolytes can be positively charged, which are called polycations, or negatively charged, called polyanions. Polyelectrolytes are of strong interest in polymer science due to their wide range of applications and because most biological macromolecules, such as, DNA, some proteins, fatty acids, etc., are polyelectrolytes. Polyelectrolytes in solutions exhibit significantly different behaviors than uncharged macromolecules and low molecular weight electrolytes (Hara 1992). The presence of charges on the polyelectrolyte chains leads to intra and intermolecular interactions that are stronger and of much larger range than uncharged polymers. These

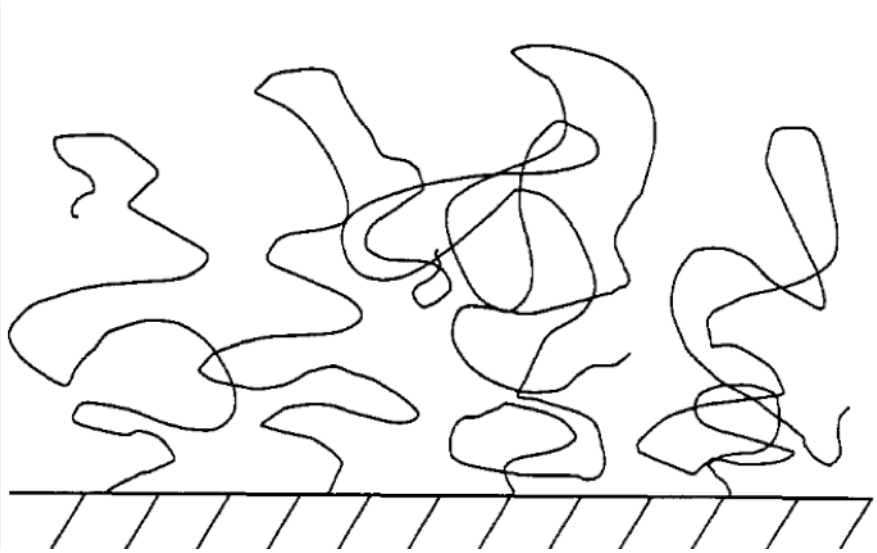

Figure 1.1 Schematic representation of a tethered polymer brush. The figure is adopted from Szleifer and Carignano 1996.

interactions give rise to distinctive conformational, thermodynamic, electrostatic and chemical properties of the polyelectrolytes. These properties can be tuned to employ the polyelectrolytes in a variety of biomedical applications ranging from biosensing to controlled drug delivery (Scranton, Rangarajan, and Klier 1995).

When one end of a polymer chain is grafted or anchored to a surface, they are called 'tethered polymers'. The properties of tethered polymers in solution environments are qualitatively different than that of polymers in bulk. This difference stems from the presence of the grafting surface that limits their configurational space and the two-dimensional anchoring gives the repulsive interaction between neighboring chains a different nature than their bulk counterparts (Szleifer and Carignano 1996). Tethered polymers change the interaction of the tethering surface with their surrounding environments which makes them promising candidates for surface modification of a variety of materials. They are found to be useful in a wide range of applications, including but not limited to, colloid stabilization (Napper 1983), biocompatible materials (Brannon-Peppas 2000), controlled drug delivery vehicles (Torchilin et al. 1994;

Ji et al. 2019; J. S. Kim et al. 2019), biosensors (Badoux, Billing, and Klok 2019; Hu et al. 2019; Andersson and Knoll 2019), etc. When the tethered polymers have charge on them, they are called 'tethered polyelectrolytes', which are the subject of interest for this study.

Along with experimental studies, theory played a vital role since the very beginning of polymer science. The work of first generation of polymer theorists tackled fundamental problems of polymer chain conformations, colligative properties and phase behavior from the perspective of physical chemistry. The second generation of polymer scientists combined the concepts of theoretical physics with polymer statistical mechanics to analyze important problems, such as, excluded volume effect in polymers. The third generation of polymer research developed the foundation of the most prominent polymer theory named as Self Consistent Field Theory (SCFT) to study equilibrium properties of inhomogeneous polymers. Various analytical techniques were employed to solve the SCFT equations and apply the theory in broad areas of applications, such as, polymer alloys, block copolymers, graft copolymers and tethered polymer layers. With the advance in computing technologies, the current generation of polymer science employs various numerical and computer simulation techniques, such as, Monte Carlo (MC), Molecular Dynamics (MD) simulations (G. Fredrickson et al. 2006).

This research endeavor focuses on understanding the structural, physicochemical and thermodynamic property changes of tethered polyelectrolytes in solution environments when they interact with other neighboring molecules and incorporate that into a molecular theory to facilitate their applications in areas of unmet biomedical needs. This molecular theory follows a single-chain mean field approach that is based on the Self Consistent Field Theory (SCFT) and takes into account the structural, thermodynamic and electrostatic properties of all the molecules involved in a system. Each of these properties shapes the nature of interactions among the biomolecules

and their environments. The molecular theory aims to explain the thermodynamic and physicochemical property changes of tethered polyelectrolytes for biosensing and drug delivery applications and leverage their tunability to achieve better performance of these systems.

1.1 Self-Consistent Field Theory (SCFT) modeling of tethered polyelectrolyte chains in solution

Self Consistent Field Theory was originally developed to treat bulk polymer systems containing freely jointed chains (Sam F Edwards 1965). It was later modified to study inhomogeneous systems where the polymers are tethered to hard surfaces (Dolan and Samuel Frederick Edwards 1974).

The basic concept of SCFT is that the polymer chains are considered to be affected by a position r dependent single field, $w(r)$, which is the average or mean of all the attractive and repulsive interactions between the polymer segments and their surrounding environments. It is called *'self-consistent'*, because the mean field is derived self consistently by assuming that the field variables are stationary with respect to the mean field $w(r)$ and then solving the equations defining the field variables simultaneously that also gives mean field $w(r)$ (G. Fredrickson et al. 2006).

SCFT has been employed extensively to study tethered polyelectrolytes for numerous applications and nicely captured their physicochemical behavior in solution environments (Pincus 1991; Zhulina and Borisov 1997). Polyelectrolytes can be categorized as 'strong' or 'weak' polyelectrolytes depending on their degree of dissociation. Strong polyelectrolytes completely dissociate in solution, such as Polystyrene Sulfonate (PSS), whereas weak polyelectrolytes are partially dissociated, such as Polyacrylic acid (PAA), nucleic acids, etc. The tethered polyelectrolyte systems behave differently in presence and absence of salt in the solution, which was captured accurately with SCFT (Pincus 1991; Borisov and Zhulina 1998; Borisov, Birshtein,

and Zhulina 1991; Zhulina, Borisov, and Birshtein 1992). In absence of salt, densely grafted strong polyelectrolytes form an 'osmotic' regime where all the counterions are trapped inside the brush and osmotic pressure creates swelling effect inside the brush. However, for sparsely grafted weak polyelectrolytes, the electrostatic attraction between the polyions and the counterions is not enough to trap the counterions inside the brush, which results in dispersing them in outer solution environment, breaking the local electroneutrality and creating a charged brush.

When salt is added to the tethered polyelectrolyte system, the cations and anions from the dissociated salt creates screening effect and diminishes electrostatic swelling that results in collapse of the brush (Brettmann et al. 2016; M. J. Uline, Rabin, and Igal Szleifer 2011). The presence of salt also ensures global electroneutrality of the polyelectrolyte system by the mobile counterions (Zhulina and Borisov 1997; Rikkert Nap, Gong, and Igal Szleifer 2006). All of the molecular theories reported in this dissertation includes salt as an integral part, because most polyelectrolytic formulations require addition of salt to control the ionic strength and charge regulation inside and outside the brush (G. Fredrickson et al. 2006).

With all these scopes of variability, tethered polyelectrolytic systems in various biomedical applications possess a wide range of parameter space. Furthermore, rapid development of new intelligent polymer-based materials makes the scenario more complicated. While combinatorial discovery chemistry provides powerful tools to study these materials, the process is often very expensive and time consuming. Theoretical study on this wide parameter space for new biomedical applications renders to be very useful in this regard, to scan the properties of these systems and map them into a generalized theory. The insights gained from the theory would enable the experimental researchers to optimize the number of experiments conducted and accelerate the materials discovery process.

Apart from SCFT, Molecular Dynamics (MD) and Monte Carlo (MC) simulations

are powerful tools to study polymeric systems with wide design space. Both of the MD and MC techniques track the motion of particles or molecules through Lagrangian or Hamiltonian dynamics. In MD simulation, the temporal evolution or trajectory of the coordinates and the momenta of a given macromolecular structure is studied (Paquet and Viktor 2015). The trajectory is important to access valuable time-dependent information about the system, such as, the accessibility of a given molecular surface, the intermolecular interaction, etc. (Lindorff-Larsen et al. 2012; Harris et al. 2013). MC simulation generates an ensemble of representative configurations under specific thermodynamic conditions for a complex polymeric system through sampling of most probable conformations (Fichthorn and Weinberg 1991; Paquet and Viktor 2015). MC simulations are not time dependent and provide an ensemble of representative configurations and conformations, which consequently gives probabilities and relevant thermodynamic observables, such as the free energy.

To most accurately model complicated many-body systems as tethered polyelectrolytes, one would intuitively think of MD or MC, as these models use particle co-ordinates for exact solution of the equation of motion of the molecules (MD) or sample the configuration space (MC) (Szleifer and Carignano 1996). However, tracking each molecule in a system and solving the equations of motion requires defining the interactions between different units, polymer segments, and solvent molecules. While using these approaches provides valuable information on the underlying physics of tethered polyelectrolytes, the computational cost of conducting these calculations is intractable and resources are often unavailable to most researchers (G. Fredrickson et al. 2006). To tackle this difficulty, coarse-grained field based models as SCFT, where the fundamental degrees of freedom is a mean-field of all the available interactions instead of particle co-ordinates, proves to be more useful to provide crucial thermodynamic and structural information at a good degree of accuracy. That is why, we choose SCFT to model tethered polyelectrolytes for various biomedical applications.

In this work, we have studied polyelectrolytic biomolecule Aptamer, which is a type of ssDNA capable of binding to a specific target molecule with high affinity and specificity. Molecular modeling of aptamers would enable us to have fundamental understanding on their property changes in various biological environments and use that for high-throughput experiments to design new aptamers with increased functionality. We have also studied a nanoparticle-polyelectrolyte mediated drug delivery system for enhanced repair in case of a cardiovascular disease. These studies can provide valuable support to experimental researchers to design new polymeric materials for highly efficient biosensing and drug delivery technologies.

1.2 Physical Significance of Molecular Modeling

Molecular modeling of tethered polymeric systems provides valuable information about the underlying mechanisms of physicochemical property changes and allows us to predict the system behavior. A major contributor in defining the structure of polyelectrolyte brush is the ionic strength of the salt present in the system and valence of the cations. Previous studies have reported that addition of a small amount of salt resulted in collapse of the polymer chains due to the decrease in charge on the polymer chains, but high concentration of salt creates high steric repulsion that results in chain stretching (Rikkert J Nap, S. H. Park, and Igal Szleifer 2018; Gong et al. 2007). The results of these theoretical studies were in qualitative agreements with collaborative experimental research (Y. Park et al. 2012).

The major property changes of the polymeric systems discussed in this dissertation are: volume fractions and fraction of protonation of all the species (polymer, water, anions and cations) and pH in different layers of the brush. The position dependent volume fraction profiles of the polymers correspond to the layer by layer assembly of the polymer brush and carry the information about whether the chains are in collapsed or extended state. This information about structure and length of the chains can

complement experimental X-ray Scattering data to understand the underpinnings of a system behavior (Pütz, Curro, and Grest 2001). The Volume fraction profiles of water, anions and cations at different positions in the system shows the inclusion or exclusion of the respective species from the brush layer, which can be experimentally measured by Atomic force Microscopy (AFM) (Holland et al. 2011; Holland, Jordan, and Geiger 2011). The volume fraction data can be used to calculate the height of the polymer brush and the number of other molecules or ions trapped in the brush, which can correspond to UV-spectroscopy data through distinct absorption peaks (Dunlap et al. 2018). The protonation profiles presents the distribution of charged monomers throughout the polymer layer. High fraction of protonation means less charged monomers and vice versa. Presence of charge in a polymer chain can also be detected by AFM, which can be accompanied by the protonation fraction from the molecular model to comprehend the charge scenario.

1.3 Assumptions of the Molecular Theory

The assumptions that we used to construct the molecular theories in this dissertation are:

- **Single chain mean field approximation:** To construct the molecular theory based on SCFT, we follow a *single chain* approach developed by Szleifer and his group (Szleifer and Carignano 1996; Rikkert Nap, Gong, and Igal Szleifer 2006). In this approach, for a many chain system, instead of looking at all the chain molecules, we look at a central chain with all its intramolecular interactions taken exactly, while taking the intermolecular interaction with a mean field approximation. This approach enables us to understand the conformational changes of the tethered polyelectrolytes depending on thermodynamic control variables, that is, surface coverage and temperature. This provides valuable

insights on the coupling that exists between the chain conformations and the thermodynamic behavior of the layer.

- **Incompressibility Constraint or Volumetric Constraint:** It is assumed that the polyelectrolyte system is incompressible, meaning all the available volume is filled with either of the species (polymer, solvent, salt and water) present in the system. Hence, the summation of volume fractions of all the species at a certain location equals to unity. Additionally, the incompressibilty constraint is a way to take into account the repulsive interactions between polymer segments that ensures self-avoidance of a chain (Szleifer and Carignano 1996).

- We neglect any volume change of the monomers due to protonation and metal binding reactions and assume that the segments have the same volume whether they are protonated and bound to other ions or not. This assumption is made due to the lack of volume change data and used only while carrying out the numerical calculations.

- The dielectric coefficient, ϵ, is assumed to be invariant with position and taken as twice as the dielectric coefficient of water, following the argument of Uline *et al* (M. J. Uline, Rabin, and Igal Szleifer 2011).

1.4 Chain Models

The solutions of the molecular models require conformational statistics of the polymer in that particular application. Based on the length scale of the system and chain length, we use two chain models listed below in our molecular theories:

1.4.1 Rotational Isomeric State Model

Rotational isomeric State (RIS) model was developed by P. J. Flory to treat the configuration dependant properties of chain molecules and to establish the connections

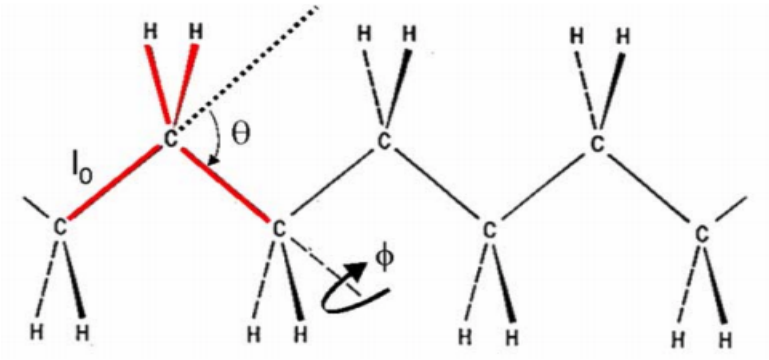

Figure 1.2 Rotational Isomeric State Model for a hydrocarbon chain. θ is the bond angle and ϕ is the rotation angle. l_0 is the bond length.

between conformational energy and the properties of the macromolecules (P. Flory 1974; Paul J Flory and Volkenstein 1969). In this model , each bond can have three possible states: trans, gauche+, and gauche− with angles ϕ=0, $+120^o$ and -120^o, respectively and the angle between bonds is θ=68^o. The continuous rotational degrees of freedom about the backbone single bonds in the polymer are replaced by a finite number of trans, gauche+, and gauche− states. RIS is generally used to treat flexible chains with intermediate chain length. For details on calculations regarding RIS, the above mentioned references can be consulted.

1.4.2 Wormlike Chain Model

Many polymers in biological systems exhibit rod-like rigidity in their structure that makes them semiflexible. A more appropriate chain model for the semi-flexible chains is Kratky-Porod model, which is generally known as Wormlike Chain model (WLC) (G. Fredrickson et al. 2006). In this model, the polymer chain is considered as a space curve, $r(s)$. s is the arc length along the polymer backbone. The detailed description of the model can be found at G. Fredrickson et al. 2006.

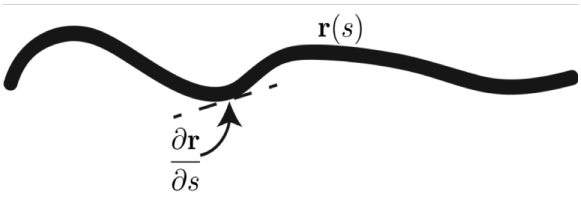

Figure 1.3 Schematic representation of a Wormlike Chain with space curve $r(s)$.

1.5 Thesis statement

This dissertation investigates the following statement:
Molecular level understanding of thermodynamic and physicochemical property changes of tethered polyelectrolytes can be leveraged to design new systems for biosensing and drug delivery applications.

1.6 Organization of the Dissertation

The rest of this dissertation is organized as follows-

- In Chapter 2, we developed a molecular theory with a biological polyelectrolyte called Aptamer to understand its thermodynamic and physicochemical property changes in an aqueous solution environment. The understanding gained from this study can aid in the selection of specific aptamers against specific target molecules of biological interest.

- In Chapter 3, aptamer behavior is studied in presence of divalent metal cations (Mg^{2+}) with a molecular theory and the cation binding is quantified to determine the nature of the ion cloud. This field theoric model helps to set up the foundation for future studies involving secondary and tertiary structures of aptamers interacting with multivalent metal ions.

- In Chapter 4, we theoretically design a localized and controlled drug delivery system for prolonged release of a drug for enhanced cardiovascular repair by

using a nanoparticle grafted polyelectrolyte as the drug carrier. The insights gained from modeling can be used to tune in the system parameters to improve drug binding results to ensure high concentration in our desired site of action for localized and sustained drug delivery.

- Chapter 5 draws conclusion of this dissertation.
- Chapter 6 discusses the possible future directions that this research can take.

Chapter 2

Modeling of Aptamers

Aptamers are a very promising class of biomolecules that have multifunctional usage for various Biomedical applications. Aptamers are single stranded DNA/ RNA oligonucleotides or peptide molecules which can bind to proteins, small molecules, cells or organs with high affinity and specificity (Figure-2.1). Aptamers are capable of forming secondary or tertiary stable structures that enables them to bind to their targets through shape specific recognition. Aptamers work in such a way that they only bind to their target proteins/cells, leaving other neighboring and non-targeting proteins/cells intact (Radom et al. 2013; Banerjee and Nilsen-Hamilton 2013). Since their discovery in 1990, numerous researches have been conducted to use aptamers as biosensors, therapeutic agents, substitution of antibodies, delivery vehicles, target validation tools and so on (Jahan and M. J. Uline 2015). Target specific Aptamers can be produced by Systematic Enrichment of Ligands by Exponential Amplification, a method usually known as 'SELEX Protocol' (Sefah et al. 2010; Bouchard, Hutabarat, and Thompson 2010).

This chapter reports a theoretical study on aptamers to model their physicochemical behaviors with a self consistent mean filed theory to aid in the future applications of aptamers.

2.1 Structure and properties of Aptamers

Aptamers are nucleic acid macromolecules typically from 15 to 60 nucleotides in length and molecular weight ranging from 10000 to 15000 Daltons. They are slightly

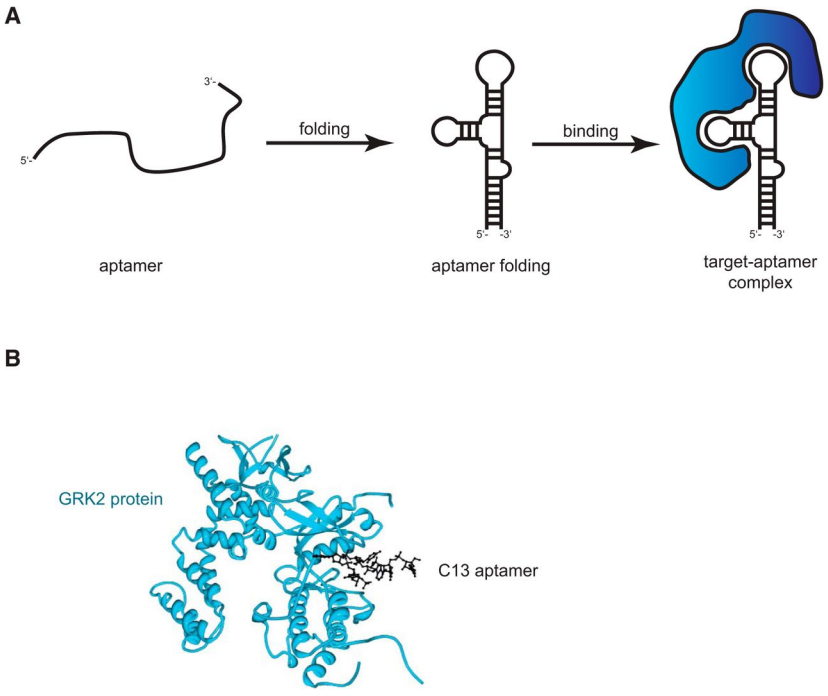

Figure 2.1 (A) Schematic representation of aptamer binding to a target protein depending on structure formation. After the adjustment of the binding conditions, the aptamer folds into a 3D structure, upon which it interacts with the target molecule (e.g., a protein), resulting in a stable target-aptamer complex. (B) The crystallographic structure of the G protein-coupled receptor kinase 2 (GRK2)-C13 complex is depicted as an example for a target-aptamer complex (Wolter and Günter Mayer 2017).

larger than small molecules but smaller than antibodies in size. Aptamers can be composed of a modified sugar backbone in $2'$ end (i.e., $2'$- fluoro, $2'$-O- methyl, phosphorothioate). Secondary structure of aptamers, either short helical arms or single stranded loops, are defined from their complementary base pairing. Tertiary or stable structures resulting from these secondary structures enables aptamers to bind to their targets through shape specific recognition. Van der Waals, hydrogen bonding, electrostatic interaction and hydrophobic interactions are responsible for strong aptamer-target binding (Pendergrast et al. 2005). They are hydrophilic and polyanionic in nature. K_D values of aptamers can range from 10 pM to 10 nM for proteins. Here, $K_D = [L][R]/[LR]$, where L denotes ligand or aptamers in our case, R is

receptor (protein) and LR stands for the ligand-receptor complex.

2.2 SELEX Protocol

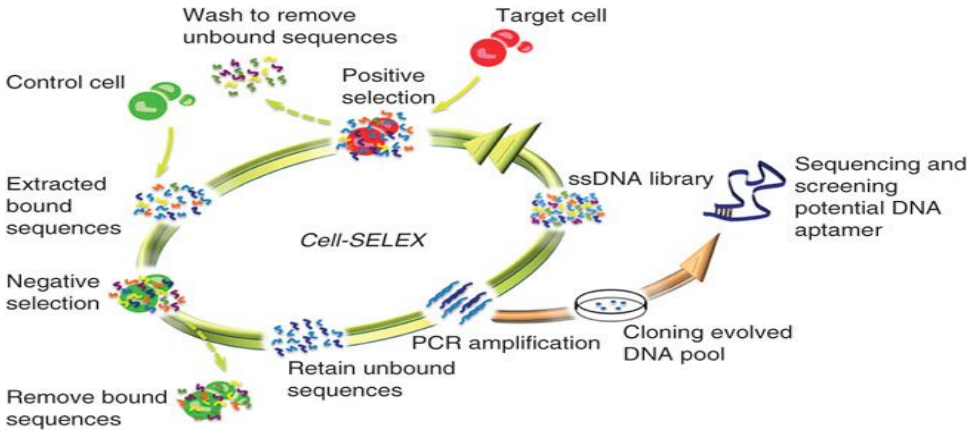

Figure 2.2 SELEX Protocol (Sefah et al. 2010).

'SELEX Protocol' was first proposed by two independent groups (Ellington and Szostak; Turek and Gold) in 1990. SELEX process requires a large library of single stranded oligonucleotide templates derived from a chemical synthesis on a standard DNA synthesizer. The library generally includes $\sim 10^{14}$ unique sequences (Bouchard, Hutabarat, and Thompson 2010). The target of interest is incubated with the library, followed by several washing steps to remove non-functional or unbound sequences. Then the aptamer-target complex undergoes an elution process where the target is separated from the binding sequences. These binding sequences then go through a negative selection where they are allowed to mix with healthy cells, preferably denoted as negative cells. The aptamers that bind to the negative cells are then separated. The unbound aptamers after this step are the desired aptamers for that target. The sequences are amplified by polymerase chain reaction (PCR) to yield a practical amount. After several rounds of selection, the enriched library is cloned, sequenced and characterized to isolate aptamers with desired characteristics (Sefah

et al. 2010; Bouchard, Hutabarat, and Thompson 2010).

2.3 Uses of Aptamers in Modern Biomedical Engineering

Aptamers can be used in various biomedical applications listed below:

2.3.1 Biosensors

Biosensors are a bimolecular probe that can measure the existence or concentration of a specific biomolecule or biological structure (Sefah et al. 2009). The most immediate commercial application of aptamers was as biosensors due to their compatibility with various analytical technologies. They can specifically detect a large variety of targets such as proteins, small molecules, nucleotides, metabolites, amino acids etc (Rimmele 2003). The interaction of aptamers with their targets can be converted to electrical signals very conveniently using different transduction processes. The compatibility of aptamers with various detection schemes like electrochemical, fluorescence, chemiluminescence, field effect transistors, potentiometry etc. surged the area of aptasensor research (Sefah et al. 2009).

In aptamer biosensing, a 'recognition aptamer' for the specific target is coupled with a 'signaling aptamer' by direct fusion of their nucleic acid sequences. For biosensing applications, SELEX can be conducted in such a way that sequences for both recognition and signaling can be selected for a target in the same round. This simple system has the major advantage of ensuring that the recognition domain does not face any adverse effect in their specificity upon binding to the signaling domain (Bunka and Stockley 2006).

Quantum-dot aptamer beacons are a recent advancement of aptamers as biosensors. Quantum-dots are flouropores having a distinct sharp emission profile. Aptamer beacons consist of multiple aptamers bound to a single quantum-dot. Each aptamer has a complimentary base pair carrying a quencher. Upon binding to the target, the

complement is displaced resulting in a large increase of fluorescence emission. These highly specific aptamer beacons have great potential to be used for early detection of diseases by binding to cell surface epitopes. Until now, aptamers have been selected toward a broad range of targets, including metal ions (e.g., K^+, Hg^{2+} and Pb^{2+}), small organic molecules (e.g., amino acids, ATP, antibiotics, vitamins and cocaine) organic dyes, peptides and proteins (e.g., thrombin, growth factors and HIV-associated peptides) and even whole cells or microorganisms (e.g., bacteria) (Günter Mayer 2009).Another interesting development of biosensing aptamers is their conjugation with gold nanoparticles. Target binding causes a conformational change in the aptamer leading to disassembly of the aggregated nanoparticles resulting in a visible color change (Bunka and Stockley 2006).

2.3.2 Substitution of Antibodies

Antibodies are naturally occurring proteins found in the body and used by the immune system to identify and neutralize antigens. Artificially produced antibodies are also used in biomedical research for detection, identification and imaging of target molecules. In recent years, aptamers have shown very good compatibility as a substitute of antibodies.

As compared to antibodies, aptamers are more stable in blood serum (W. Tan et al. 2011). Chemically modified aptamers have better nuclease resistance than antibodies. They are easily producible in commercial basis with a cost much lower than antibodies. Antibodies only work extracellularly, but aptamers show both intracellular and extracellular functionality (Banerjee 2010). The most important advantage of aptamers over antibodies is that the body does not show any immune response against aptamers (Famulok and Mayer 1999; Foy et al. 2007). Prescribing antibody always has a chance for immune response in the patient and once administered is difficult to have control over the drug effect. With aptamer, however, the patients so

far treated did not show any kind of toxicity. For all these reasons, aptamers can successfully replace antibodies for the treatment of macular degeneration, non-small cell lung cancer, and thrombotic thrombocytopenic purpura, acute coronary syndrome, von Willebrand factor-related disorder, angiomas, acute myeloid leukemia, and renal cell carcinoma etc (Sundaram et al. 2013; Ng et al. 2006).

2.3.3 Therapeutic agents

Aptamers can modulate protein function which enables them to be used as therapeutic agents. Chemical modifications of aptamers lead their increased half-life, nuclease resistance and improved pharmacokinetics allowing their rigorous use in clinical applications. Even in unmodified form, aptamers can be used for treatment of transient conditions like blood clotting with their low half-life and rapid clearance by the kidneys (Banerjee and Nilsen-Hamilton 2013). Conjugation of aptamers with PEG lead to their increased half-life in blood. All kinds of modifications in aptamer structure led to a significant enrichment of the aptamer in kidneys, liver, spleen, heart, and mediastinal lymph nodes, representing modulation in their pharmacokinetic properties (W. Tan et al. 2011).

Superior targeting performance of aptamers raised the interest of using them for cancer therapy. An aptamer named AS1411 is undergoing clinical trials, which can specifically target a bcl-2 binding protein, nucleolin, responsible for cell proliferation. Upon binding, AS1411 can enter the cancer cell and causes its death by apoptosis (W. Tan et al. 2011). Anti-thrombin aptamers have been developed to increase clotting time of human plasma. These aptamers are undergoing clinical trials for the treatment of Acute Coronary Syndrome (ACS) (Günter Mayer 2009). Aptamers can also be used as antiviral drug agents by preventing replication of escape mutants (Banerjee 2010).

2.3.4 Target validation tools

Target validation is the determination of whether a drug target is involved in disease pathology. Aptamers can inhibit target function by blocking or knocking out gene expression (Pendergrast et al. 2005). This makes them particularly important as target validation tools . They bind with high affinity and specificity with target molecules. Protein level function of aptamers can provide information complementary to that obtained from gene-level validation approach. Aptamers can validate both intracellular and extracellular targets. They can be easily delivered to the intracellular target by using standard transfection techniques (Pendergrast et al. 2005).

2.3.5 Drug carriers

Aptamers can be assembled with different functional groups which provide the means to use them as delivery vehicles that specifically address certain malignant cell subtype (Song et al. 2008). They can be conjugated with nanoparticles for targeted delivery of chemotherapeutic agents to cancer cells (Figure-2.3). The best characterized aptamer in this regard is A10 which binds to the prostate specific membrane antigen (PSMA) responsible for the onset and progression of cancer. This aptamer can be conjugated with polymer coated nanoparticle encapsulated with chemotherapeutics (i.e., Docetaxel) to its $5'$-amino end. This chemotherapeutic treatment aided by aptamers can reduce the size of cancer upto a total remission.

Other than chemotherapeutics, aptamers can be used for delivery of cell specific small interfering RNA (siRNA) molecules. In this regard, siRNA molecules have been coupled to aptamer A10 either directly by nucleotidic extensions or indirectly through the assembly of tetrameric streptavidin-biotin complexes consisting of two biotinylated aptamers and two biotinylated siRNA molecules per streptavidin moiety. Both approaches were successful in the cell specific siRNA-mediated reduction of the corresponding mRNA and protein levels. Aptamer-toxin conjugates were also

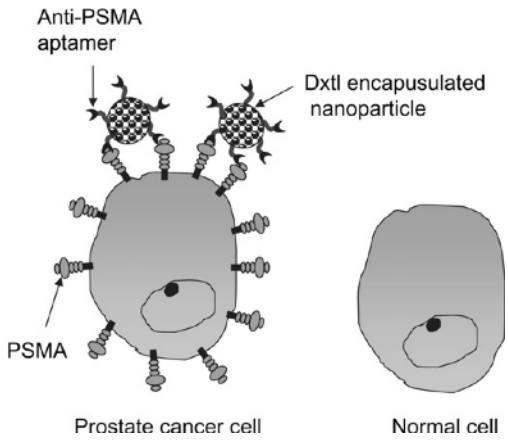

Figure 2.3 Targeted delivery of the anticancer drug docetaxel (Dxtl) encapsulated by the nanoparticle functionalized with an anti-prostate specific membrane antigen (anti-PSMA) aptamer. The nanoparticle aptamer bioconjugate selectively delivers the drug to prostate cancer cells expressing the PSMA on their surface and not to normal cells, which do not have the PSMA (Khati 2010).

generated and applied to give specificity for the toxin gelonin, a ribosome-inactivating protein (Günter Mayer 2009).

Aptamer-based targeted delivery can also be used to selectively inactivate bacterial and viral pathogens in infected cells. DNA aptamers have been developed to bind vaccinia-virus-infected cells with dissociation constant in nanomolar range. Transcription of HIV-1 can be inhibited by targeted delivery of siRNA using anti-gp120 RNA aptamer (Khati 2010).

2.4 Importance of Molecular Modeling with Aptamers

Production of aptamers with SELEX protocol is a very time consuming and labor-intensive task. To select aptamer for a single target, it takes 15-18 rounds of selection and each round can take 2-3 days (Carlson 2007). A theoretical model for selection of aptamers *in-silico* prior to the experimental SELEX can make the entire process a lot easier and commercially viable. Structural, thermodynamic and electrostatic properties are studied in our model which can be used to generate a theoretical

databank containing a large number of aptamer conformations. This model takes into account the size, shape, electrical properties and physical conformations of the aptamers to study their structural and thermodynamic changes with varying biological environments. This model lays the foundation to develop a predictive approach to select the specific aptamer for a specific target that shows the most stable and strongest binding. This approach will make the use of aptamers in biosensing, target validation and other drug delivery applications more efficient. For example, using this model will enable us to select an aptamer as a biosensing probe that will detect a specific pathogen more accurately in human body. The accuracy will be ensured through the understanding of all the chemical and thermodynamic aspects related to the aptamer-target binding. Structural modification of aptamers with different functional groups can enhance their stability and binding efficacy. Our model can lead to the addition of a specific functional group to the aptamer chain in the most accurate position for a specific application. To choose aptamer as a drug agent, this model can ensure strongest binding with the pathogens and will work most effectively to stop the signaling pathway for the progression of a certain disease.

2.5 Molecular Modeling of Aptamers

The molecular model in this work is developed to represent surface-grafted ssDNA aptamers as a co-polymer with a combination of four monomer units- adenine (A), guanine (G), Cytosine (C) and Thymine (T) in a coarse-grained level. We explicitly considered the physical and chemical properties of these nucleobases in a solution environment to capture their behavior as accurately as possible. We studied two chain sequences: diblock co-polymer of A and G (A_6G_6, a block of six adenine monomers followed by a block of six guanine monomers) and diblock of T and C (T_6C_6, a block of six thymine monomers followed by a block of six cytosine monomers) (Figure-1). Each of these chains contain 12 monomers at varying grafting densities and either

$NaCl$ or $MgCl_2$ salt concentrations, while keeping the solution temperature fixed at 298 K.

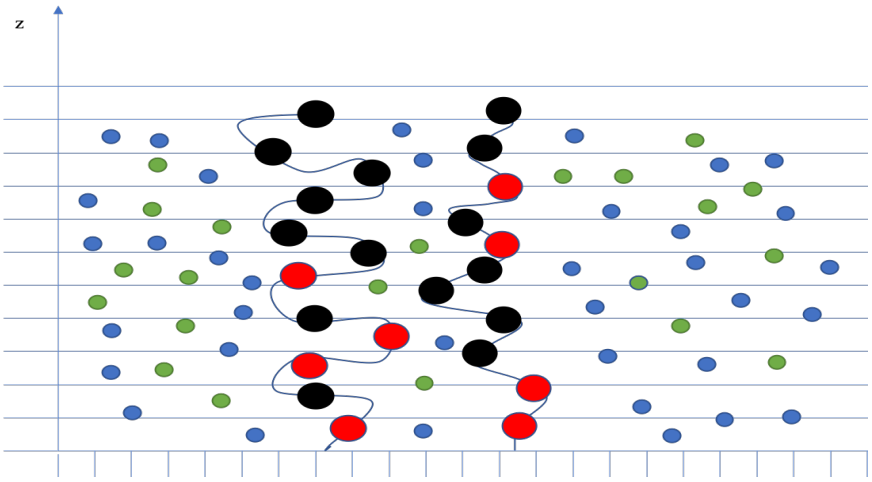

Figure 2.4 Schematic representation of the end-grafted polymer in the salt solution environment. The circles on the polyelectrolyte segments represent acid groups; the red segments are negatively charged, and the black segments are protonated and therefore charge neutral. The cations are colored blue to denote positive charge and are either monovalent in the case of NaCl or divalent in the case of $MgCl_2$. The negative ions are shown as small green circles.

The theoretical model is constructed using a **Self Consistent Field Theory (SCFT)** approach for a single polyelectrolyte chain in a field of interacting species (M. J. Uline, Rabin, and Igal Szleifer 2011; Szleifer and Carignano 1996; M. J. Uline, Meng, and Igal Szleifer 2010; Munnik et al. 2018; Jahan and M. Uline 2018). The polyelectrolyte chains are end-tethered to a surface and submerged in a salt and water bath, containing either $NaCl$ or $MgCl_2$ salts. In this molecular model, N_p polyelectrolyte chains are end-grafted to a surface with cross sectional area A. We assumed the system to be homogeneous in x and y directions, but heterogeneous in z direction. Within the field theory framework, the lateral heterogeneity is accounted for by discretizing the system space into a number of layers. The concentrations of the salts are converted to a density field to determine their contribution to the field. The model construction is initiated by calculating the total Helmholtz free energy of

the system, which is given by,

$$F = -TS_{conf} - TS_{mix} + F_{chem} + F_{elect} + E_{rep} \tag{2.1}$$

Here, S_{conf} is the conformational entropy of the grafted polymer chains, S_{mix} is the mixing or translational entropy of all the free species: water (w), protons (H^+) and hydroxyl ions (OH^-), cations (Na^+, Mg^{2+}) and anions (Cl^-,OH^-). F_{chem} is the free energy associated with the equilibrium reactions that the monomers undergo in this system. We have explicitly considered three equilibrium reactions for each monomer- (1) protonation and deprotonation via acid-base equilibrium reaction, (2) Mg^{2+} binding or Na^+ binding. By deriving the individual terms of the Helmholtz free energy, free energy equation for aptamers containing Adenine, Guanine, Thymine and Cytosine bases in planar surface is given by:

$$\begin{aligned}
f &= \frac{\beta F}{A} \\
&= \sigma_p \sum_{\alpha} P(\alpha) \ln P(\alpha) \\
&+ \int \langle \rho_A(z) \rangle [f_{HA}(z)(\ln f_{HA}(z) + \beta\mu^0_{AH}) + (1 - f_{HA}(z))(\ln(1 - f_{HA}(z)) + \beta\mu^0_{A^-}]dz \\
&+ \int \langle \rho_G(z) \rangle [f_{HG}(z)(\ln f_{HG}(z) + \beta\mu^0_{HG}) + (1 - f_{HG}(z))(\ln(1 - f_{HG}(z)) + \beta\mu^0_{G^-}]dz \\
&+ \int \langle \rho_T(z) \rangle [f_{HT}(z)(\ln f_{HT}(z) + \beta\mu^0_{HT}) + (1 - f_{HT}(z))(\ln(1 - f_{HT}(z)) + \beta\mu^0_{T^-}]dz \\
&+ \int \langle \rho_C(z) \rangle [f_{HC}(z)(\ln f_{HC}(z) + \beta\mu^0_{HC}) + (1 - f_{HC}(z))(\ln(1 - f_{HC}(z)) + \beta\mu^0_{C^-}]dz \\
&+ \beta \int [\langle \rho_q(z) \rangle \psi(z) - \frac{1}{2}\epsilon_w (\frac{d\psi(z)}{dz})^2]dz + \int \rho_w(z)(\ln \rho_w(z) v_w - 1)dz \\
&+ \int \rho_{H^+}(z)(\ln \rho_{H^+}(z) v_w - 1 + \beta\mu^0_{H^+})dz + \int \rho_{OH^-}(z)(\ln \rho_{OH^-}(z) v_w - 1 \\
&+ \beta\mu^0_{OH^-})dz + \int \rho_+(z)(\ln \rho_+(z) v_w - 1 + \beta\mu_+)dz \\
&+ \int \rho_-(z)(\ln \rho_-(z) v_w - 1 + \beta\mu_-)dz
\end{aligned} \tag{2.2}$$

The Free energy equation subjected to volume constraint by introducing Lagrange multipliers, $\beta\pi(z)$ is:

$$\begin{aligned} w =& f + \beta \int \pi(z)(\sigma_p \sum_{\alpha} P(\alpha)[v_A(z;\alpha) + v_G(z;\alpha) + v_T(z;\alpha) + v_C(z;\alpha)] \\ &+ \rho_+(z)v_+ + \rho_-(z)v_- + \rho_w(z)v_w \\ &+ \rho_{H^+}(z)v_{H^+} + \rho_{OH^-}(z)v_{OH^-} - 1)dz \end{aligned} \tag{2.3}$$

Extremization of equation(2.3) with respect to densities, degree of protonation, electric potential and probability distribution function gives following expressions:

$$\rho_w(z)v_w = \exp[-\beta\pi(z)v_w] \tag{2.4}$$

$$\rho_{H^+}(z)v_w = \exp[-\beta\pi(z)v_w + \beta\mu^0_{H^+} + \beta\psi(z)] \tag{2.5}$$

$$\rho_{OH^-}(z)v_w = \exp[-\beta\pi(z)v_w + \beta\mu^0_{OH^-} - \beta\psi(z)] \tag{2.6}$$

$$\rho_+(z)v_w = \exp[-\beta\pi(z)v_+ + \beta\mu_+ + \beta\psi(z)] \tag{2.7}$$

$$\rho_-(z)v_w = \exp[-\beta\pi(z)v_- + \beta\mu_- - \beta\psi(z)] \tag{2.8}$$

$$\frac{f_{HA}(z)}{1 - f_{HA}(z)} = \frac{\phi^+_H(z)}{\phi_w(z)K^0_G} \tag{2.9}$$

$$\frac{f_{HG}(z)}{1 - f_{HG}(z)} = \frac{\phi^+_H(z)}{\phi_w(z)K^0_G} \tag{2.10}$$

$$\frac{f_{HT}(z)}{1 - f_{HT}(z)} = \frac{\phi^+_H(z)}{\phi_w(z)K^0_T} \tag{2.11}$$

$$\frac{f_{HC}(z)}{1 - f_{HC}(z)} = \frac{\phi^+_H(z)}{\phi_w(z)K^0_C} \tag{2.12}$$

The probability distribution function (pdf) is derived from the functional minimization with $P(\alpha)$,

$$\begin{aligned}
P(\alpha) = \frac{1}{Q}\exp[&-\int n_A(\alpha;z)v_A\ln(1-f_{HA}(z))dz \\
&-\int n_G(\alpha;z)v_G\ln(1-f_{HG}(z))dz - \int n_T(\alpha;z)v_T\ln(1-f_{HT}(z))dz \\
&-\int n_C(\alpha;z)v_C\ln(1-f_{HC}(z))dz + \beta\int \psi(z)n_A(\alpha;z)dz \\
&+\beta\int \psi(z)n_G(\alpha;z)dz + \beta\int \psi(z)n_T(\alpha;z)dz \\
&+\beta\int \psi(z)n_C(\alpha;z)dz - \beta\int \pi(z)n_A(\alpha;z)v_A dz \\
&-\beta\int \pi(z)n_G(\alpha;z)v_G dz - \beta\int \pi(z)n_T(\alpha;z)v_T dz - \beta\int \pi(z)n_C(\alpha;z)v_C dz]
\end{aligned} \tag{2.13}$$

Extremization of the free energy with respect to the electrostatic potential yields Poisson equation,

$$\epsilon_w \frac{d^2\psi(z)}{dz^2} = -\langle\rho_q(z)\rangle \tag{2.14}$$

$$\epsilon_w \frac{d\psi(z)}{dz}|_{z=0} = 0, \lim_{r\to\infty}\psi(z) = 0 \tag{2.15}$$

Equations (2.4) through (2.15) are solved simultaneously following the procedure described in previous publications using this general approach (M. J. Uline, Rabin, and Igal Szleifer 2011; Szleifer and Carignano 1996; Rikkert J Nap, S. H. Park, and Igal Szleifer 2018). These integro-differential equations are solved numerically by discretizing the space for a discretization length of 0.3 nm for 100 discrete layers. Solution of these sets of non-linear coupled equations yields the unknowns of the model, that are the Lagrange multiplier $\pi(z)$ and the electrostatic potential $\psi(z)$. The inputs necessary to solve the system of equations are the bulk concentrations of the salts, bulk pH, grafting density, volumes of different species, a set of polymer conformations and the equilibrium reaction constants. The pKa values for A, G, T and C are 3.5, 1.6, 9.7 and 4.2, respectively (Bloomfield and Crothers 2000). The volume of Mg^{2+} is $0.18nm^3$, and the volumes for Na^+ and Cl^- are $0.05nm^3$. The set

of polymer conformations are derived using a Rotational Isomeric State (RIS) model (Paul J Flory and Volkenstein 1969).

2.6 Results and Discussions

In the molecular model, the aptamer chains are grafted in a planar surface and is assumed to be inhomogeneous in the direction perpendicular to the grafting surface. The aptamer chains are submerged in a bath of anions, cations, H^+, OH^- and water molecules. The number of polymer molecules is fixed, but the grafting surface is in contact with a bath of ions and water. Therefore, we choose our system to be in grand canonical ensemble. It has been assumed that the system is in a good solvent bath, i.e.; there is no attractive interactions between the monomers. So, Chi parameter (χ) is considered to be zero and therefore not included in the free energy equation.

Aptamers may contain four nucleotides: adenine, guanine, cytosine and thymine. We took two aptamer chains, one containing Adenine and Guanine; another one containing Thymine and Cytosine. Bulk pH of the system is chosen to be 4.0 due to acidic nature of the aptamer chains. Each chain contains n=12 monomers, having six of each nucleobase.

We varied the bulk salt concentration and surface coverage of aptamer chains along with the type of salt to observe the changes in the structural and chemical properties. We calculated the change in volume fraction and protonation profile with the change in distance from grafting surface. Two different salts, $NaCl$ and $MgCl_2$ are used to observe the effect of cation size on polymer volume distribution.

2.6.1 Effect of salt concentration and surface coverage on aptamer volume fractions: aptamer containing Adenine and Guanine

$NaCl$ Salt Solution

Figure-2.5 and 2.6 shows the volume profile of the aptamer chains in $NaCl$ solution at two different surface coverages. At lower surface coverage (0.0001 $molecules/nm^2$), the aptamer chains are highly flexible and have relatively higher volume fractions near the tethering surface (Figure-2.5). But at higher surface coverage (at 0.007 $molecules/nm^2$), the flexibility is much lower and volume fractions are almost uniform throughout the one-dimensional space.

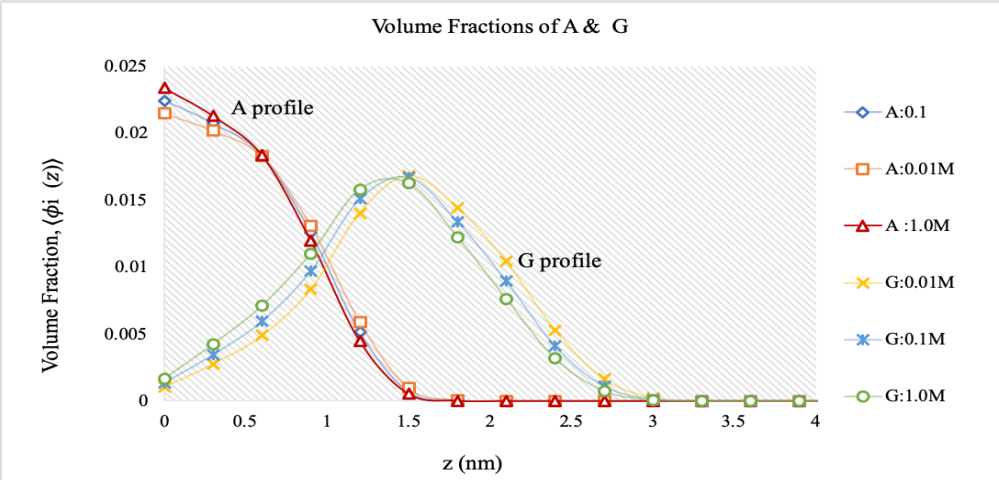

Figure 2.5 Aptamer volume fraction profile in $NaCl$ salt at low surface coverage (0.0001 $molecules/nm^2$).

$MgCl_2$ Salt Solution

In $MgCl_2$ salt solution, the aptamer chains show similar volume profile like NaCl salt in low surface coverage (Figure-2.7). So at lower surface coverage, cation size does not affect the spatial distribution of aptamer chains very much. But at higher surface coverage (Figure-2.8), there is a significant change in volume fraction profile. Volume fractions near the tethering surface decreases from 0.9 to 0.65. This is due to the

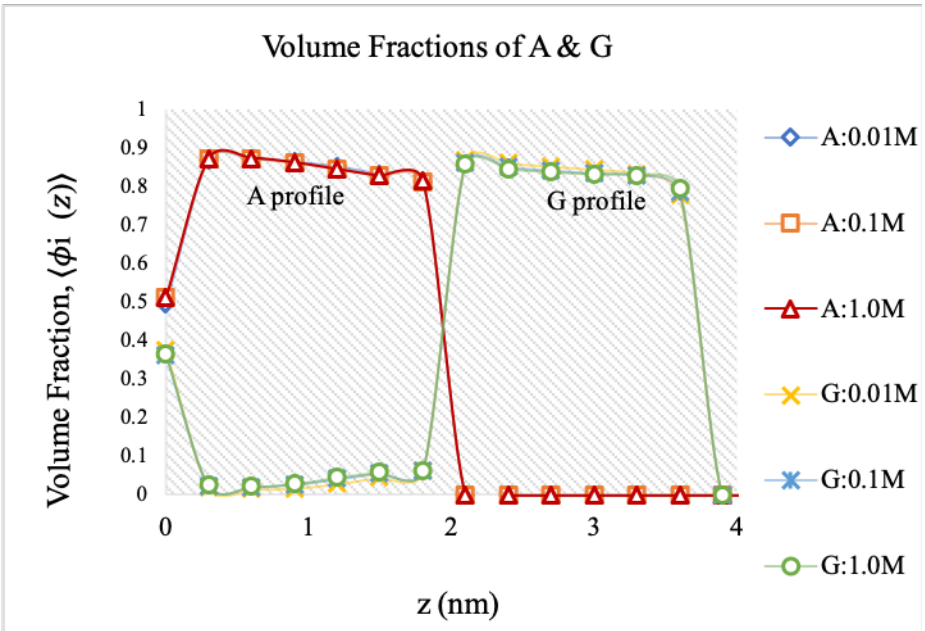

Figure 2.6 Aptamer volume fraction profile in $NaCl$ salt at high surface coverage (0.007 $molecules/nm^2$).

increased steric hindrance caused by increasing the cation size from Na^+ to Mg^{2+}. To minimize the steric effect, the aptamer chains change their spatial distribution to achieve the most stable structure.

2.6.2 Effect of salt concentration and surface coverage on protonation profiles for aptamer containing Adenine and Guanine

$NaCl$ Salt Solution

Figure-2.9 and Figure-2.10 shows the protonation profile of the aptamer chains at lower and higher surface coverages respectively in NaCl solution. At lower surface coverage (Figure-2.9), the equilibrium protonation fraction is 0.6, which means that the layer is neutralized by the counterions present in the solution. This represents a significant amount of sodium in the brush at lower surface coverage of the aptamer chains. But at higher surface coverage, the protonation fraction is higher (nearly 1.0) indicating the presence of less amount of sodium ions in the brush to neutralize the

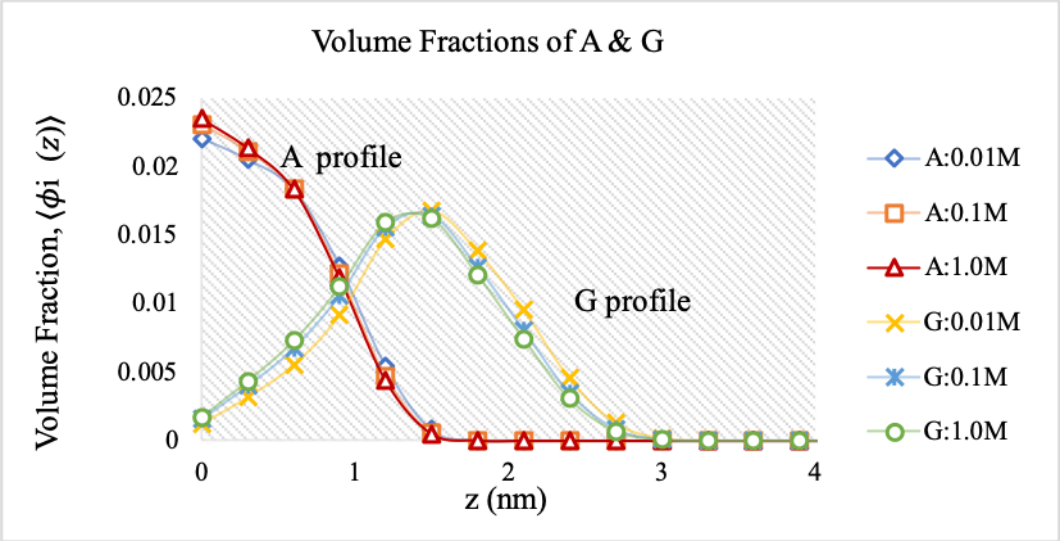

Figure 2.7 Aptamer volume fraction profile in $MgCl_2$ at lower surface coverage (0.0001 $molecules/nm^2$).

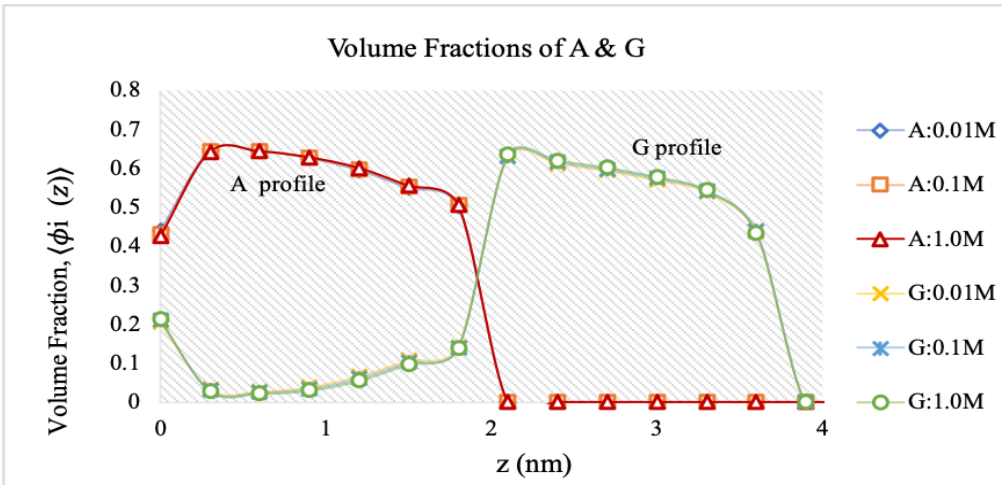

Figure 2.8 Aptamer volume fraction profile in $MgCl_2$ salt at high surface coverage (0.002 $molecules/nm^2$).

charged polymers.

We can also see that protonation profiles of two different bases Adenine and Guanine are different at different surface coverages. At lower surface coverage, Adenine is protonated, but Guanine remains nearly unprotonated indicating the presence of a large volume fraction of sodium ions. But at higher surface coverage, Adenine is

fully protonated at lower salt concentration and Guanine is protonated significantly with a decrease in sodium ion concentration along the chain.

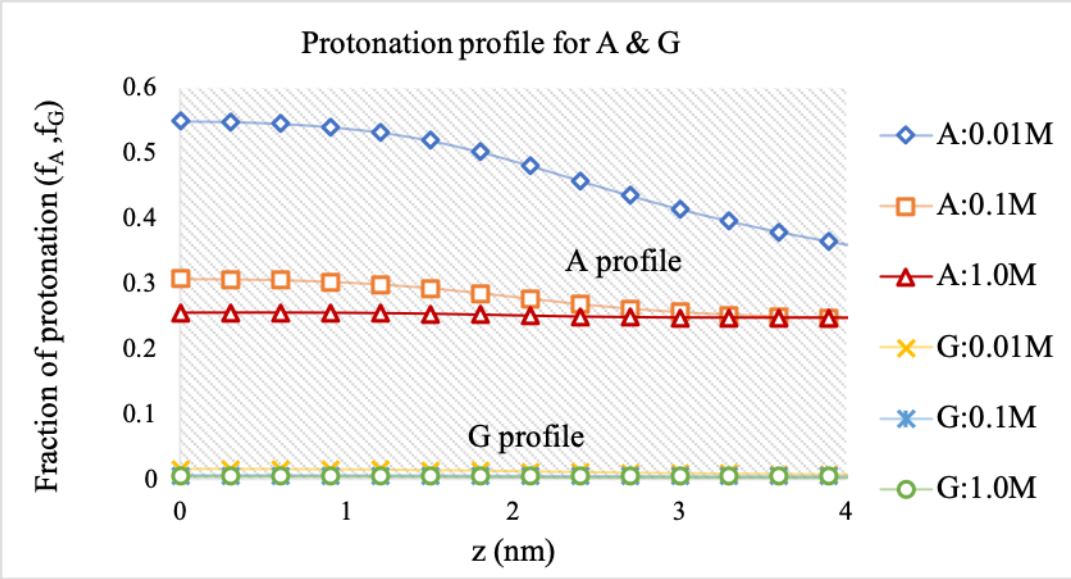

Figure 2.9 Aptamer protonation profile in $NaCl$ at lower surface coverage (0.0001 $molecules/nm^2$).

$MgCl_2$ Salt Solution

Figure-2.11 and Figure-2.12 shows the protonation profile of the aptamer chains at lower and higher surface coverages respectively in $MgCl_2$ solution. At lower surface coverage, the equilibrium protonation fraction falls from 0.6 to 0.375 in effect of changing cation type from Na^+ to Mg^{2+}. Hence, bigger cations can enter the brush to neutralize it more easily than the smaller ones. At higher surface coverage, some Mg^{2+} ion can enter the brush to neutralize it unlike the Na^+ ions. We can conclude from figures- 2.11 and 2.12 that at lower surface coverage and lower salt concentrations, cations can enter the brush to neutralize them along with the protons. But at higher surface coverage and lower salt concentrations, the cations are repelled from the brush to minimize the steric hindrance. In other words, the system pays in chemical free energy to reduce the electrostatic repulsions and to avoid localization of a

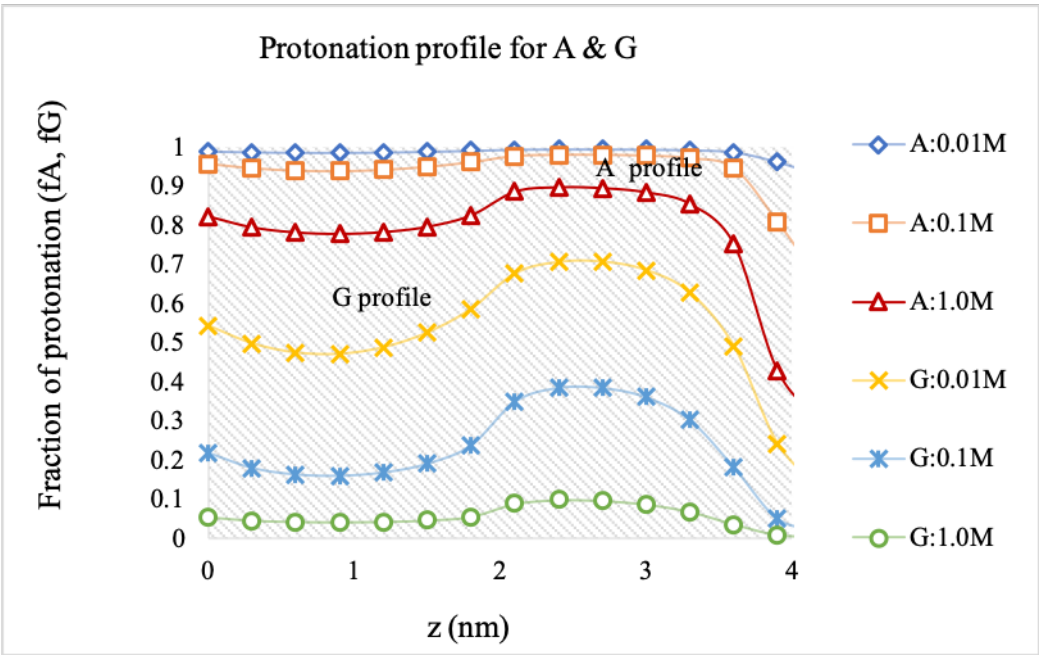

Figure 2.10 Aptamer protonation profile in $NaCl$ salt at high surface coverage (0.007 $molecules/nm^2$).

very high concentrations of ions, i.e.; counterion confinement (M. J. Uline, Rabin, and Igal Szleifer 2011).

2.6.3 Effect of salt concentration and surface coverage on aptamer volume fractions: aptamer containing Thymine and Cytosine

$NaCl$ Salt Solution

Figure-2.13 and Figure-2.14 shows volume profiles of aptamer chains containing Thymine and Cytosine in NaCl salt solution at two different surface coverages. At lower surface coverage (Figure-2.13), the chains are more flexible and have relatively higher volume fraction near the tethering surface than the bulk. But at higher surface coverage (Figure-2.14), the chains are more stretched and have higher volume fraction on the mid-layer.

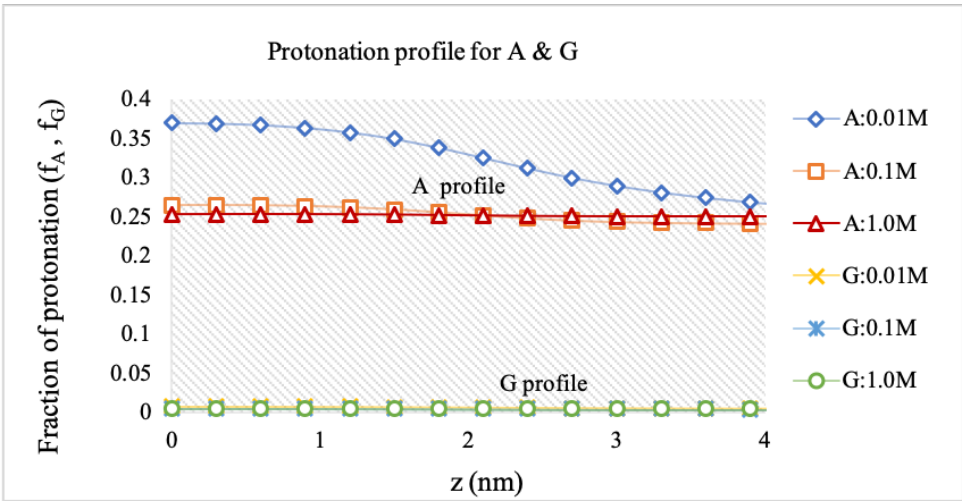

Figure 2.11 Aptamer protonation profile in $MgCl_2$ at lower surface coverage (0.0001 $molecules/nm^2$).

$MgCl_2$ Salt Solution

Figure- 2.15 and Figure-2.16 shows volume profiles of aptamer chains containing Thymine and Cytosine in $MgCl_2$ salt solution at two different surface coverages. At lower surface coverage, the chains have higher flexibility. But at higher surface coverage, the chains comprise to their flexibility to compensate the steric effect due to charge regulation along the chain.

2.6.4 Effect of salt concentration and surface coverage on protonation profiles for aptamer containing Thymine and Cytosine

$NaCl$ Salt Solution

Figure-2.17 and Figure-2.18 shows the protonation profile of the aptamer chains containing Thymine and Cytosine at lower and higher surface coverages respectively in $NaCl$ solution. At lower surface coverage (Figure-2.17), the equilibrium protonation fraction is 1.0 for Thymine, but 0.68 for Cytosine which represents the presence of sodium ion on the brush. But at higher surface coverage (Figure-2.18), the protona-

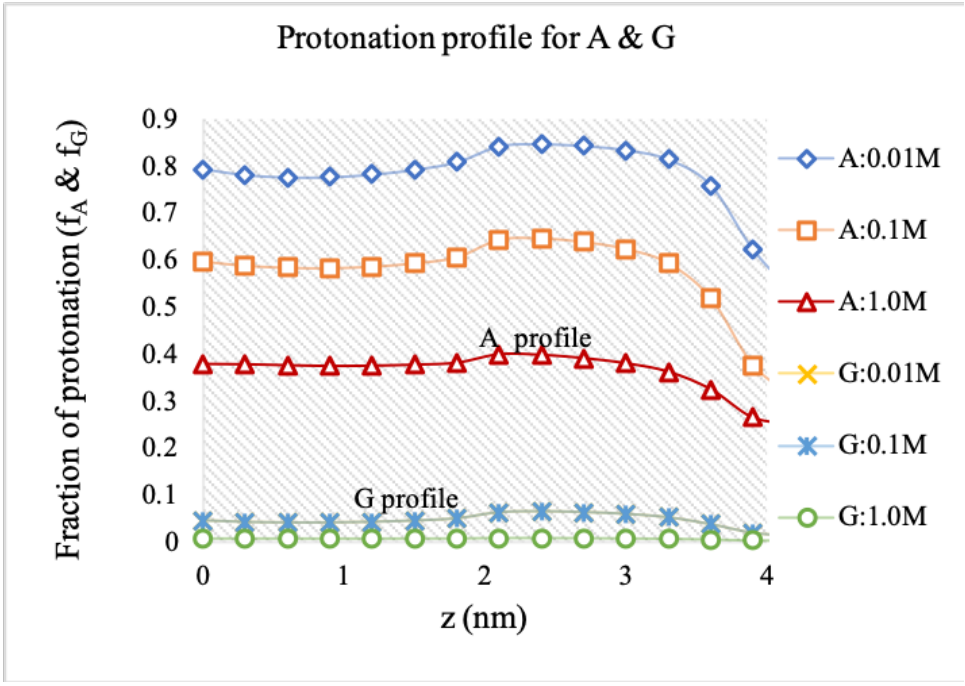

Figure 2.12 Aptamer protonation profile in $MgCl_2$ salt at high surface coverage (0.005 $molecules/nm^2$).

tion fraction is higher (nearly 0.9) indicating the presence of less amount of sodium ions in the brush to neutralize the charged polymers.

$MgCl_2$ Salt Solution

For $MgCl_2$ salt solution, the protonation along the aptamer chain containing Thymine and Cytosine is more uniform along the brush in lower surface coverage (Figure-2.19). But as the surface coverage increases, protonation fraction increases at the middle of the layers. That means magnesium ions are repelled from the brush due to higher charge regulation on the chains and the brush is neutralized by counterions present in the solution.

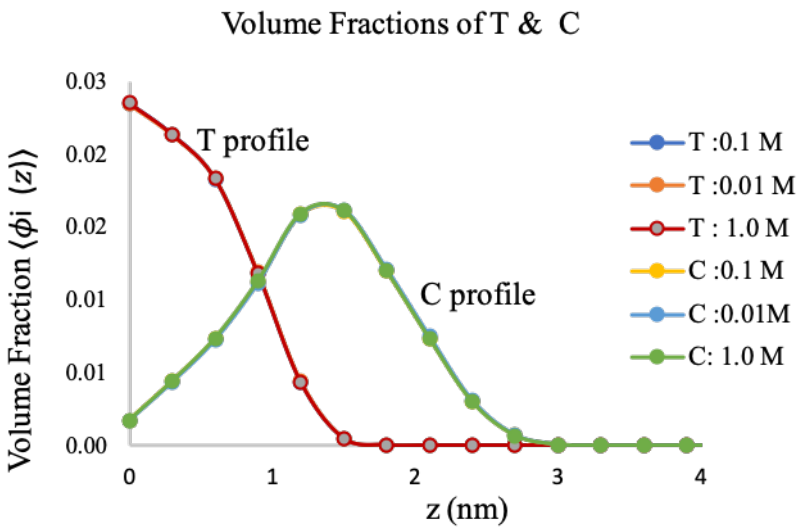

Figure 2.13 T and C Aptamer volume fraction profile in $NaCl$ salt at lower surface coverage (0.0001 $molecules/nm^2$).

2.7 Conclusions

A theoretical molecular model is developed to capture the structural, electrostatic and thermodynamic behavior of aptamers in response to the change of their surrounding environments. We considered two aptamer chains, one containing Adenine and Guanine, and another containing Thymine and Cytosine nucleobases. This model takes into account the size, shape, electrical properties and physical configurations of the aptamers along with the size, shape and physical properties of other chemical species associated with a particular biological environment. Simulating the molecular model provides us fundamental insights on structure and property changes of the aptamers with changes in their surrounding environment.

We studied the variation of chain types, salt concentration and grafting density of the aptamer chains. The results imply that the structure of the aptamer chains varies significantly due to charge regulation effects. Protonation profiles of monomer blocks are highly dependent on the distance from the interface. Neutralization of the negative charge is highly dependent on both the surface coverage of aptamers

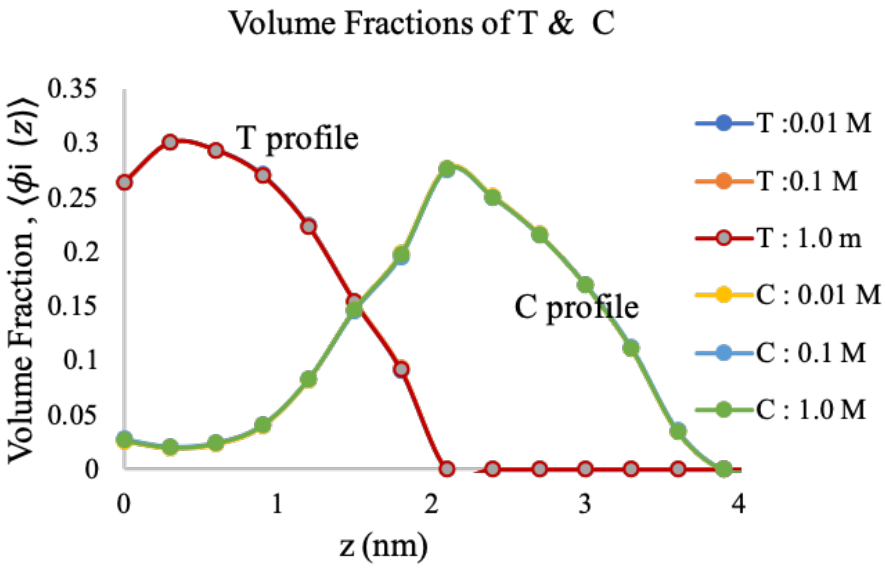

Figure 2.14 T and C Aptamer protonation profile in $NaCl$ at higher surface coverage (0.002 $molecules/nm^2$).

and the valence of the cations. Mg^{2+} is still present in the aptamer layer for the high surface coverage case. But Na^+ is nearly excluded from the brush due to high steric repulsion inside the brush for higher amount of charged monomers. The system decides to relieve the electrostatic repulsions by paying in acid-base equilibrium.

Finally, it can be concluded that this model captures the physical property changes very well for the aptamer chains at varying surface coverages, types of salt and different salt concentrations. This model can aid in generating a theoretical databank for ssDNA aptamers to select a specific aptamer for a specific target molecule very quickly and cost effectively.

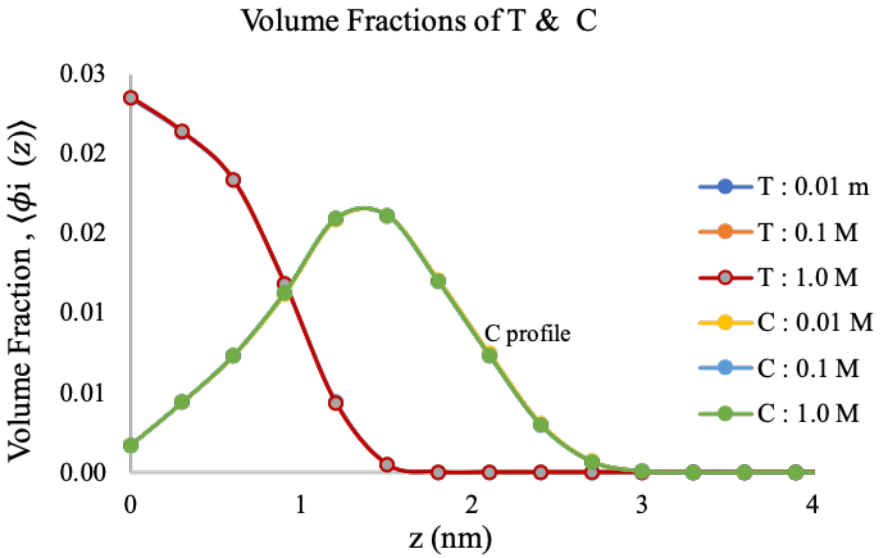

Figure 2.15 T and C Aptamer volume fraction profile in $MgCl_2$ at lower surface coverage (0.0001 $molecules/nm^2$).

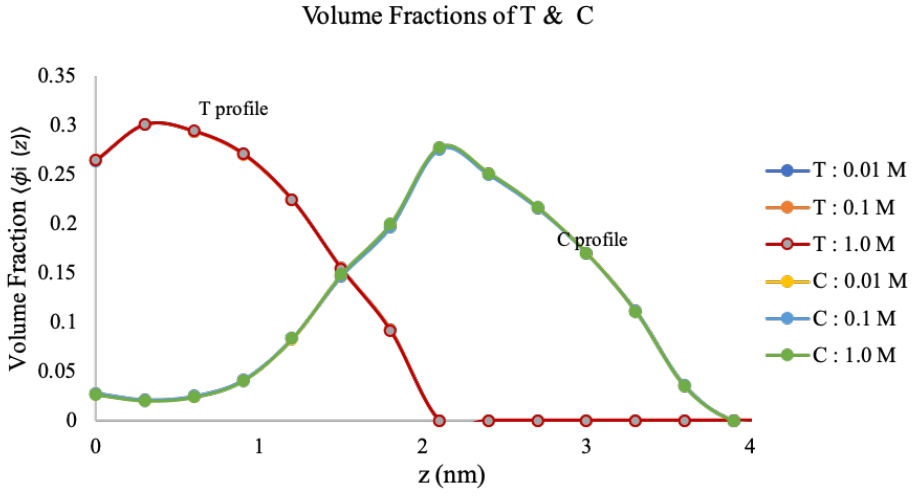

Figure 2.16 T and C Aptamer volume fraction profile in $MgCl_2$ salt at high surface coverage (0.002 $molecules/nm^2$).

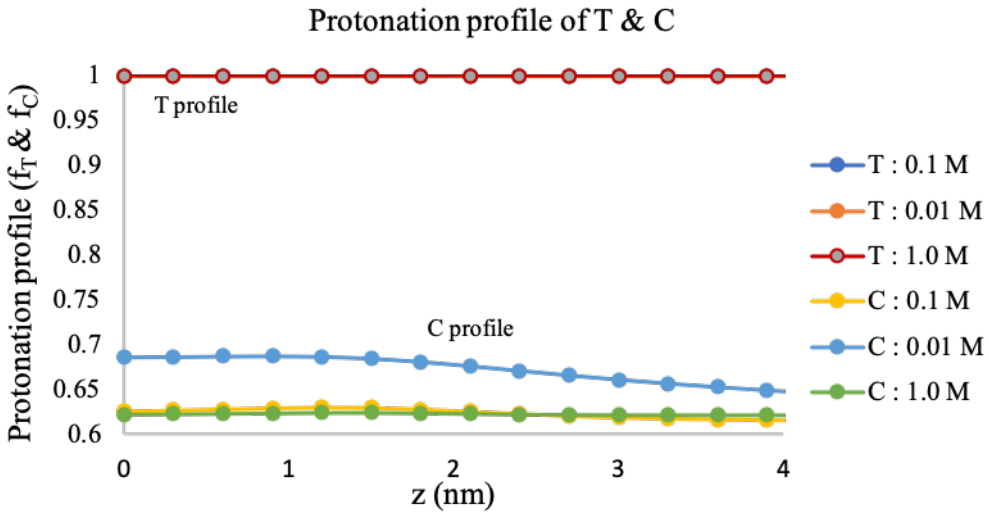

Figure 2.17 T and C Aptamer volume fraction profile in $NaCl$ at low surface coverage (0.0001 $molecules/nm^2$).

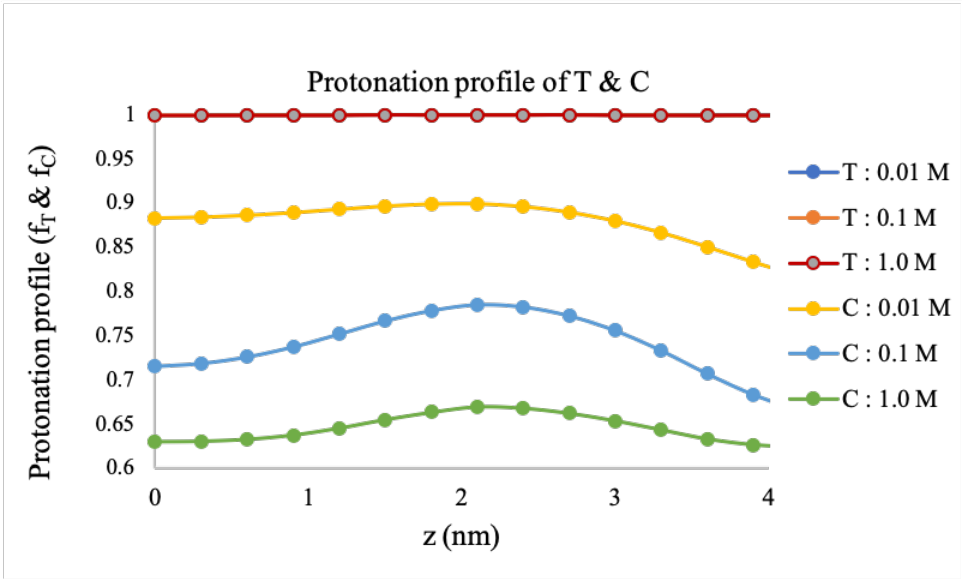

Figure 2.18 T and C Aptamer volume fraction profile in $NaCl$ salt at high surface coverage (0.002 $molecules/nm^2$).

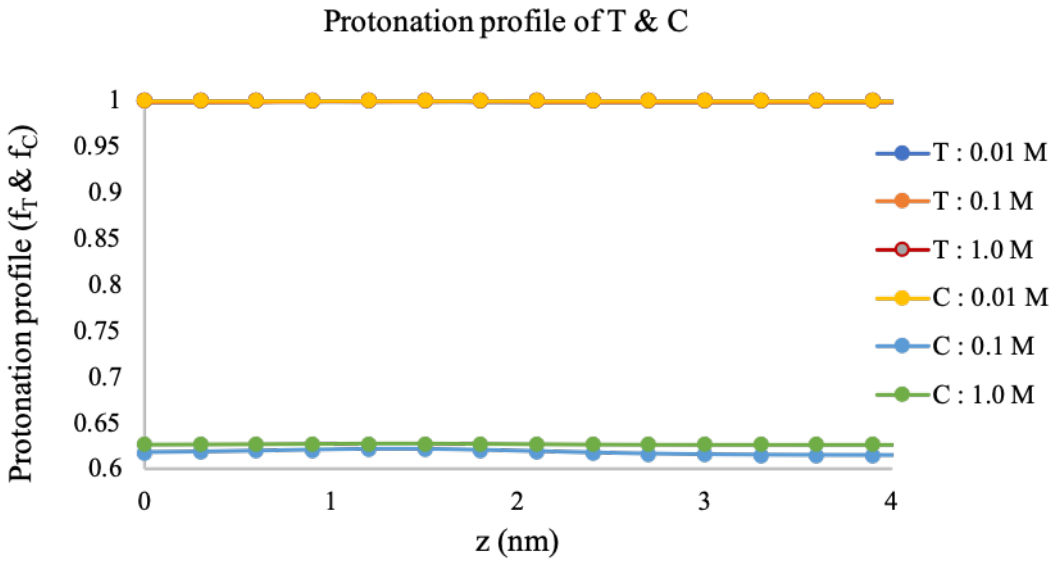

Figure 2.19 T and C Aptamer protonation fraction profile in $MgCl_2$ at low surface coverage (0.0001 $molecules/nm^2$).

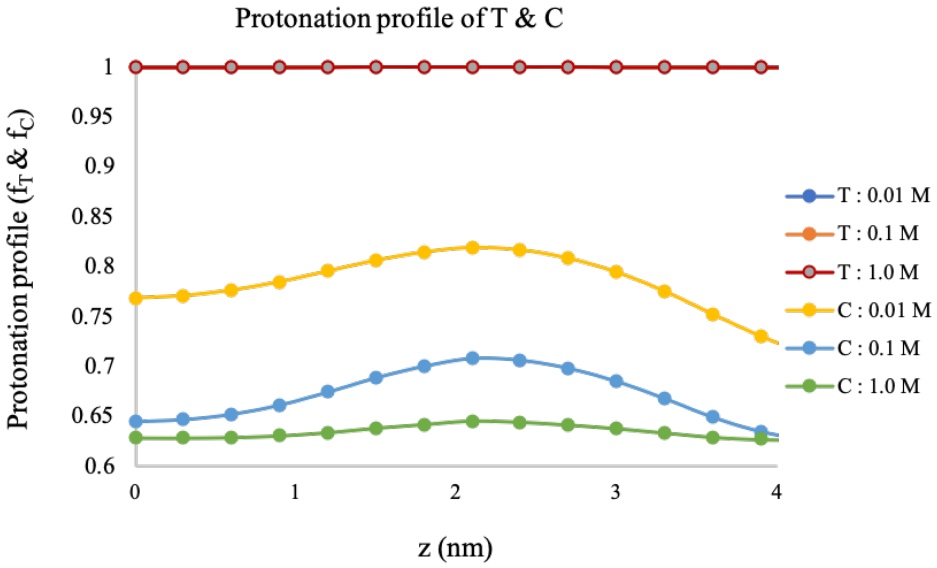

Figure 2.20 T and C Aptamer protonation fraction profile in $MgCl_2$ salt at high surface coverage (0.002 $molecules/nm^2$).

Chapter 3

Quantifying Divalent Cation Binding To ssDNA Aptamers

3.1 Introduction

Aptamers are an important class of biomolecules consisting of single stranded DNA (ssDNA), RNA, or peptides that can fold into unique secondary and tertiary structures for shape-specific target recognition(Keefe, Pai, and A. Ellington 2010). Due to the highly specific and selective nature of their target binding, aptamers are widely studied for a range of applications from biosensing (R. Liu et al. 2018; Cho, J.-W. Lee, and A. D. Ellington 2009) to drug design (Dua et al. 2018; G. Zhou et al. 2018; Foster and DeRosa 2014). A recent work reported a major breakthrough in biosensor research by using aptamers with field-effect transistors to overcome the 'Debye length limitations' (Nakatsuka et al. 2018). Aptamers are polyelectrolytic in nature with their monomer units (nucleobases) participating in acid-base equilibrium and counterion binding reactions with the surrounding solution environments. Charge regulation and counterion binding in aptamers, or polyelectrolytes in general, are modulated by the metal ions present in the system that can non-trivially alter their chemical and structural properties (M. J. Uline, Rabin, and Igal Szleifer 2011; Rikkert J Nap and Igal Szleifer 2018; Rikkert J Nap, Solveyra, and Igal Szleifer 2018; Zwanikken et al. 2011; R. Kumar, Sumpter, and Kilbey 2012; Lewis et al. 2013). Presence of metal ions affects the performance of the aptamers as biosensing probes or therapeutics (Juewen Liu, Cao, and Lu 2009; W. Zhou et al. 2014; J.-S. Lee, Han, and Mirkin 2007) due to

the electrostatic screening of the charges on their surface that changes their structure and chemistry. These interactions of aptamers with metal ions are complicated in nature owing to the fact that multiple binding sites on the nucleobases are capable of such interactions, following different binding pathways and thus having varying energy landscapes (Saenger 1984; Reshetnikov et al. 2011). In this work, we have particularly addressed magnesium ion (Mg^{2+}) binding because of its relevance to almost all nucleic acid related biological processes in the intracellular environment (Ono et al. 2011; Anastassopoulou and Theophanides 2002; Pascal, Grover, and Westhof 2011).

A myriad of computational studies has been conducted with Molecular Dynamics (MD) (Mocci and Laaksonen 2012) and Monte Carlo (MC)(Mills, Anderson, and Record Jr 1985) simulations to elucidate the nature of metal ion binding to nucleic acids. Most of such theoretical studies are based on double stranded DNA (dsDNA) - monovalent cation (such as Na^{+}, K^{+}) interactions (Savelyev and MacKerell Jr 2015; Howard, Lynch, and Pettitt 2010; Gebala et al. 2016; Gebala et al. 2015). Among the few that included multivalent cations, Hayes *et al* (Hayes et al. 2014) employed a hybrid structure based MD model to explicitly count the number of excess Mg^{2+} ions bound to RNA sequences in the presence of background potassium chloride with a Manning condensation estimated by a Non-linear Poisson Boltzmann equation. Li *et al* (Li, Nordenskiöld, and Mu 2011) used implicit Mg^{2+} binding to dsDNA sequences with classical MD simulation to study the effect of counterion condensation on DNA structure and conformational dynamics. While atomistic MD simulations give a full distribution of the ion atmosphere around the nucleic acids, they suffer from drawbacks due to the enormous computational cost and the choice of force fields that might lead to over or underestimation of the same ion cloud (Savelyev and MacKerell Jr 2015; Jacobson and Saleh 2016). These studies also rely heavily on parameterization to match experimental studies, which imposes unrestrained bias

toward their agreement with experimental results (Jacobson and Saleh 2016). On the other hand, almost all theoretical studies consider nucleic acid chains in bulk conditions; therefore, characteristics of nucleic acid strands end-tethered to a surface remain elusive.

Along this line, this study addresses metal ion binding to surface-anchored nucleic acid oligomers with a Self Consistent Field Theory (SCFT) approach to construct a comprehensive and statistically robust model for quantifying the number of Mg^{2+} ions bound to each chain, while capturing the ion-binding effect on their structure and properties. The molecular model analyzes Mg^{2+} binding to nucleic acid oligomers containing adenine (A) and guanine (G) nucleobases, while trying to capture, as much as possible, the details of experimental studies for a similar system. Metal ion binding to the monomers is explicitly included with equilibrium binding reactions by using experimentally derived (Holland et al. 2011) binding free energies for relevant binding modes (Holland, Jordan, and Geiger 2011). The molecular model characterizes the spatial variation of the structure and properties of the oligonucleotide chains along the distance from the grafting surface, at varying ionic strength and grafting densities, and quantifies the number of bound ions at thermodynamic equilibrium with the oligonucleotides. The model explicitly accounts for the thermodynamic, structural and electrostatic properties of all the species involved in the system, while remaining free of adjustable parameters. This field theoric model helps to set up the foundation for future studies involving secondary and tertiary structures of aptamers interacting with multivalent metal ions.

3.2 Theoretical Methodology

The theoretical model in this work is developed to represent surface-grafted ssDNA oligomers as a co-polymer with two monomer units- adenine (A) and guanine (G), in a coarse-grained level. We explicitly considered the physical and chemical properties

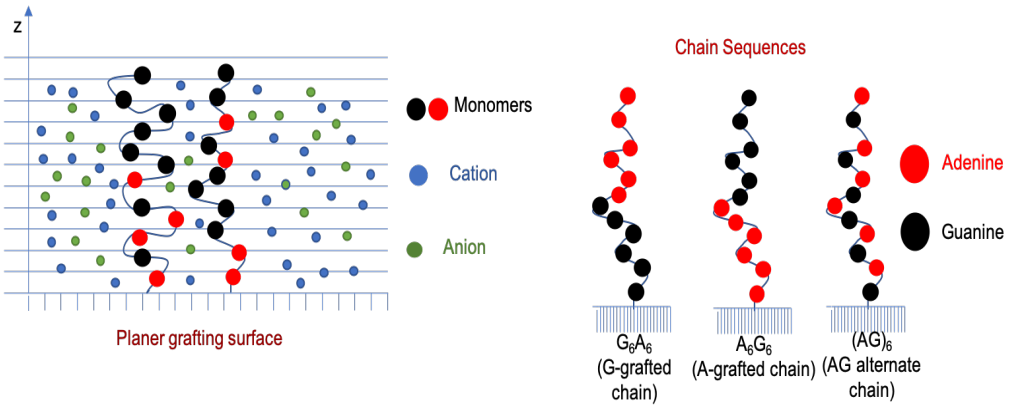

Figure 3.1 Schematic representation of an end-grafted polymer in a salt solution environment (left) and chain sequences used for molecular modeling (right).

of these nucleobases in a solution environment to capture their behavior as accurately as possible. We studied three chain sequences: diblock co-polymer of A and G with A-end grafted to the surface (A_6G_6, a block of six adenine monomers followed by a block of six guanine monomers), diblock of A and G with G-end grafted to the surface (G_6A_6, a block of six guanine monomers followed by a block of six adenine monomers) and alternating sequence of A and G ($(AG)_6$, one adenine monomer followed by a guanine monomer in an alternating manner) (Figure-1). Each of these chains contain 12 monomers at varying grafting densities and $MgCl_2$ concentrations, while keeping the solution temperature and background NaCl concentration fixed at 298 K and 10 mM, respectively. NaCl is added to the system to comply with the relevant experimental study (Holland, Jordan, and Geiger 2011).

The theoretical model is constructed using a **Self Consistent Field Theory (SCFT)** approach for a single polyelectrolyte chain in a field of interacting species (M. J. Uline, Rabin, and Igal Szleifer 2011; Szleifer and Carignano 1996; M. J. Uline, Meng, and Igal Szleifer 2010; Munnik et al. 2018; Jahan and M. Uline 2018). The polyelectrolyte chains are end-tethered to a surface and submerged in a salt and water bath, containing both $NaCl$ and $MgCl_2$ salts. The motivation behind our

study is to find out the extent of Mg^{2+} ion binding to the polyelectrolytes and how it changes the structure and properties of the polyelectrolyte chains. In this molecular model, N_p polyelectrolyte chains are end-grafted to a surface with cross sectional area A. We assumed the system to be homogeneous in x and y directions, but heterogeneous in z direction. Within the field theory framework, the lateral heterogeneity is accounted for by discretizing the system space into a number of layers. The concentrations of the salts are converted to a density field to determine their contribution to the field. Cation binding to the polyelectrolytes are considered within the scope of reaction equilibrium calculations, rather than condensation near the charged monomers (Rikkert J Nap, S. H. Park, and Igal Szleifer 2018), with binding reactions relevant to the experimental study of a similar system (Holland, Jordan, and Geiger 2011). We start constructing the model by calculating the total Helmholtz free energy of the system, which is given by,

$$F = -TS_{conf} - TS_{mix} + F_{chem} + F_{elect} + E_{rep} \tag{3.1}$$

Here, S_{conf} is the conformational entropy of the grafted polymer chains, S_{mix} is the mixing or translational entropy of all the free species: water (w), protons (H^+) and hydroxyl ions (OH^-), cations (Na^+, Mg^{2+}) and anions (Cl^-,OH^-). F_{chem} is the free energy associated with the equilibrium reactions that the monomers undergo in this system. We have explicitly considered three equilibrium reactions for each monomer- (1) protonation and deprotonation via acid-base equilibrium reaction, (2) Mg^{2+} binding and (3) Na^+ binding.

$$A^- + H^+ \Longleftrightarrow AH \tag{3.2}$$

$$G^- + H^+ \Longleftrightarrow GH \tag{3.3}$$

$$A^- + Mg^{2+} \Longleftrightarrow AMg^+ \tag{3.4}$$

$$G^- + Mg^{2+} \Longleftrightarrow GMg^+ \tag{3.5}$$

$$A^- + Na^+ \Longleftrightarrow ANa \tag{3.6}$$

$$G^- + Na^+ \Longleftrightarrow GNa \tag{3.7}$$

F_{elect} is the total electrostatic energy due to the charged species and E_{rep} is the repulsive interactions between all the species due to steric hindrance. T is the temperature of the system which is held constant at 298 K. Expansion of all the energy and entropy terms gives the total Helmholtz free energy of the system,

$$\begin{aligned}
\frac{\beta F}{A} &= \sigma_p \sum_\alpha P(\alpha) \ln P(\alpha) + \int \rho_w(z)(\ln \rho_w(z) v_w - 1) dz \\
&+ \int \rho_{H^+}(z)(\ln \rho_{H^+}(z) v_w - 1 + \beta\mu^0_{H^+}) dz \\
&+ \int \rho_{OH^-}(z)(\ln \rho_{OH^-}(z) v_w - 1 + \beta\mu^0_{OH^-}) dz \\
&+ \int \rho_{Na^+}(z)(\ln \rho_{Na^+}(z) v_w - 1 + \beta\mu_{Na^+}) dz \\
&+ \int \rho_{Mg^{2+}}(z)(\ln \rho_{Mg^{2+}}(z) v_w - 1 + \beta\mu_{Mg^{2+}}) dz \\
&+ \int \rho_{Cl^-}(z)(\ln \rho_{Cl^-}(z) v_w - 1 + \beta\mu_{Cl^-}) dz \\
&+ \beta \int [\langle \rho_q(z) \rangle \psi(z) - \frac{1}{2}\epsilon_w (\frac{d\psi(z)}{dz})^2] dz \\
&+ \int \langle \rho_A(z) \rangle [f_{A^-}(z) \ln f_{A^-}(z) + f_{AH}(z) \ln f_{AH}(z) \\
&+ f_{ANa}(z) \ln f_{ANa}(z) + f_{AMg^+}(z) \ln f_{AMg^+}(z) \\
&+ f_{A^-}(z)\beta\mu^0_{A^-} + f_{AH}(z)\beta\mu^0_{AH} + f_{ANa}(z)\beta\mu^0_{ANa} + f_{AMg^+}(z)\beta\mu^0_{AMg^+}] \\
&+ \int \langle \rho_G(z) \rangle [f_{G^-}(z) \ln f_{G^-}(z) + f_{GH}(z) \ln f_{GH}(z) + f_{GNa}(z) \ln f_{GNa}(z) \\
&+ f_{GMg^+}(z) \ln f_{GMg^+}(z) + f_{G^-}(z)\beta\mu^0_{G^-} + f_{GH}(z)\beta\mu^0_{GH} \\
&+ f_{GNa}(z)\beta\mu^0_{GNa} + f_{GMg^+}(z)\beta\mu^0_{GMg^+}]
\end{aligned} \tag{3.8}$$

The first term in equation (3.8) stands for the structural or conformational energy (TS_{conf}) of the polyelectrolyte chains with $P(\alpha)$ being the probability of the polymer to be in a conformational state α and $\sigma_p = \frac{N_p}{A}$ is the grafting density on the surface.

The second through seventh term represents the total mixing energy TS_{mix} of all the species. $\rho_i(z)$ is the position dependent density of species i. ${\mu^0}_i$ and v_i are the standard chemical potential and the volume of species i, respectively.

The second term is the translational energy of the undissociated water molecules. Third and fourth term stands for the translational entropy of H^+ and OH^- ions respectively, from dissociation of water. The fifth, sixth and seventh terms come from the translational entropy of the anions and cations (Mg^{2+}, Na^+ and Cl^-) produced by the dissociation of salts ($MgCl_2$ and $NaCl$). We assumed that the salts in this system are completely dissociated. The eighth term represents the contribution of electrostatic energy F_{elect}. $\psi(z)$ is the electrostatic potential and ϵ_w is the dielectric constant of water. $\langle\rho_q(z)\rangle$ is the ensemble average charge density of the system, given by,

$$\begin{aligned}\langle\rho_q(z)\rangle = &\sum_{i=Na^+,Mg^{2+},Cl^-,H^+,OH^-} ez_i\rho_i(z) - e\langle\rho_A(z)\rangle(f_{A^-}(z) - f_{AMg^+}(z)) \\ &- e\langle\rho_G(z)\rangle(f_{G^-}(z) - f_{GMg^+}(z))\end{aligned} \tag{3.9}$$

Here, $f_i(z)$ is the fraction of a monomer in different states, such as deprotonated or charged (A^-, G^-), protonated (AH, GH) or cation-bound (AMg^+, GMg^+) etc., along the distance from the grafting surface.

The ninth and tenth terms are derived from the reaction equilibrium of equations (2), (3) and (4), (5), respectively. The reaction equilibrium energies include the entropy of mixing between charged and uncharged groups as well as the standard chemical potentials of these groups. Any volume change of the polyelectrolyte segments due to protonation and ion-binding is neglected. The system is in contact with a bath of anions, cations, protons and hydroxyl ions and therefore, best described by semi-grand canonical ensemble. The proper thermodynamic potential (W) is given

by,

$$W = F - \sum_{\gamma=w,Na^+,Mg^{2+},Cl^-,H^+,OH^-} \mu_\gamma N_\gamma \tag{3.10}$$

Here, N_γ is the total number of molecules of species γ and μ_γ is the exchange chemical potential of those species.

3.2.1 Extremization of the free energy

The free energy equation is extremized subjected to two constraints. One is the incompressibility constraint originating from the repulsive interactions between different species,

$$\langle\phi_p(z)\rangle + \phi_w(z) + \phi_{Na^+}(z) + \phi_{Mg^{2+}}(z) + \phi_{H^+}(z) + \phi_{OH^-}(z) + \phi_{Cl^-}(z) = 1 \tag{3.11}$$

Here, $\langle\phi_p(z)\rangle$ is the ensemble average polymer volume fraction which is given by,

$$\begin{aligned}\langle\phi_p(z)\rangle = {} & \langle\rho_A(z)\rangle(f_{A^-}(z)v_{A^-} + f_{AH}(z)v_{AH} + f_{ANa}(z)v_{ANa} + f_{AMg^+}(z)v_{AMg^+}) \\ & + \langle\rho_G(z)\rangle(f_{G^-}(z)v_{G^-} + f_{GH}(z)v_{GH} + f_{GNa}(z)v_{GNa} + f_{GMg^+}(z)v_{GMg^+})\end{aligned} \tag{3.12}$$

$\langle\rho_i(z)\rangle$ is the average number density of monomer i at position z, expressed as,

$$\langle\rho_{i=A,G}(z)\rangle = \sigma_p \sum_\alpha P(\alpha) n_{i=A,G}(\alpha; z) v_{i=A,G} \tag{3.13}$$

$\phi_i(z)$ is the volume fraction of free species i in the system as a function of the distance from the grafting surface and defined as $\phi_i(z) = \rho_i v_i$.

The second constraint arises from the fact that the total number of each monomers are fixed. Hence, the fractions of a monomer at different derivative species should sum up to unity,

$$f_{A^-}(z) + f_{AH}(z) + f_{ANa}(z) + f_{AMg^+}(z) = 1 \tag{3.14}$$

$$f_{G^-}(z) + f_{GH}(z) + f_{GNa}(z) + f_{GMg^+}(z) = 1 \tag{3.15}$$

Under these two constraints, the total thermodynamic potential per unit area is given by,

$$\begin{aligned}
\frac{\beta W}{A} = \frac{\beta F}{A} &- \sum_{k=w,Cl^-,OH^-} \beta\mu_k \int \rho_k(z)dz \\
&- \beta\mu_{H^+} \int [\rho_{H^+}(z) + f_{AH}(z)\langle\rho_A(z)\rangle \\
&+ f_{GH}(z)\langle\rho_G(z)\rangle]dz \\
&- \beta\mu_{Na^+} \int [\rho_{Na^+}(z) + f_{ANa}(z)\langle\rho_A(z)\rangle + f_{GNa}(z)\langle\rho_G(z)\rangle]dz \\
&- \beta\mu_{Mg^{2+}} \int [\rho_{Mg^{2+}}(z) + f_{AMg^+}(z)\langle\rho_A(z)\rangle + f_{GMg^+}(z)\langle\rho_G(z)\rangle]dz \\
&+ \beta \int \lambda_1(z)\langle\rho_A(z)\rangle(f_{A^-}(z) + f_{AH}(z) + f_{ANa}(z) + f_{AMg^+}(z) - 1)dz \\
&+ \beta \int \lambda_2(z)\langle\rho_G(z)\rangle(f_{G^-}(z) + f_{GH}(z) + f_{GNa}(z) + f_{GMg^+}(z) - 1)dz \\
&+ \beta \int \pi(z)(\langle\phi_p(z)\rangle + \phi_w(z) + \phi_{Na^+}(z) + \phi_{Mg^{2+}}(z) + \phi_{H^+}(z) \\
&+ \phi_{OH^-}(z) + \phi_{Cl^-}(z) - 1)dz
\end{aligned} \tag{3.16}$$

Here, $\pi(z)$, $\lambda_1(z)$ and $\lambda_2(z)$ are Lagrange multipliers to incorporate the constraints into the free energy equation.

Extremization of the thermodynamic potential equation (3.16) with respect to the relevant variables gives the equations for spatial variation of $\rho_i(z)$, $f_i(z)$, $\psi(z)$ and $P(\alpha)$.

From functional extremization, the density profiles of the free species are given by the following equations,

$$\rho_w(z)v_w = \exp[-\beta\pi(z)v_w] \tag{3.17}$$

$$\rho_{H^+}(z)v_w = \exp[\beta\mu_{H^+} - \beta\mu^0_{H^+} - \beta\pi(z)v_{H^+} - \beta\psi(z)e] \tag{3.18}$$

$$\rho_{OH^-}(z)v_w = \exp[\beta\mu_{OH^-} - \beta\mu^0_{OH^-} - \beta\pi(z)v_{OH^-} + \beta\psi(z)e] \tag{3.19}$$

$$\rho_{Na^+}(z)v_w = \exp[\beta\mu_{Na^+} - \beta\mu^0_{Na^+} - \beta\pi(z)v_{Na^+} - \beta\psi(z)e] \tag{3.20}$$

$$\rho_{Mg^{2+}}(z)v_w = \exp[\beta\mu_{Mg^{2+}} - \beta\mu^0_{Mg^{2+}} - \beta\pi(z)v_{Mg^{2+}} - 2\beta\psi(z)e] \tag{3.21}$$

$$\rho_{Cl^-}(z)v_w = \exp[\beta\mu_{Cl^-} - \beta\mu^0_{Cl^-} - \beta\pi(z)v_{Cl^-} + \beta\psi(z)e] \tag{3.22}$$

Functional extremization with respect to the monomer fractions $f_i(z)$ yields the governing equations for chemical equilibrium reactions for both monomers A and G,

$$\frac{f_{A^-}(z)}{f_{AH}(z)} = K^0_{AH}\frac{\exp\left(-\beta\pi(z)\Delta v_{AH}\right)}{\rho_{H^+}(z)v_w} \tag{3.23}$$

$$\frac{f_{A^-}(z)}{f_{ANa}(z)} = K^0_{ANa}\frac{\exp\left(-\beta\pi(z)\Delta v_{ANa}\right)}{\rho_{Na^+}(z)v_w} \tag{3.24}$$

$$\frac{f_{A^-}(z)}{f_{AMg^+}(z)} = K^0_{AMg^+}\frac{\exp\left(-\beta\pi(z)\Delta v_{AMg^+}\right)}{\rho_{Mg^{2+}}(z)v_w} \tag{3.25}$$

$$\frac{f_{G^-}(z)}{f_{GH}(z)} = K^0_{GH}\frac{\exp\left(-\beta\pi(z)\Delta v_{GH}\right)}{\rho_{H^+}(z)v_w} \tag{3.26}$$

$$\frac{f_{G^-}(z)}{f_{GNa}(z)} = K^0_{GNa}\frac{\exp\left(-\beta\pi(z)\Delta v_{GNa}\right)}{\rho_{Na^+}(z)v_w} \tag{3.27}$$

$$\frac{f_{G^-}(z)}{f_{GMg^+}(z)} = K^0_{GMg^+}\frac{\exp\left(-\beta\pi(z)\Delta v_{GMg^+}\right)}{\rho_{Mg^{2+}}(z)v_w} \tag{3.28}$$

The quantity $K^0_i = \exp\left(-\beta\Delta G^0_i\right)$ corresponds to the chemical equilibrium constant that is derived from the standard chemical free energy ΔG^0_i of the respective formation reactions for AH, GH, ANa, GNa, AMg^+ or GMg^+. Δv_i denotes the volume change due to the reactions. The change in the standard free energy for the reaction $A^- + Mg^{2+} \Longleftrightarrow AMg^+$ is given by $\Delta G^0_{AMg^+} = \mu^0_{AMg^+} - \mu^0_{A^-} - \mu^0_{Mg^{2+}}$ and the volume change of reaction is $\Delta v_{AMg^+} = v_{AMg^+} - v_{A^-} - v_{Mg^{2+}}$. The reaction constants and change in volumes for other reactions can be derived in a similar manner.

Extremization of the free energy with respect to the electrostatic potential yields Poisson equation,

$$\epsilon_w\frac{d^2\psi(z)}{dz^2} = -\langle\rho_q(z)\rangle \tag{3.29}$$

$$\epsilon_w\frac{d\psi(z)}{dz}|_{z=0} = 0, \lim_{r\to\infty}\psi(z) = 0 \tag{3.30}$$

The probability distribution function (pdf) is derived from the functional minimization with $P(\alpha)$,

$$P(\alpha) = \frac{1}{e}\exp[-\int n_A(\alpha;z)v_A(\ln f_{A^-}(z) + \beta\mu^0_{A^-} + \beta\pi(z)v_{A^-} - \beta e\psi(z))dz \\ - \int n_G(\alpha;z)v_G(\ln f_{G^-}(z) + \beta\mu^0_{G^-} + \beta\pi(z)v_{G^-} - \beta e\psi(z))] \tag{3.31}$$

Equations (3.17) through (3.31) are solved simultaneously following the procedure described in previous publications using this general approach (M. J. Uline, Rabin, and Igal Szleifer 2011; Szleifer and Carignano 1996; Rikkert J Nap, S. H. Park, and Igal Szleifer 2018). These integro-differential equations are solved numerically by discretizing the space for a discretization length of 0.3 nm for 100 discrete layers. Solution of these sets of non-linear coupled equations yields the unknowns of the model, that are the Lagrange multiplier $\pi(z)$ and the electrostatic potential $\psi(z)$. The inputs necessary to solve the system of equations are the bulk concentrations of the salts, bulk pH, grafting density, volumes of different species, a set of polymer conformations and the equilibrium reaction constants. The equilibrium constants for the binding reactions between the monomers (Adenine and Guanine) and the Mg^{2+} cations are obtained from the binding free energies of the second harmonic generation (SHG) and atomic force microscopy (AFM) studies of Holland *et al* (Holland, Jordan, and Geiger 2011) by using the previously mentioned equation for equilibrium constant K_i^0 . The binding free energies are -32.1 KJ/mol and -35.6 KJ/mol for Adenine and Guanine, respectively. The pKa values for G and A are 1.6 and 3.5, respectively (Bloomfield and Crothers 2000). The volume of Mg^{2+}_{aq} is $0.18nm^3$, and the volumes for Na^+_{aq} and Cl^-_{aq} are $0.05nm^3$. We did not include a change in volume upon binding in this analysis. The set of polymer conformations are derived using a Rotational Isomeric State (RIS) model (Paul J Flory and Volkenstein 1969).

3.3 Results and Discussions

To elucidate the effects of Mg^{2+} binding on the structure and properties of a short chain surface-grafted A-G oligomer, we studied three different chains: A-G diblock with A-end grafted to the surface (A_6G_6), A-G diblock with G-end grafted to the surface (G_6A_6), and A-G co-polymer with alternating A and G along the chain ($(AG)_6$) (referring to Figure-3.1). We studied the variation of the $MgCl_2$ concentration and the polymer surface coverage for the same chain types as well as quantifying the number of bound Mg^{2+} ions to each chain in different solution conditions, while keeping the background $NaCl$ concentration and pH constant at 10 mM and 7.0, respectively. We presented the quantitative results for all the chain sequences and the qualitative results for A-grafted chains only, as the results for the other chain systems do not deviate quantitatively from the A-grafted system. Our results provide valuable insight into the molecular details of this polyelectrolyte system in various biologically relevant environments.

3.3.1 Effect of sequence heterogeneity on Mg^{2+} binding

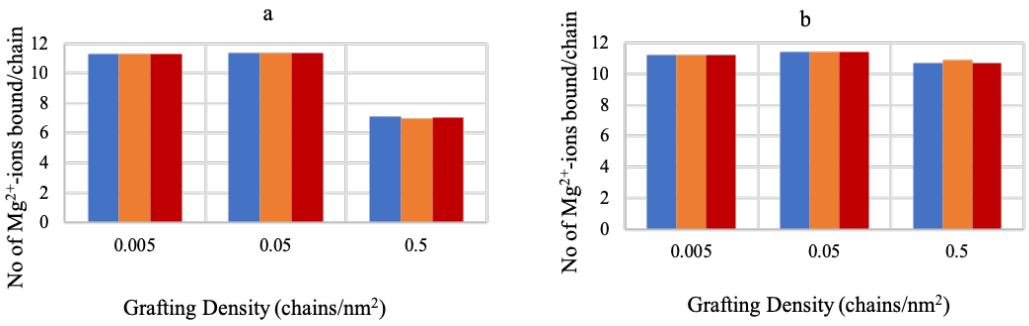

Figure 3.2 No. of bound Mg^{2+} to different sequences at varying grafting densities for (a) 3 mM $MgCl_2$ and (b) 180 mM $MgCl_2$. The color bars correspond to A-grafted chain (blue), G-grafted chain (yellow) and A-G alternate chain (red).

The number of bound Mg^{2+} per chain is calculated from the volume fraction of

the polymer and the fraction of the Mg^{2+}-bound monomers by using the following equation,

$$N_{Mg^{2+}}/chain = \frac{\int \langle \phi_p(z) \rangle f_{PMg^+}(z) dz}{\sigma_p v_p} \tag{3.32}$$

Figure-3.2(a) and 3.2(b) shows the number of bound Mg^{2+} with A_6G_6, G_6A_6 and $(AG)_6$ sequences at different grafting densities for 3 mM and 180 mM $MgCl_2$ content. The data in both plots demonstrates that despite the sequence heterogeneity and variation on the grafting ends, all three sequences bind similar amounts of Mg^{2+} ions at different grafting densities and salt concentrations, except for 0.5 $chains/nm^2$ and 3 mM condition. The relatively low cation binding at this condition can be attributed to the unavailability of enough Mg^{2+} ions in low concentration of salt and high grafting density of polymer chains. These results are in agreement with the experimental findings that Mg^{2+} ions do not aggregate around the strongest binder (Guanine) and are uniformly distributed throughout the length of the chains (Holland et al. 2011). This agrees with the notion that non-specific interactions due to the electrostatics of the sugar-phosphate backbone dominates ion binding to ssDNA chains, as the non-specific part of the free energy for Adenine and Guanine (-21 KJ/mol, from Holland et. al) (Holland, Jordan, and Geiger 2011) is much higher than the specific part of the free energies (-11.1 KJ/mol and -14.6 KJ/mol, respectively, from Holland et. al) (Holland, Jordan, and Geiger 2011) and the specific free energies are all within a few KJ of each other, hence making the ion binding less distinctive.

3.3.2 Effect of ionic strength and grafting density

Figure-3.3 (a), 3.3 (b) and 3.3 (c) are the volume fraction profiles of the A-grafted chains (A_6G_6) along the distance from the grafting surface for low (0.005 $chains/nm^2$), medium (0.05 $chains/nm^2$) and high (0.5 $chains/nm^2$) grafting densities, for a range of $MgCl_2$ concentrations. At low grafting density (figure-3.3 (a)), as we increase the

$MgCl_2$ salt concentration from 3 mM to 180 mM, the chain structures contract towards the grafting surface and we get a distinct peak of the highest volume fractions at a distance close to the surface. This change in the chain structure is due to the reduction in negative charge of the polyelectrolytes by binding to Mg^{2+} ions that lowers the repulsive interaction between the monomers.

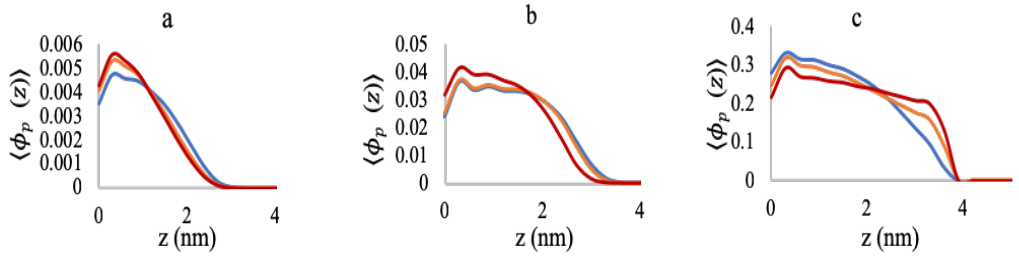

Figure 3.3 Total polymer volume fraction profiles as a function of distance from the grafting surface at (a) 0.005 $chains/nm^2$ (b) 0.05 $chains/nm^2$ (c) 0.5 $chains/nm^2$. Blue lines correspond to 3 mM $MgCl_2$, yellow lines correspond to 50mM $MgCl_2$ and red lines correspond to 180 mM $MgCl_2$.

Although at first glance, the collapse does not seem to be very prominent, it is significant for the length scales of the polyelectrolytes in our system (chain length of only 12 monomers). But for higher grafting density (figure 3.3 (b)), the peak is less distinctive at 3 mM and 50 mM $MgCl_2$ concentrations than 180 mM and nearly plateaus down from 0.8 nm to 2 nm. Herein, the high grafting density creates steric repulsion and the system faces a competition between charge screening and steric repulsion to stabilize the polyelectrolyte structures. At low $MgCl_2$ salt concentrations (3 mM and 50 mM), the system energetically favors chain stretching to accommodate both charge repulsion and steric hindrance. But when we further increase the $MgCl_2$ salt concentration to 180 mM, charge screening by Mg^{2+} ion dominates over steric repulsion and we get a distinct chain collapse near the grafting surface. Figure-3.3(c) corresponds to volume fraction profiles of the polyelectrolyte chains at high grafting density (0.5 $chains/nm^2$) and shows a clearly opposite picture than figure-3.3

(a) and 3.3 (b), with the chains stretching while we increase the salt concentration. In this case, at 3 mM $MgCl_2$, the number of bound Mg^{2+} ions are sufficient for mitigating the charge repulsion inside the brush. Further increase in the salt concentration induces additional steric hindrance due to the volume exclusion and the chains pay in conformational entropy to stretch the chains and accommodate more Mg^{2+} ions inside the brush. This phenomenon of polyelectrolyte chains stretching with increasing counterion concentration is well known as the 're-entrant phenomena' and is experimentally verified by several studies (Yu et al. 2016; Wu et al. 2007).

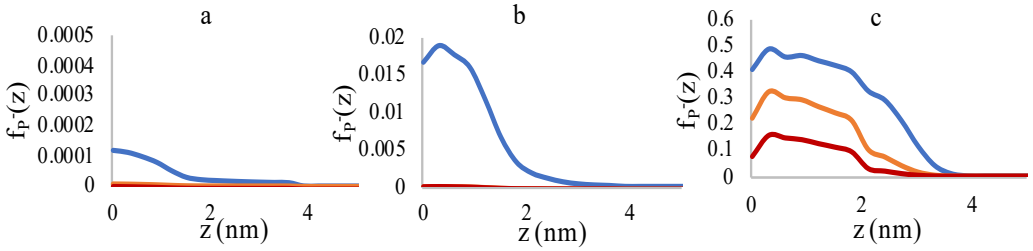

Figure 3.4 Deprotonated polymer fraction profiles at 3 mM (blue lines), 50 mM (yellow lines) and 180 mM (red lines) $MgCl_2$ concentrations. (a) 0.005 $chains/nm^2$ (b) 0.05 $chains/nm^2$ (c) 0.5 $chains/nm^2$.

Figure-3.4 represents the profiles of the deprotonated (negatively charged) polymer fraction ($f_{P^-}(z)$). This quantity is calculated from the individual monomer-species fractions by ,

$$f_{P^-}(z) = \frac{f_{A^-}(z)\langle\phi_A(z)\rangle + f_{G^-}(z)\langle\phi_G(z)\rangle}{\langle\phi_p(z)\rangle} \tag{3.33}$$

In Figure-3.4 (a), at 0.005 $chains/nm^2$ grafting density, almost 100% of the polymers are bound to Mg^{2+} for 50 mM and 180 mM salts and even for 3 mM salt, a very small fraction is deprotonated ($f_{P^-}(z) \sim 0.0001$), with the rest of the polymers being Mg^{2+}-bound. At 0.05 $chains/nm^2$ (Figure - 3.4 (b)), the polymers are still (nearly) entirely bound to Mg^{2+} at 50 mM and 180 mM salt concentrations. But for 3 mM salt, the fraction of negatively charged polymers slightly increases. As we further

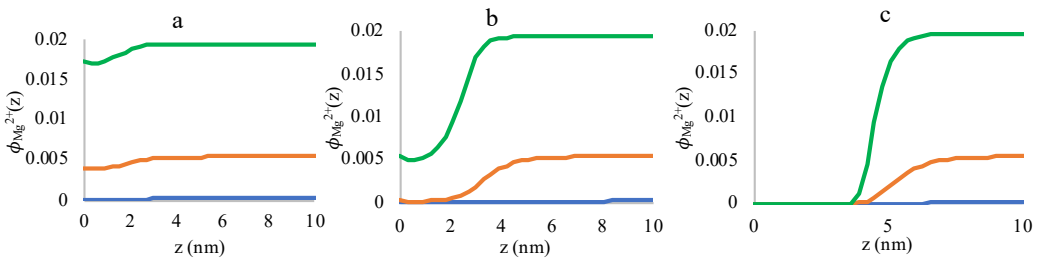

Figure 3.5 Free Mg^{2+} volume fraction profiles as a function of distance from the grafting surface at (a) 0.005 $chains/nm^2$ (b) 0.05 $chains/nm^2$ and (c) 0.5 $chains/nm^2$ grafting densities for 3 mM (blue lines), 50 mM (Yellow lines) and 180 mM (green lines) $MgCl_2$ concentrations.

increase the grafting density up to 0.5 $chains/nm^2$ in figure- 3.4 (c), ionic strength shows a more prominent effect on the chain structure and chemistry. Now at 3 mM $MgCl_2$, about 50% of the polymers are negatively charged. Increase of the ionic strength to 50 mM and 180 mM decreases the negative charge by binding to more Mg^{2+} to reduce the negative charge inside the brush.

The 're-entrant phenomena' shown in figure-3.3(c) can be further explained using figure-3.4(c) and figure-3.5. At 3 mM $MgCl_2$, about half of the polymers are negatively charged and another half is positively charged due to the formation of AMg^+ and GMg^+ complexes with the monomers. Hence, the brush environment is nearly neutralized with low or no residual positive or negative charges and the brush becomes collapsed for that grafting density. Therefore, increasing the salt concentration does not contribute to the global charge neutralization inside the brush; rather, the availability of more Mg^{2+} ions, that have very high affinity towards binding to the negatively charged monomers, creates high steric hindrance. As a result, we see stretching of the chains and the system pays in conformational entropy to reduce steric repulsion inside the brush.

Figure-3.5 represents the volume fractions of free Mg^{2+} ions inside the brush and the surrounding medium. At low grafting density (0.005 $chains/nm^2$, figure-

3.5(a)), there are significant amounts of free Mg^{2+} ions inside the brush at all salt concentrations, which is depicted by the small deviation in the free Mg^{2+} volume fractions from the bulk value. Here,

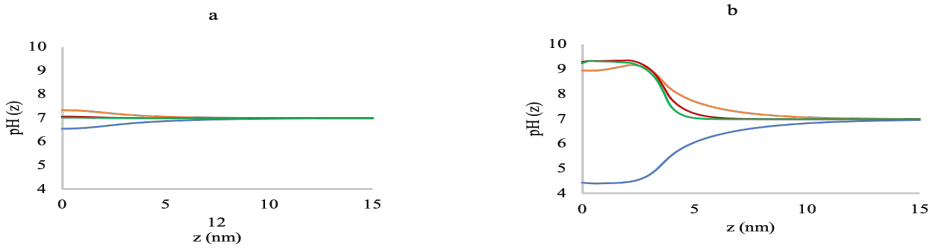

Figure 3.6 pH profiles along the distance from grafting surface at (a) 0.005 $chains/nm^2$ and (b) 0.5 $chains/nm^2$ for 0 mM (blue lines), 3 mM (yellow lines), 50 mM (red lines) and 180 mM (green lines) $MgCl_2$ concentrations.

along with the ion binding, localization of the free Mg^{2+} ions screen the negative charges inside the brush, which results in a collapse of the polyelectrolyte chains (referring to figure-3.3 (a)). But as we increase the grafting density to 0.05 $chains/nm^2$ (figure-3.5 (b)), the amount of free Mg^{2+} ions inside the brush drops noticeably from the bulk value, compared to the low grafting density brush. However, the system still entropically favors localization of free Mg^{2+} ions while staying at a collapsed state (figure-3.3 (b)). Further increase in the grafting density up to 0.5 $chains/nm^2$ gives rise to the above mentioned re-entrant phenomena (figure-3.3 (c)). At this point, the brush region acts like a barrier to the free Mg^{2+} ions and the brush is completely devoid of free Mg^{2+} ions at all the salt concentrations (figure-3.5 (c)). For a grafting density this high, the brush is so dense that the binding to the Mg^{2+} ions increases the volume of the monomers that also increase the steric hindrance, even at low $MgCl_2$ salt concentration. Increasing the $MgCl_2$ salt concentration promotes binding to more Mg^{2+} ions, which is energetically more favorable than bringing the free ions from the bulk and localizing them inside the brush. Hence, the system pays in conformational entropy to stretch the chains to avoid high steric repulsion in the

brush and the re-entrant phenomena arises.

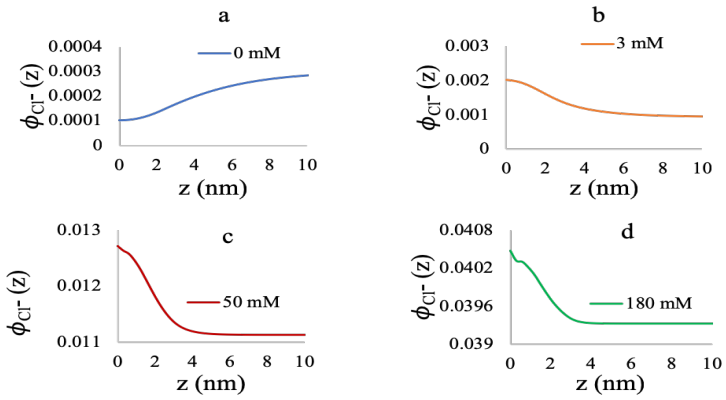

Figure 3.7 Chloride volume fractions at 0.005 $chains/nm^2$ for 0 mM (a), 3 mM (b), 50 mM (c) and 180 mM (d) $MgCl_2$ concentrations.

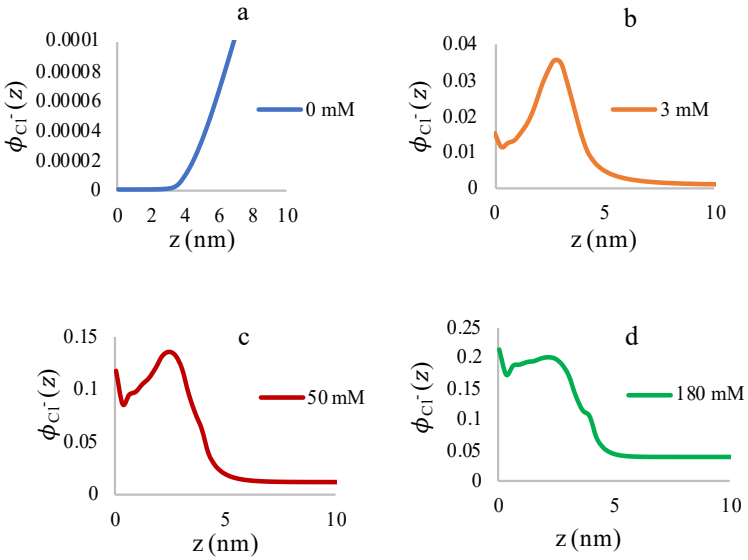

Figure 3.8 Chloride volume fractions at 0.5 $chains/nm^2$ for 0 mM (a), 3 mM (b), 50 mM (c) and 180 mM (d) $MgCl_2$ concentrations.

Figure-3.6 (a) and 3.6 (b) shows the change in local pH inside the brush along the distance from the grafting surface for low (0.005 $chains/nm^2$) and high (0.5 $chains/nm^2$) grafting densities, respectively, for varying ionic strengths. pH profiles, when no $MgCl_2$ was added in the system, are included in the figures to compare the

systems response with added $MgCl_2$ salt. At no added $MgCl_2$ (0 mM), the system only had 10 mM $NaCl$ as a background electrolyte to modulate charge regulation inside the brush. For lower grafting density, the pH inside the brush (Figure-3.6 (a)) only deviates by ~ 0.5 from the bulk. But for higher grafting density, the available Na^+ ions are not enough to reduce the negative charges on the polyelectrolytes and the local pH is much lower with the lowest value of ~ 4.5 (Figure-3.6 (b)).

When we add $MgCl_2$ in the system, even as low as 3 mM, the negatively charged monomers readily bind to Mg^{2+} to form AMg^+ and GMg^+ complexes that are positively charged. Production of the positively charged complexes creates a significant change in pH inside the brush for all grafting densities. For lower grafting density (Figure-3.6 (a)), at 3 mM $MgCl_2$, the pH change is only for one unit. As the $MgCl_2$ concentration is increased, the pH surge subsides and at 180 mM, the system is almost charge neutral. But for high grafting density (Figure-3.6 (b)), addition of only 3 mM $MgCl_2$ creates a pH increase of more than four units (from $pH = 4.5$ to $pH = 9.0$). As the $MgCl_2$ content is increased, unlike the lower grafting density case, the pH further increases up to ~ 9.5. This dramatic change in the local pH with the increase in $MgCl_2$ is consistent with the change in free chloride volume fraction profiles in Figure-3.7 and 3.8.

In figure-3.7, volume fractions of free chloride ions along the distance from the grafting surface are reported at low grafting density of the brush for varying $MgCl_2$ concentrations. When there is no $MgCl_2$ in the system (figure-3.7 (a)), the free chloride ions from the dissociation of $NaCl$ salt are excluded from the system due to the repulsion of highly negatively charged monomers inside the brush and resides in the bulk. But when $MgCl_2$ is added, positively charged monomer-cation complex takes the place of the deprotonated monomers. At this stage, free chloride ions contribute as counterions to minimize the repulsion due to the positively charged species inside the brush. At 50 mM and 180 mM $MgCl_2$ (Figure-3.7 (c) and 3.7

(d), respectively), the free chloride ion concentration inside the brush is significantly higher than the bulk and the local pH is close to neutral. But for $MgCl_2$ salt concentration as low as 3 mM, the available chloride ions are not enough to neutralize the positive charge in the brush and the pH is highest for the specific grafting density.

Figure-3.8 presents the free chloride volume fractions inside the chain as a function of distance from the grafting surface at high grafting density (0.5 $chains/nm^2$). In the absence of $MgCl_2$, almost all the chloride ions are excluded from the system due to the repulsion by highly negatively charged chains, and the counterions (Na^+) are excluded due to high steric hindrance of the crowded brush. As we add $MgCl_2$ salt in the system, formation of positively charged complex now gives rise to electrostatic repulsion inside the brush. It would be thermodynamically favorable for the system to employ negatively charged chloride counterions to mitigate the electrostatic repulsion. But the system is already highly dense with the added Mg^{2+} ions bound to the polymers and further accommodation of any more species creates high steric hindrance. Hence, the system prefers to stay in a positively charged condition inside the brush with a maximum pH of 10.0 and the free chloride ions mostly resides in the outer periphery of the brush with high volume fractions near the bulk (figure-3.8(b), 3.8(c), 3.8(d)).

In summary, the results in this section portray the complex and coupled interplay between the grafting density of the chains and the ionic strength to govern the structure, ion binding and local environment inside the brush. The system generates the thermodynamic equilibrium state by adjusting between conformational entropy, electrostatic potential and repulsive interactions.

3.4 Conclusions

Divalent metal ion binding to surface-grafted nucleic acid oligomers is investigated by studying the effects of the ionic strength and grafting density on the oligomer

structure and chemistry with a field theoric molecular model. The cation binding is explicitly included in the model utilizing experimentally derived binding free energies of the relevant reactions. Quantitative assessment of the ion cloud around the oligomers shows an uniform distribution of ions around different sequences and reinforces the dominance of non-specific electrostatic attraction between the nucleobases and the cations as the driving force for cation-binding (Holland et al. 2011; Bai et al. 2007). Analysis of the system with the variation in ionic strength and polymer grafting density shows a complex coupling between the chain conformation and the ion cloud to maintain the stability of the system by achieving the minimum energy state. At lower grafting density, when the polymers are sparsely grafted, cation binding and ion condensation around the charged oligomers leads to charge neutralization inside the brush which is accompanied by a chain collapse. At high grafting density, however, cation binding results in the reversal of the oligomer charge that can no longer be neutralized by the anions due to anion exclusion from the brush to avoid steric repulsion and hence, we get a highly stretched polymer brush. Our results also show that the ionic strength has a more prominent effect on the structure and properties of the oligomer brushes when they are densely grafted, compared to their sparsely grafted counterpart. It is important to note that this work considers the Mg^{2+} ion explicitly, without taking into account the solvation effect. Mg^{2+} has a strong hydration shell compared to the bulk and binds to nucleotides via a solvent-mediated-ion pairing (Y. Lee, Thirumalai, and Hyeon 2017). However, to accurately capture the thermodynamics of Mg^{2+}-nucleotide interactions, it is necessary to treat Mg^{2+} explicitly (Hayes et al. 2014). This work provides a basis for further theoretical study involving Mg^{2+}-solvation effect on tethered ssDNA-Mg^{2+} binding. Furthermore, this work does not include the possibility of secondary or tertiary structure formation for these particular sequences of nucleic acid oligomers, as no structure formation is evidenced by a relevant experimental study (Holland et al. 2011). However, the pos-

sibility of secondary or tertiary structure formation will be included in our future studies of these polyelectrolyte systems. In its current state, this model can serve as a foundation for field theoric studies of more complex systems to dissect the ion binding scenario around aptamers and single stranded nucleic acids. Although, originally constructed to mimic surface-anchored nucleic acid aptamers for the robust design of aptamer-based biosensors and therapeutics, this molecular model can also be employed to understand the molecular level interactions of other natural or synthetic polyelectrolytes with metal ions in a solution environment for applications ranging from colloid chemistry to drug design for controlled release.

Chapter 4

Modeling of a polyelectrolyte-small molecule drug binding for controlled drug delivery

4.1 Introduction

A leading cause of heart failure is left ventricular (LV) remodeling caused by over-expression of matrix metalloproteinases (MMPs) following a myocardial infarction (MI). MI is commonly known as heart attack and occurs due to the damage of heart muscles when blood flow stops to part of the heart. The most common triggering event is the disruption of an atherosclerotic plaque in an epicardial coronary artery, which leads to a clotting cascade, sometimes resulting in total occlusion of the artery (Thygesen, Alpert, White, et al. 2007; Pfeffer and Braunwald 1990). Atherosclerosis is the gradual buildup of cholesterol and fibrous tissue in plaques in the wall of coronary arteries (Members et al. 2008; Agewall et al. 2016). Plaques can become unstable, rupture, and additionally promote the formation of a blood clot that occludes the artery. When a severe enough plaque rupture occurs in the coronary arteries, it leads to MI. If impaired blood flow to the heart lasts long enough, it triggers a process called the ischemic cascade; the heart cells in the territory of the occluded coronary artery die and do not grow back. A collagen scar forms in their place. Recent studies indicate that another form of cell death, apoptosis, also plays a role in the process of tissue damage following an MI (Kutty, Jones, and Moorjani 2013; Agewall et al. 2016). As a result, the person's heart will be permanently damaged. This myocardial scarring also puts the person at risk for potentially life-threatening abnormal heart

rhythms (arrhythmias), and may result in the formation of a ventricular aneurysm that can rupture with catastrophic consequences.

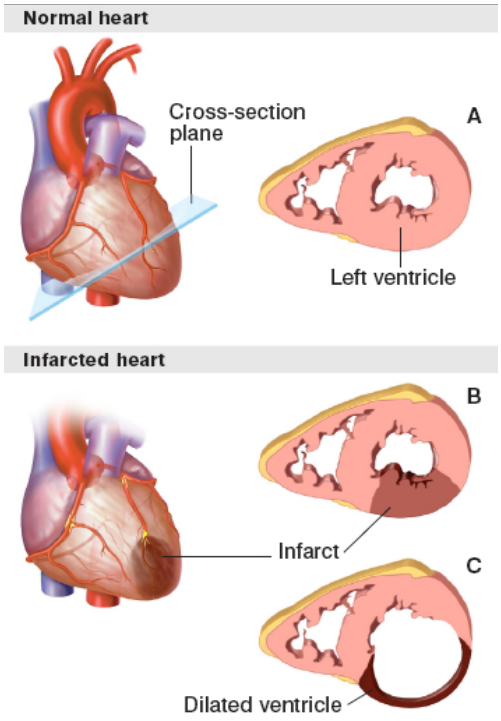

Figure 4.1 Schematic diagram of a human heart in normal condition and after Myocardial Infarction (MI). Figure adopted from *Complications of myocardial infarction Kernel Description* n.d.

Many cytokines and proteolytic enzymes are released following acute MI. Among them, matrix metalloproteinases (MMPs) are an important class of proteolytic enzymes. Matrix metalloproteinases, collectively called matrixins, are proteinases that participate in the degradation of the extracellular matrix (ECM). More than one type of MMP is present in the circulation after cardiomyocyte injury. Tissue inhibitors of metalloproteinases (TIMPs) are specific inhibitors of matrixins that participate in controlling the local activities of MMPs in tissues. The pathological effects of MMPs and TIMPs in cardiovascular disease processes that involve vascular remodeling, atherosclerotic plaque instability, and left ventricular remodeling after myocardial infarction are of considerable interest.

MMPs generally consist of a prodomain, a catalytic domain, a hinge region, and a hemopexin domain (Figure-4.2). They are either secreted from the cell or anchored to the plasma membrane. MMPs can be activated by proteinases in vivo. In vitro activation is triggered by chemical agents, such as thiol modifying agents, oxidized glutathione, SDS, chaotropic agents and reactive oxygens. Low pH and heat treatment can also lead to activation (Visse and Nagase 2003). These agents most likely work through the disturbance of the cysteine-zinc interaction of the cysteine switch. The initial cleavage occurs within the propeptide and that this reaction is intramolecular rather than intermolecular. Proteolytic activation of MMPs is a stepwise process. The initial Proteolytic attack occurs at an exposed loop region between the first and the second helices of the propeptide. Once a part of the propeptide is removed, this probably destabilizes the rest of the propeptide, including the cysteine switch-zinc interaction, which allows the intermolecular processing by partially activated MMP intermediates or other active MMPs (Creemers et al. 2001). Hence, the final step in activation is conducted by an MMP. Activated MMPs can participate in processing other MMPs. The stepwise activation system may have evolved to accommodate finer regulatory mechanisms to control destructive enzymes, in as much as TIMPs may interfere with activation by interacting with the intermediate MMP before it is fully activated.

Following MI, the left ventricle (LV) undergoes a continuum of molecular, cellular, and extracellular responses that manifest clinically as changes in LV size, shape, and function (Zamilpa and Lindsey 2010) . This process in known as cardiovascular remodeling. Cardiovascular remodeling or left ventricular (LV) remodeling is the process by which ventricular size, shape, and function are regulated by mechanical, neurohormonal, and genetic factors. The process of left ventricular (LV) remodeling begins rapidly, usually within the first few hours after an infarct, and continues to progress (Cohn, Ferrari, Sharpe, et al. 2000). The acute loss of myocardium results in

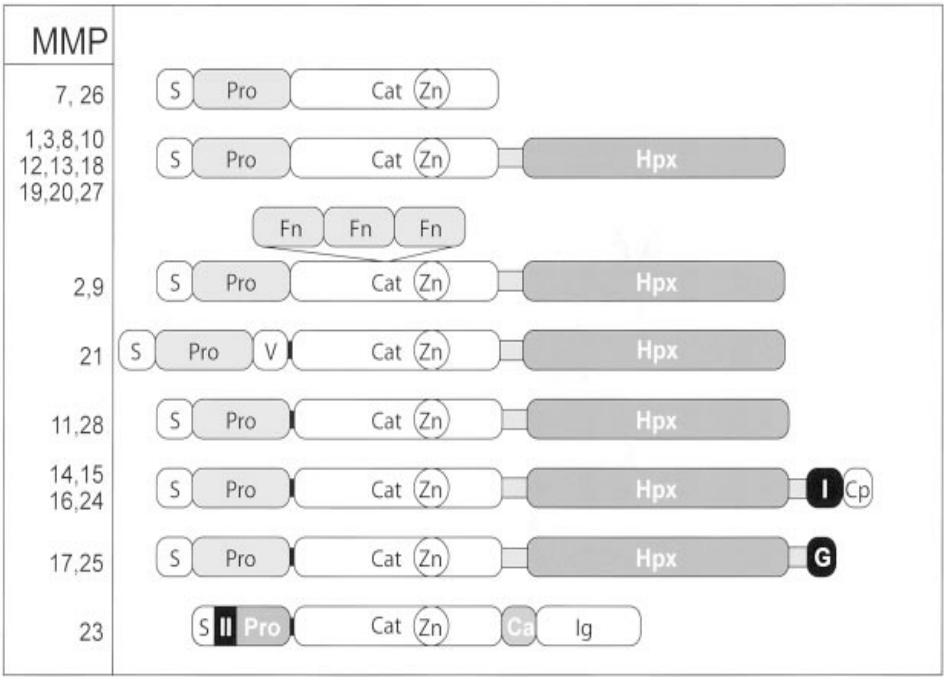

Figure 4.2 Domain structure of MMPs. The domain organization of MMPs is as indicated: S, signal peptide; Pro, propeptide; Cat, catalytic domain; Zn, active-site zinc; Hpx, hemopexin domain; Fn, fibronectin domain; V, vitronectin insert; I, type I transmembrane domain; II, type II transmembrane domain; G, GPI anchor; Cp, cytoplasmic domain; Ca, cysteine array region; and Ig, IgG-like domain. Figure adopted from Visse and Nagase 2003.

an abrupt increase in loading conditions that induces a unique pattern of remodeling involving the infarcted border zone and remote noninfarcted myocardium (Sutton and Sharpe 2000). The term LV remodeling encompasses LV wall thinning, LV dilation, and infarct expansion; inflammation and necrotic myocyte resorption; fibroblast accumulation and scar formation; and endothelial cell activation and neovascularization. LV remodeling is influenced by variations in inflammatory response (neutrophil and macrophage influx), hemodynamic load, molecular changes (neurohormonal activation and cytokine production), and extracellular responses (fibrosis and activation extracellular proteases including matrix metalloproteinases (MMPs) and serine proteases) (Zamilpa and Lindsey 2010). Myocyte necrosis and the resultant increase in load trigger a cascade of biochemical intracellular signaling processes that initiates

and subsequently modulates reparative changes that include dilatation, hypertrophy, and the formation of a discrete collagen scar (Zamilpa and Lindsey 2010; Sutton and Sharpe 2000).

Matrix metalloproteinases (MMPs) comprise a family of zinc-dependent endopeptidases that can cleave all components of the extracellular matrix (ECM) and thereby exert influence on LV remodeling (Jian Liu et al. 2003). MMPs are elevated after MI, and a cause and effect relationship between MMPs and LV remodeling has been demonstrated through the use of MMP inhibitors and MMP-null mice. Lindsey et al showed that there is an upregulation in MMP-9 after MI and MMP-9 gene deletion results in attenuation of LV remodeling (Lindsey et al. 2006). Activation of the secreted MMPs requires cleavage of an approximately 10 kD propeptide in the amino terminus through the cysteine switch mechanism. In the latent enzyme, a cysteine in the propeptide domain interacts with the active site Zn^{2+} and prevents enzyme activity. When the propeptide domain is cleaved, the bond is dissociated and the active site is exposed. Calcium is required for full activity and the MI sites has a high deposition of calcium in it, which activates the MMPs (Lindsey 2004). Figure-4.3 shows the chronological events after MI explaining the role of MMPs in the remodeling process.

LV remodeling is a very dynamic process which involves overexpression of several MMP types at different stages of the disease progression (Lindsey 2004). In normal physiological condition, there is a balance between the number of MMPs and TIMPs which is disrupted after MI resulting in various chronic and acute cardiovascular diseases including LV remodeling (Eckhouse et al. 2014; Purcell et al. 2014; Dixon and Spinale 2011). This dynamic nature of the disease progression makes MMP inhibition and thus the treatment after MI very intricate.

Several different types of MMPs are overexpressed during the LV remodeling process that entails the administration of broad spectrum MMP inhibitors (Fingleton

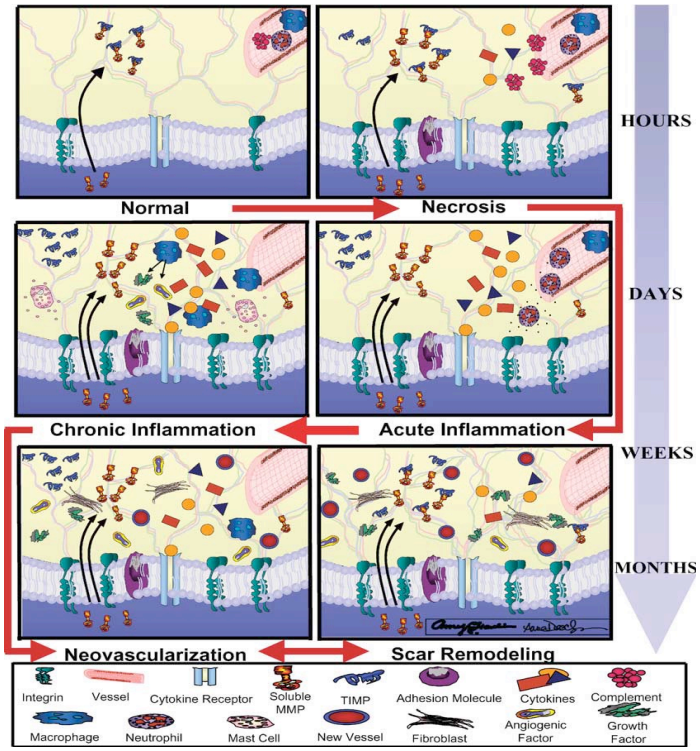

Figure 4.3 The chronological progression of MI, from necrosis to a remodeling scar. MMPs are involved throughout the entire sequence. The normal LV (top left panel) is depicted with a low level of MMPs and an equal number of TIMPs. During necrosis (top right panel), complement activation upregulates adhesion molecule expression to stimulate cytokine and MMP synthesis and release. Coupled with metabolic changes, the net effect is cardiac myocyte loss through necrotic and apoptotic pathways. During the acute and chronic inflammatory reactions (middle panels), neutrophils, macrophages, and mast cells infiltrate to release additional MMPs, cytokines, growth factors, angiogenic factors, and histamine. During neovascularization (bottom left panel), growth and angiogenic factors stimulate endothelial cells to produce and react to MMPs to support new vessel growth. Scar remodeling (bottom right panel) continues through weeks and months, and is coordinated by fibroblast changes in integrin profiles and effects on ECM synthesis and degradation. MMPs continue to factor in these events. Figure adopted from Lindsey 2004.

2008; Rao 2005). A variety of exogenous or synthetic compounds have been found to effectively inhibit several MMP types in animal trial. They include small molecule antibiotic tetracycline molecule doxycycline (DOXY), collagen peptidomimetics and nonpeptidomimetic inhibitors, bisphosphonates, and metal chelators (Kaludercic et

al. 2008; Hidalgo and Eckhardt 2001). Direct inhibition of MMPs by binding to metal ions such as Ca^{2+} and Zn^{2+} is seen at concentrations of DOXY well above expected serum concentrations ($50g/mL$) (Jian Liu et al. 2003). Another broad-spectrum small molecule MMP inhibitor that has been shown to be beneficial in the left ventricular remodeling process and in several animal models of congestive heart failure is PD166793 (PD). (Kaludercic et al. 2008; Jahan et al. 2017), which is of particular interest in our study to design a localized and controlled drug delivery system for MMP inhibition.

PD166793 ($C_{17}H_{18}BrNO_4S$) is a cell-permeable biphenyl-sulfonylvaline compound [(S)-2-(4′-Bromo-diphenyl-4- sulfonylamino-3-methylbutyric acid)] with a molecular weight of 412.3 kDa. They inhibit MMPs by chelating to the active zinc site and preventing the overexpression on the MMPs (figure-4.4). The higher plasma concentration and longer elimination half life of PD166793 compared to other MMP inhibitors makes them a promising candidate to use as a MMP inhibitor drug. PD166793 has shown to completely prevent angiotensin-II-tachypacing-induced diastolic dysfunction in an animal study (Paolocci et al. 2006). Another study showed high bioavailability of PD166793, almost comparable to oral dosage, in infarcted swine heart (Spinale et al. 1999). MMP inhibition by PD166793 also have shown to preserve LV geometry, attenuating LV remodeling and improving LV function during the transition to heart failure (Kaludercic et al. 2008; Peterson 2004; Peterson 2006). PD was not found to exhibit cytotoxicity at therapeutic concentration in ex vivo experiments of infarcted rat heart and thus, did not compromise cardiac cell viability (Romero-Perez et al. 2009).

Inhibition of MMPs is particularly complicated due to the presence of 25 different types of MMPs in human body, that are responsible for a myriad of diseases including but not limited to angiogenesis, metastasis, cardiac and vascular remodeling and periodontal diseases (Kaludercic et al. 2008; Fingleton 2007; Verma and Hansch

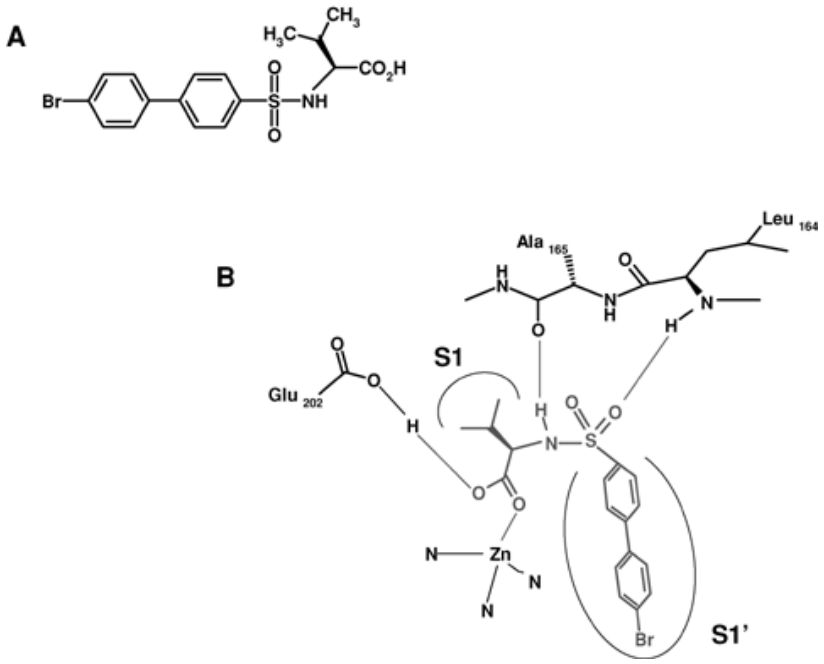

Figure 4.4 Structure of PD166793 (panel A). The tight binding of the inhibitor in the catalytic site of the enzyme is due to carboxylic acid-zinc ligation, the carboxylate hydrogen bonding with Glu202 and hydrogen bonding between the sulfonamide moiety and Leu164 and Ala165. In addition, S1' pocket present in MMP-3 is occupied by 4'-bromo- substituted biphenyl ring system resulting in a more potent inhibition (panel B). Figure adopted from Kaludercic et al. 2008

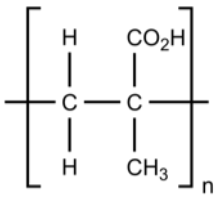

Figure 4.5 Structure of Polymethyl Acrylic Acid (PMAA).

2007). Pharmacological inhibition of MMPs requires administration of broad spectrum inhibitors at therapeutic quantities to inhibit several MMP types. But systemic administration of therapeutic MMP inhibitors is clinically proved problematic due to dose-limiting side effects (Spinale 2007; Dormán et al. 2010). Localized delivery of the inhibitors can provide non-invasive and sustained clinically favorable solution to

this problem (Eckhouse et al. 2014; Purcell et al. 2014). Hydrogel mediated local delivery of rTIMP has shown effective MMP inhibition to MI induced porcine heart for as long as 14 days (Eckhouse et al. 2014; Purcell et al. 2014). But the physiological events that take place during LV remodeling and causes severe changes in LV size, shape and function might take place for a much prolonged time, from days to months (Lindsey 2004). This fact leaves scope for development of a MMP inhibition system that locally delivers exogeneous inhibitor drugs for a prolonged period in a sustainable way.

Controlled or Intelligent drug delivery systems are gaining more traction in recent years due to their ability to achieve spatial and temporal control over the drug release profile, that eradicates many of the side-effects and disadvantages of traditional drug delivery approaches (Gao et al. 2019). These systems are capable of releasing drugs at the desired site of action at an amount required by disease progression. The release profile can also be adjusted to achieve a prolonged drug release based on the physiological response due to the disease progression (Alvarez-Lorenzo and Concheiro 2008).

Stimuli responsive polymers can play a pivotal role in designing controlled drug delivery systems (Gao et al. 2019; Badeau and DeForest 2019; Jahan and M. J. Uline 2018). Stimuli-responsive polymers can be triggered by changes with surrounding biological environments. These dynamic systems can leverage biological signals found locally within the body as well as exogenous cues administered with spatiotemporal control, paving the ways for next-generation diagnostics and personalized medicine (Badeau and DeForest 2019). These materials can change their structures and other physicochemical properties when exposed to any external or internal stimuli, such as, pH, temperature, light, ionic strength, mechanical force (i.e; compression, tension, and shear), biomolecules, and magnetic or electric fields (Stuart et al. 2010; C. Huang et al. 2011; Wiggins, Brantley, and Bielawski 2013; Wei et al. 2017; Nucara et al.

2017; Zheng et al. 2017). In light of these existing research on stimuli-responsive polymers, we can consider using such materials for MMP inhibition to achieve target drug release profile at high concentration without any harmful side effects generally posed by traditional drug delivery systems.

The development and successful implementation of controlled drug delivery system largely depends on suitable carriers that can transmit the drug to the desired site, while ensuring high concentration in a specific area (B. Kumar et al. 2017; Gonzalez Solveyra and Igal Szleifer 2016). Nanotechnology offers a promising paradigm for drug delivery and theranostic applications by combining nanomaterials and biological substances. Nanoparticles functionalized with polymers can be a very good drug carrier for site specific delivery of bioactive agents. Biocompatible nanoparticles with appropriate size and surface characteristics can increase both the concentration and bioavailability of drugs, while minimizing harmful side affects. Nanoparticle mediated delivery of polymer bound chemotherapeutic drugs has significantly improved the anti-tumor efficacy and alleviated their side effects (Chen et al. 2019). Polymer grafted magnetic nanoparticles have been successfully used to increase the antibiotic efficiency of otherwise ineffective Penicillin-G against bacteria (Wang et al. 2015). A similar strategy with polymer grafted nanoparticle can be used to increase the efficacy of MMP inhibitor drug for enhanced cardiovascular repair.

This study aims to design a localized and controlled delivery system for prolonged release of MMP inhibitor drug PD166793 in conjugation of polymer grafted nanoparticles. We have used polymethyl acrylic acid (PMAA) as the polymer which is grafted to spherical silica nanoparticle to bind to the drug (figure-4.6). PMAA is electrolytic in nature, and hence, capable to protonating and deprotonating in aqueous solutions, making them responsive to change in pH. This pH responsiveness can be leveraged to tune in the properties of the drug delivery system to achieve higher efficiency. This theoretical study subjects to aid our experimental collaborators to gain fundamental

understanding of the binding mechanism of the nanoparticle anchored PMAA and drug. The insights gained from modeling can be used to tune in the system parameters to improve drug binding results to ensure high concentration in our desired site of action for localized and sustained drug delivery.

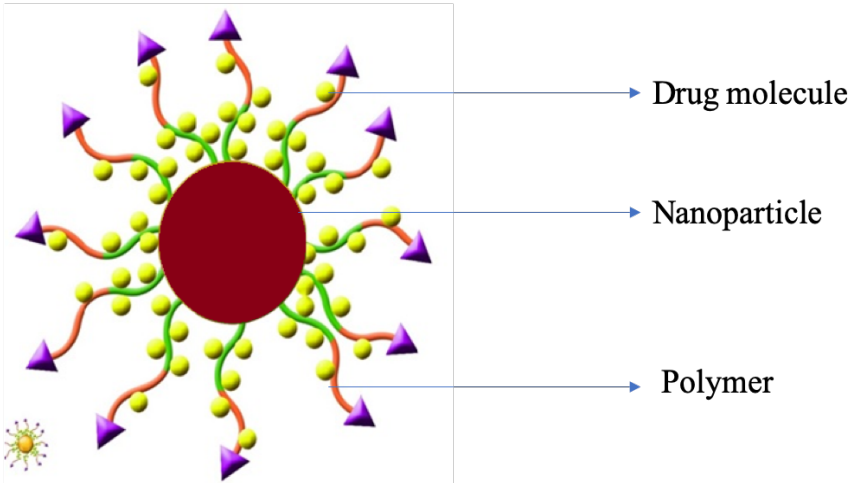

Figure 4.6 Schematic representation of a polymer-drug conjugate, where one end of the polymer chains are grafted to a spherical nanoparticle surface(*Figure not drawn to scale*).

4.2 Theoretical Methodology

Let us assume, a polyelectrolyte chain is end-tethered to a spherical nanoparticle surface (figure-4.6) and submerged in a $NaCl$ salt and water bath. Drug molecules are bound to the polymer brush by a ligand-receptor binding reaction. The system is homogeneous in all directions except along the radius, r that is perpendicular to the sphere surface. The coordinate system is defined as $r = 0$ at the surface of the sphere. At each r, the system is homogeneous in θ and ϕ directions. The polyelectrolyte chain is consisted of n=150 monomers and is treated as a semi-flexible chain by taking chain rigidity into account . The chain is theoretically modeled with a Worm Like Chain Model following the procedure developed by Fredrickson and co-workers (G.

Fredrickson et al. 2006).

The polymer chain is considered as a space curve $r(s)$ in which s is a parameter denoting arch length along the polymer backbone. The bending/internal energy of the chain is given by,

$$\frac{E(r_\alpha; s_1, s_2)}{k_B T} = \frac{l_p}{2} \int_{s_1}^{s_2} (\frac{d^2 r_\alpha(s)}{ds^2})^2 ds \tag{4.1}$$

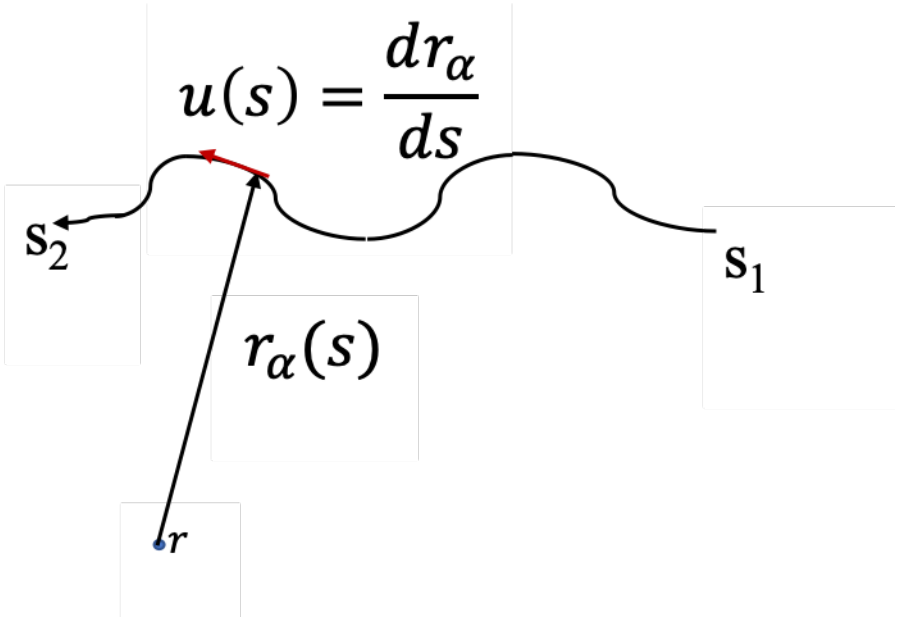

Figure 4.7 Space curve $r_\alpha(s)$ for polymer conformation α. $u(s)$ is the slope of the tangent on the curve.

Here, l_p = bending elasticity of the polymer, α is the conformational state of the space curve r, k_B is the Boltzmann constant and T is the equilibrium temperature of the system.

Volume fraction of the polymer and bound drug is denoted by $\phi_p(r)$ and $\phi_D(r)$ respectively. The system consists of three equilibrium reactions,

$$A^- + H^+ \Longleftrightarrow AH \tag{4.2}$$

$$D^- + H^+ \Longleftrightarrow DH \tag{4.3}$$

$$AH + DH \Longleftrightarrow AH - DH \tag{4.4}$$

Equations (4.2) and (4.3) represents the acid-base equilibrium reaction of polymer and drug respectively and equation (4.4) stands for binding between the polymer and drug molecules. Fractions of protonated deprotonated and drug-bound polyelectrolyte are given by $f_{A^-}(r)$, $f_{AH}(r)$ and $f_{AD}(r) = 1 - f_{A^-}(r) - f_{AH}(r)$ and $f_{DH}(r)$ gives fraction of protonated and deprotonated drugs respectively. Fraction of drug bound is given by $f_{DA}(r) = 1 - f_{D^-}(r) - f_{DH}(r)$.

The total Helmholtz free energy of the system containing polymer, solvent, salt anions and cations is given by,

$$\begin{aligned}
\frac{\beta F}{A(R)} &= \frac{\phi_p}{N v_p} \int P[r_\alpha][\beta E[r_\alpha; 0, 1] + \ln P[r_\alpha]] D r_\alpha \\
&+ \frac{1}{2 v_p^2} \int \int G(r) \chi(|r - r'|) \langle \phi_p(r) \rangle \langle \phi_p(r') \rangle dr dr' \\
&+ \frac{1}{v_p} \int \int G(r) \chi(|r - r'|) \langle \phi_p(r) \rangle \phi_d(r') dr dr' \\
&+ \int \sum_{i=H^+, OH^-} \rho_i(r) G(r) (\ln \rho_i(r) v_w - 1 + \beta \mu_i^0) dr \\
&+ \int \sum_{i=w,+,-} \rho_i(r) G(r) (\ln \rho_i(r) v_w - 1) dr + \int \rho_D(r) G(r) (\ln \rho_D(r) v_w - 1) dr \\
&+ \frac{1}{v_p} \int G(r) \langle \phi_p(r) \rangle [f_{A^-}(r) (\ln f_{A^-}(r) + \beta \mu_{A^-}^0) + f_{AH}(r) (\ln f_{AH}(r) + \beta \mu_{AH}^0) \\
&+ (1 - f_{A^-}(r) - f_{AH}(r)) (\ln(1 - f_{A^-}(r) - f_{AH}(r)) + \beta \mu_{AD}^0)] dr \\
&+ \int G(r) \rho_D(r) [f_{D^-}(r) (\ln f_{D^-}(r) + \beta \mu_{D^-}^0) + f_{DH}(r) (\ln f_{AH}(r) + \beta \mu_{DH}^0) \\
&+ (1 - f_{D^-}(r) - f_{DH}(r)) (\ln(1 - f_{D^-}(r) - f_{DH}(r)) + \beta \mu_{AD}^0)] dr \\
&+ \beta \int G(r) [\langle \rho_q(r) \rangle \psi(r) - \frac{1}{2} \epsilon_w (\frac{d\psi(r)}{dr})^2] dr
\end{aligned} \tag{4.5}$$

The first term in equation (4.5) represents the conformational or structural entropy of the polyelectrolyte. $P[r_\alpha]$ stands for the probability of finding a chain in conformational state α. ϕ_p is the total volume fraction of polymer in the system and v_p is

the volume of the monomers. N is the number of monomer segments in the polymer. Volume fraction of a polyelectrolyte conformation α is given by,

$$\hat{\phi}_\alpha = v_p N \int_0^1 \delta(r - r_\alpha(s))ds \tag{4.6}$$

The ensemble average volume fraction of the polyelectrolyte is given by,

$$\langle \phi_p(r) \rangle = \phi_p \int P[r_\alpha^{'}](\int_0^1 \delta(r - r_\alpha^{'})ds)Dr_\alpha^{'} \tag{4.7}$$

δ represents Dirac delta function to enforce a finite integral $\int \delta(r)dr = 1$.

The second and third terms are the non-electrostatic intermolecular interaction energy between the polyelectrolyte segments and water and the polyelectrolyte segments and drug molecules, respectively, where χ denotes the Flory-Huggins interaction parameter measuring the strength of water-polymer effective repulsions (Ren, Nap, and Szleifer 2008). The fourth term describes the translational entropy of the dissociated H^+ and OH^- ions along with their respective standard chemical potentials. The fifth term represents the translational entropy of water (w), anions (Cl^-) and cations ((Na^+) . The sixth term stands for translational entropy of the drug molecules. The seventh and eighth term describes the chemical equilibrium energy arising from equilibrium reactions given by equations (4.2), (4.3), (4.4). Here, A^- is the charged monomer, H^+ is proton , AH is the protonated monomer, D^- is charged drug molecule, DH is protonated drug molecule and $AH - DH$ is the bound drug-polymer complex . The acid base equilibrium energy includes the entropy of mixing between charged and uncharged groups as well as the standard chemical potential of these groups. Any volume change of the polyelectrolyte segments due to protonation is neglected (M. J. Uline, Rabin, and Igal Szleifer 2011).

The last term represents the contribution of electrostatic energy. $\psi(r)$ denotes the electrostatic potential and ϵ is the dielectric constant which is taken to be that of water(M. J. Uline, Rabin, and Igal Szleifer 2011). $\langle \rho_q(r) \rangle$ is the ensemble average

number density of charges at r which is given by,

$$\langle \rho_q(r) \rangle = \sum_{i=+,-,H^+,OH^-} e z_i \rho_i(r) - e\rho_D(r) f_{D^-}(r) - e\langle \rho_p(r) \rangle f_{A^-}(r) \tag{4.8}$$

z_i corresponds to the valence of the species i, $f_{D^-}(r)$ is the fraction of charged drug molecules and $f_{A^-}(r)$ is the fraction of polymer that is charged.

The excluded volume interaction of molecules are taken into account by assuming that the system is incompressible at every point which is mathematically presented as,

$$\langle \phi_p(r) \rangle + \phi_w(r) + \phi_+(r) + \phi_-(r) + \phi_{H^+}(r) + \phi_{OH^-}(r) + \phi_D(r) = 1 \tag{4.9}$$

This packing constraint is included by using Lagrange multiplier $\pi(r)$. Density of a species i is related to volume fraction $\phi_i(r)$ with $\phi_i(r) = \rho_i v_i$.

The ensemble that we are considering is one with a fixed number of grafted polymers at the surface in equilibrium with a constant chemical potential of a solution and drug molecules. Therefore, the total thermodynamic potential is given by,

$$\begin{aligned} \frac{\beta w}{A(R)} =& \frac{\beta F}{A(R)} + \beta \int G(r)\pi(r)[\langle \phi_p(r) \rangle + \phi_w(r) + \phi_+(r) + \phi_-(r) + \phi_{H^+}(r) \\ &+ \phi_{OH^-}(r) + \phi_D(r) - 1]dr - \beta\mu_+ \int G(r)\rho_+(r)dr \\ &- \beta\mu_- \int G(r)\rho_-(r)dr - \beta\mu_{D^-} \int G(r)\rho_D f_{D^-}(r)dr \end{aligned} \tag{4.10}$$

The equilibrium values of $P(\alpha)$, $\rho_i(r)$, $\rho_D(r)$, $f_{A^-}(r)$ and $f_{D^-}(r)$ are determined by functional extremization of equation (4.10). The Lagrange multiplier enforces the sum of all volume fractions to be equal to unity at every r.

The volume fractions and protonation fractions of different species from functional extremization are given by,

$$\rho_w(r) v_w = \exp[-\beta\pi(r) v_w] \tag{4.11}$$

$$\rho_{H^+}(r) v_w = \exp[\beta\mu^0_{H^+} - \beta\pi(r) v_{H^+} - \beta\psi(r) e] \tag{4.12}$$

$$\rho_{OH^-}(r)v_w = \exp[\beta\mu^0_{OH^-} - \beta\pi(r)v_{OH^-} + \beta\psi(r)e] \tag{4.13}$$

$$\rho_{+}(r)v_w = \exp[\beta\mu_{+} - \beta\pi(r)v_{+} - \beta\psi(r)e] \tag{4.14}$$

$$\rho_{-}(r)v_w = \exp[\beta\mu_{-} - \beta\pi(r)v_{-} + \beta\psi(r)e] \tag{4.15}$$

$$\frac{f_{D^-}(r)}{f_{DH}(r)} = K^0_{DH}\frac{\phi_w(r)\exp(\beta\mu_{D^-})}{\phi_{H^+}(r)} \tag{4.16}$$

$$\frac{f_{A^-}(r)}{f_{AH}(r)} = K^0_{AH}\frac{\phi_w(r)}{\phi_{H^+}(r)} \tag{4.17}$$

Here, K^0_{DH}=$\exp(-\beta\Delta G^0_{DH})$ is the equilibrium constant of the protonation reaction of drug and K^0_{AH}=$\exp(-\beta\Delta G^0_{AH})$ is the equilibrium constant of the protonation reaction of the polyelectrolyte.

Extremization of the free energy with respect to the electrostatic potential, $\psi(r)$, yields Poisson equation and it's boundary conditions,

$$\epsilon_w\frac{d^2\psi(r)}{dr^2} = -\langle\rho_q(r)\rangle \tag{4.18}$$

$$\epsilon_w\frac{d\psi(r)}{dr}|_{r=0} = 0, \lim_{r\to\infty}\psi(r) = 0 \tag{4.19}$$

Minimizing the free energy for the polymer probability distribution yields $P[r_\alpha]$, and lays the foundation to numerically solve this system of equations. To solve this system, we consider a self-consistent external field $w(r)$ that acts on and influences the structure and properties of the polyelectrolyte chain. Here,

$$P[r_\alpha] = \frac{1}{Q[w(r)]}\int\exp[\frac{l_p}{2}\int_0^1(\frac{d^2r_\alpha(s)}{ds^2})^2ds + w(r_\alpha(s))]ds \tag{4.20}$$

External field $w(r)$ is given by,

$$\begin{aligned} w(r) =& \beta\pi(r)v_p + \frac{1}{v_p}\int\langle\phi_p(r^{'}))\rangle\beta\chi(|r-r'|)dr^{'} \\ &+ \frac{1}{v_p}\int\phi_d(r^{'}))\beta\chi(|r-r'|)dr^{'} + v_p\ln[1-f_{A^-}(r)-f_{AH}(r)] \\ &- \frac{\phi_p}{Nv_p}f_{A^-}\psi(r) \end{aligned} \tag{4.21}$$

$Q[w(r)]$ is the single chain partition function given by,

$$Q[w(r)] = \frac{1}{V}\int \exp[[\frac{l_p}{2}\int_0^1 (\frac{d^2 r_\alpha(s)}{ds^2})^2 ds + w(r_\alpha(s))]ds]\delta(r_\alpha(1)-\epsilon)Dr_\alpha \qquad (4.22)$$

ϵ gives the value of $r(s)$ for the grafted end of the chain. Total volume of the polymer chain $V = Nv_p$.

Equation (4.22) is solved to get the value of $\langle\phi_p(r)\rangle$ following the procedures described in previous publications (G. Fredrickson et al. 2006; Matsen 2006; Trombly, Pryamitsyn, and Ganesan 2011; Jiang 2013). Then the solution is used to calculate the volume fraction and protonation fraction of other species in the system and also to solve Poisson equation (equation-4.19).

4.3 Results and Discussions

The theoretical model for the nanoparticle grafted polyelectrolyte-drug conjugate was used to simulate the drug-binding experiments in our experimental collaborators lab to elucidate the physical mechanism of polymer-drug binding and how the solution environments affect the extent of drug binding. PMAA surface coverage is taken as 0.5 $chains/nm^2$, chain length is 150 monomers, pKa of PMAA and drug (PD166793) is 5.0 and 4.0, respectively. We have also calculated the total number of drug molecules bound to the chain by using the following equation,

$$N_{drug} = \frac{\int r^2\langle\phi_p(r)\rangle\rho_D(r)dr}{\int r^2\langle\phi_p(r)\rangle dr} \qquad (4.23)$$

Here, N_{drug} is the total number of drug molecules bound and $\rho_D(r)$ is the position r dependent density of drug molecules.

The first set of simulation is run to mimic the drug binding experiments in PBS buffer solution with neutral pH = 7.4, which also represents physiological pH. Figure-4.8 represents the volume fraction profile of PMAA and figure- 4.9 represents the fraction of polymer bound to the hydrogen ion, also known as fraction of protonation

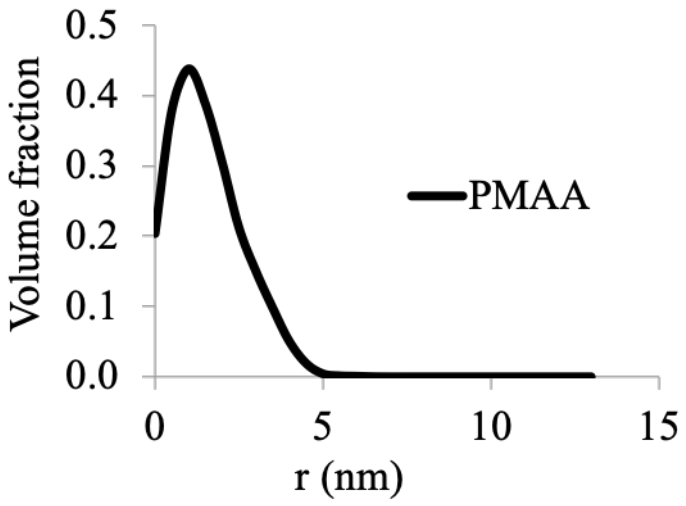

Figure 4.8 Volume fraction of PMAA as a function of distance from the nanoparticle surface at pH = 7.4

(f_H) and fraction of polymer bound to the drug (f_D). PMAA volume fraction is high near the nanoparticle surface which represents a collapsed state. Figure-4.9 shows that protonation of PMAA is very low (about ~ 0.25), which implies that the PMAA chains are highly (about $\sim 70\%$) charged. This high negative charge creates strong electrostatic repulsion inside the PMAA brush and drive the drug molecules outside the polyelectrolyte brush region and decreases drug binding, which is indicated by low drug binding fraction, f_D, which occurs only at the protonated PMAA sites. Using equation (4.23), the total number of drug molecules is only ~ 100, which is a very low amount and does not meet the therapeutic quantity. The combined effect of chain collapse and electrostatic repulsion lowers the amount of drug binding to the polymer chains. This result agrees with the experimental results which also yielded poor drug binding at physiological pH.

Next, we simulate the experimental condition to mimic an acidic pH (=5.5). At this condition, the drug binding is much higher experimentally than the physiological pH case. Figure-4.10 shows the volume fraction profile of PMAA and figure-4.11

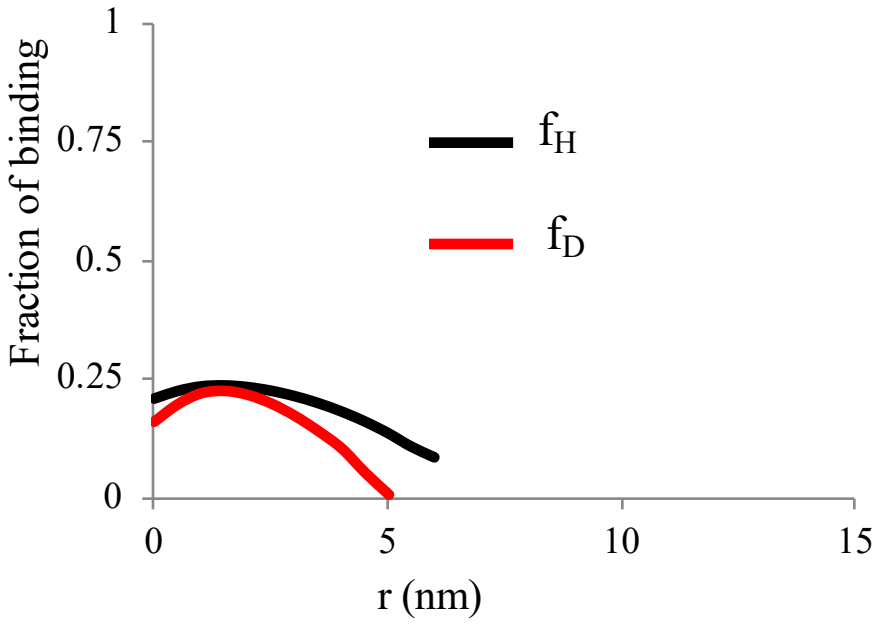

Figure 4.9 Fraction of protonation and fraction of drug binding to PMAA at pH = 7.4

presents the fraction of protonation (f_H) and fraction of polymer bound drug (f_D) profiles, at that pH from the theoretical model. Figure- 4.10 shows that the polymer is relatively stretched and extended to longer distance from the grafting surface than neutral pH case. Figure-4.11 shows that protonation fraction of PMAA is very high (~ 0.9), which implies that the number of charged monomers are very low and hence, the electrostatic repulsion is reduced inside the brush. As a result, fraction of drug binding to the polymer is increased to ~ 0.75, which is much higher than the previous case. High fraction of protonation for the polymer significantly reduces negative charge on them and hence, reduces electrostatic repulsion. This reduction in repulsive interaction increases the extent of drug binding for the nanoparticle grafted polymer-drug conjugate system, which we calculate as ~ 21000 drug molecules, using equation (4.23). This quantity is about 210 times higher than the physiological pH case and

also meets the therapeutic window.

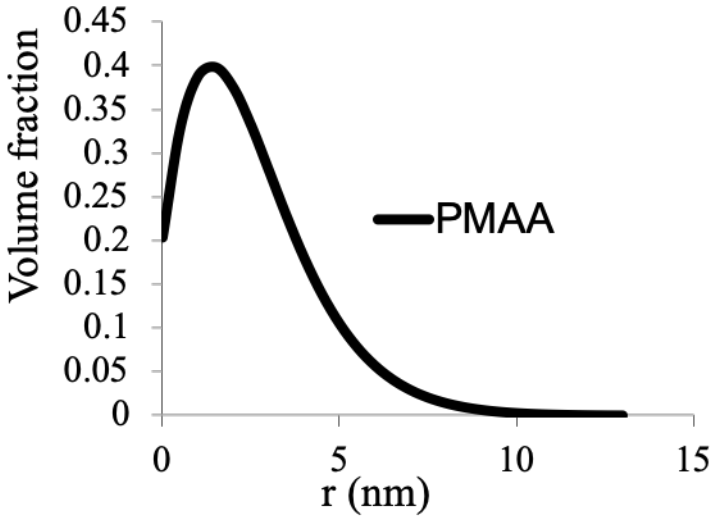

Figure 4.10 Volume fraction of PMAA as a function of distance from the nanoparticle surface at acidic pH = 5.5

Simulation of the PMAA-drug conjugate system at two different conditions (pH = 7.4 and pH = 5.5) manifests the complex interplay of polymer structure, energetic and entropic contributions to stabilize the system. At neutral pH, the solvent where the PMAA-drug conjugate resides in, does not have enough protons (H^+) available to neutralize the charge that is already present in PMAA, that gives rise to the high electrostatic repulsion. However, when the pH is reduced to an acidic level at 5.5, more protons are available in the system that can bind to negatively charged PMAA to increase their fraction of protonation. This change in charged state decrease the electrostatic repulsion and allows more drug to bind to the PMAA chains.

4.4 Conclusions and Future Work

The insights gained from the molecular modeling of the PMAA-drug conjugate in section-4.3 can be used to further improve drug binding to ensure higher concentration

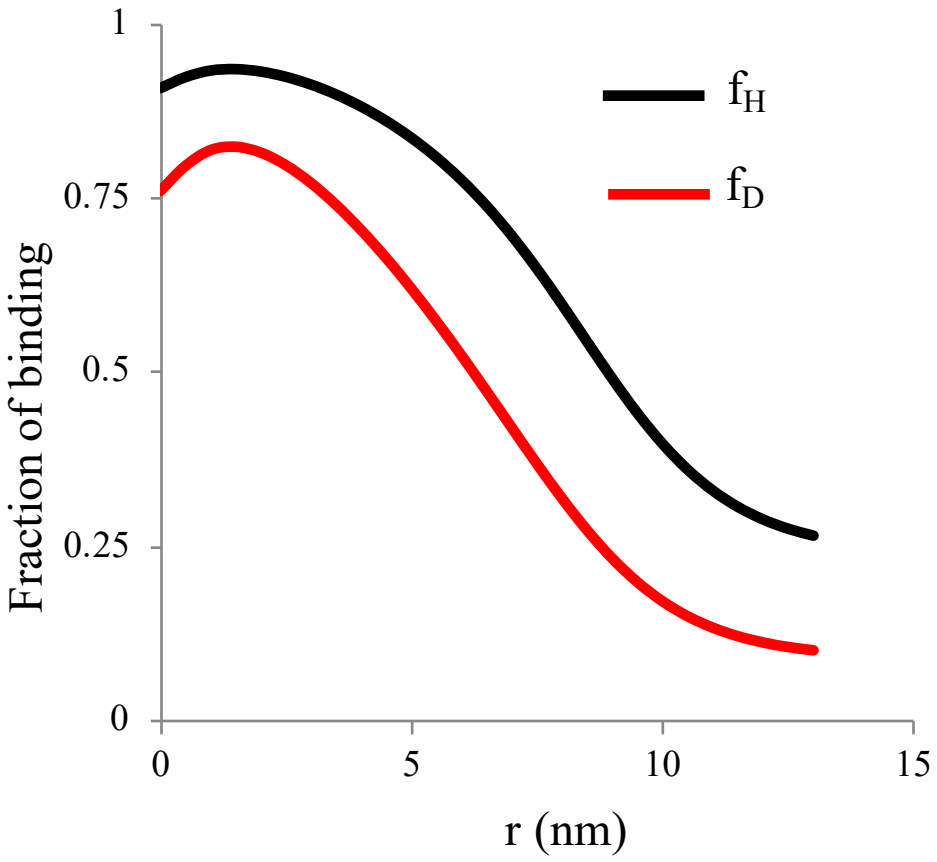

Figure 4.11 Fraction of protonation and fraction of drug binding to PMAA at acidic pH = 5.5

of drug for localized delivery.

From the results at acidic pH (figures-4.10 and 4.11), we can conclude that the mechanisms responsible for high drug binding are extension of PMAA chain and reduction of negative charge on PMAA. The complex interplay between conformational entropy of the polymer chains and repulsive energy between the charged species determine the ability of drug binding for this system. This combined effect leads to the entrapment of more drug molecules inside the polymer brush and results in much higher drug binding than the neutral pH (figures-4.8 and 4.9).

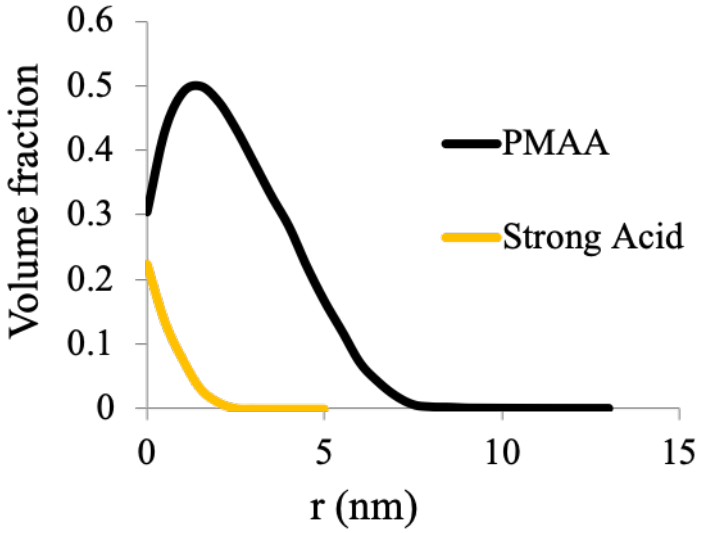

Figure 4.12 Volume fraction of PMAA and strong polyelectrolyte as a function of distance from the nanoparticle surface at neutral pH = 7.4.

From this observations gained by molecular modeling, we can safely hypothesize that if we can modify or manipulate the PMAA-drug conjugate in a way at the physiological condition ($pH = 7.4$) so that the polymer structure remains at extended state and the protonation fraction of the PMAA is low, we might be able to achieve higher drug binding similar to acidic pH condition.

As a proof of concept, we added a strong polyacid in our theory. The strong polyacid is also grafted to the nanoparticle surface along with the PMAA chains. The length of the polyacid is taken as 100 monomers per chain, surface coverage is 0.1 $chain/nm^2$, and $pKa = -1.0$. Figures-4.12 and 4.13 presents the simulation results of the molecular model at $pH = 7.4$ with added strong polyacid. Figure-4.12 shows that in presence of the added strong polyacid, the PMAA chain is relatively extended than previous physiological pH case. Figure-4.13 shows that the fraction of protonation (f_H) in PMAA is much higher than before, which reduces the electrostatic repulsion inside the brush. This results in increasing the fraction of drug binding (fD) to a significant extent. The number of drug molecules bound to the polymer is calculated

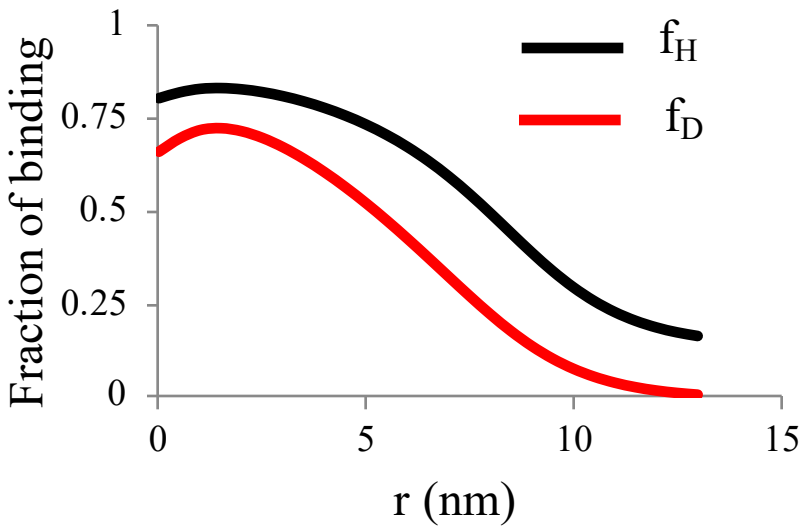

Figure 4.13 Fraction of protonation and fraction of drug binding to PMAA at neutral pH=7.4 with added strong polyelectrolyte.

as $\sim$ 12000, which is much larger than the previous physiological pH simulation. The strong polyacid here acts as a buffer for the pH inside the brush. However, there are a few conditions to be met to for this buffering to occur, such as,

- The cations of the polyacid have to be large enough to have high steric repulsions with the polymer brush.
- The system must charge regulate and neutralize the charge through acid-base equilibria.
- The strong polyacid cannot be too long, or else, the electrostatic repulsions lower the drug concentration in the brush.

This molecular model can be further extended to tune the structural and electrostatic properties of the system to increase the efficiency of the local delivery system. Release of the drug can be achieved by chemically grafting the strong polyacid to the nanoparticle with an enzymatic cleavage chemical group. Localization of the nanoparticles can be enhanced by attaching ligands to end groups of the PMAA.

Chapter 5

Conclusions

In this dissertation, we have reported the development of three SCFT based molecular theories for tethered polyelectrolyte chains in three different biomedical applications. All of these molecular theories take into account all the structural, thermodynamic, electrostatic and chemical properties of all the species involved in the system. The results show the complex interplay that exist between thermodynamic variables and the conformational statistics of the polymers.

The first molecular theory (Chapter 2) in this work is developed to study a polyelectrolytic biomolecule, aptamer, in biological environment. The aim is to understand the underlying physics of aptamer behavior due to the changes in system pH, salt concentration, types of salt and grafting densities and how that governs the change in aptamer conformational statistics and chemical properties.Two different diblock chains, one containing Adenine (A) and Guanine (G) nucleobases and another containing Thymine (T) and Cytosine (C) nucleobases are considered. The results imply that the structure of the aptamer chains varies significantly due to charge regulation effects and the protonation profiles of monomer blocks are highly dependent on the distance from the interface. Neutralization of the negative charge is highly dependent on both the surface coverage of aptamers and the valence of the cations. Mg^{2+} is still present in the aptamer layer for the high surface coverage case. But Na^{+} is nearly excluded from the brush due to high steric repulsion inside the brush for higher amount of charged monomers.The system decides to relieve the electrostatic repulsions by paying in acid-base equilibrium. This model captures the

physical property changes very well for the aptamer chains at varying surface coverages, types of salt and different salt concentrations. This model can aid in generating a theoretical databank for ssDNA aptamers to select a specific aptamer for a specific target molecule very quickly and cost effectively.

The second molecular theory (chapter 3) uses the understanding on aptamer behavior gained from the previous chapter to study aptamers that bind to a divalent metal cation, Mg^{2+}. This theory closely follows the experimental works of Geiger and his group (Holland et al. 2011; Holland, Jordan, and Geiger 2011) as reference system to choose the system parameters.The molecular model characterizes the spatial variation of the structure and properties of the oligonucleotide chains along the distance from the grafting surface, at varying ionic strength and grafting densities, and quantifies the number of bound ions at thermodynamic equilibrium with the oligonucleotides. The model explicitly accounts for the thermodynamic, structural and electrostatic properties of all the species involved in the system, while remaining free of adjustable parameters. Quantitative assessment of the ion cloud around the oligomers shows an uniform distribution of ions around different sequences and reinforces the dominance of non-specific electrostatic attraction between the nucleobases and the cations as the driving force for cation-binding (Holland et al. 2011; Bai et al. 2007). Analysis of the system with the variation in ionic strength and polymer grafting density shows a complex coupling between the chain conformation and the ion cloud to maintain the stability of the system by achieving the minimum energy state. At lower grafting density, when the polymers are sparsely grafted, cation binding and ion condensation around the charged oligomers leads to charge neutralization inside the brush which is accompanied by a chain collapse. At high grafting density, however, cation binding results in the reversal of the oligomer charge that can no longer be neutralized by the anions due to anion exclusion from the brush to avoid steric repulsion and hence, we get a highly stretched polymer brush. Our results also show

that the ionic strength has a more prominent effect on the structure and properties of the oligomer brushes when they are densely grafted, compared to their sparsely grafted counterpart. In its current state, this model can serve as a foundation for field theoric studies of more complex systems to dissect the ion binding scenario around aptamers and single stranded nucleic acids.

The third molecular theory (Chapter 4) is developed with a goal to design a polymer mediated controlled drug delivery system for prolonged release of a MMP inhibitor drug for enhanced cardiovascular repair. The theory accounts for a polyelectrolyte, PMAA, grafted to a spherical nanoparticle surface that works as an intelligent carrier for a small molecule drug, PD166793. The results indicate that PMAA shows poor binding results at physiological pH due to the complex interplay of chain collapse and repulsive energy between PMAA and drug originated from higher availability of charged species. However, lowering the system pH to an acidic level extends the chain and lowers the charge on both the polymer and the drug, which results in a much higher drug binding. This understanding from the molecular theory can be leveraged to tune the system parameters to achieve higher efficiency of such systems and also to step forward towards customized drug delivery.

As opposed to field theoric models, other theoretical methods available to study similar systems are atomistic and coarse grained particle-based simulations (G. H. Fredrickson, Ganesan, and Drolet 2002). In both of these systems, the fundamental degrees of freedom to be sampled are the bond and torsional angles associated with the atoms or particles. The atomistic simulation methods involve tracking the Newtonian motion of each atom and building a classical description of the polymeric system with atomic resolution. The equilibrium and non-equilibrium properties and potential functions of bonded and non-bonded interactions of the system are determined by quantum chemical calculations. These calculations are usually carried out with either Molecular Dynamics (MD) or Monte Carlo (MC) techniques. MD tech-

niques consider motions of all the atoms involved, while MC employ random sampling to reduce the computational cost. Although atomistic simulation has the potential to provide most accurate description of a polymeric system in atomic level, they have a massive drawback. It is very difficult to equilibrate large systems of polymers at realistic densities due to the vast number of atoms to track and the associated stochasticity. That is why, it is extremely difficult so simulate such systems beyond a few nano-seconds at a high computational cost, which makes extraction of meaningful information about structure and thermodynamics almost impossible. This limitation is particularly acute for multiphase, inhomogeneous systems, which are often those of primary interest (G. H. Fredrickson, Ganesan, and Drolet 2002).

A less complicated and reasonable alternative to fully atomistic simulation is coarse-grained simulation (Kremer and Müller-Plathe 2001; G. H. Fredrickson, Ganesan, and Drolet 2002). In this method, atoms are lumped into larger particles and all the monomers in a polymer chain is replaced by a single effective chain. The interactions taken into account in this approach are that of the united particle with each other and the calculations are carried out by employing standard MD and MC techniques. This is computationally less exhaustive due to the reduction in the number of atoms through coarse-graining. However, even with extensive coarse-graining the many-body system and reducing the available degrees of freedom, calculations involving polymeric systems with this method remain to be computationally expensive.

While the atomistic and coarse-grained MD and MC simulation methods track the bond and torsion angles of all the available atoms in a system at high computational cost, our molecular model approximates the available force field with functional integrals over one or more fluctuating chemical potential fields that are confined to a simulation domain. In our model, a molecule or a single chain is considered to be affected by a self-consistent mean field of all the attractive and repulsive interac-

tions with the surrounding environment. Intramolecular interactions in this model are taken exactly and intermolecular interactions are taken within the mean filed approximation. A major difference of this model with MD and MC is the degree of parametrization. MD and MC heavily depends on parametrizing the interactions between bonds, which often severely lack accuracy (Savelyev and MacKerell Jr 2015; Jacobson and Saleh 2016). Inversely, our mean field treatment allows us to account for individual molecular interactions within a single chain and with its surrounding mean-field with a high degree of accuracy for a wide range of polymeric materials. The filed theoric molecular level modeling approach employed in this dissertation have been proved to be a powerful tool in understanding tethered polyelectrolyte systems (M. J. Uline, Rabin, and Igal Szleifer 2011; Szleifer and Carignano 1996; Shvartzman-Cohen et al. 2004; Matsen 2006; Szleifer and Carignano 2000; Rikkert Nap, Gong, and Igal Szleifer 2006). In the current state, the molecular models presented here can provide fundamental information of the physicochemical properties of tethered polyelectrolytes in various biomedical applications and can be leveraged to design new systems with increased functionality and efficacy.

Chapter 6

Future Work

The molecular theories developed in this work can be extended to study new systems of polyelectrolytic materials for advanced drug delivery and other biomedical applications.

6.1 Modeling of a hydrogel mediated drug delivery system

6.1.1 Hydrogel

A hydrogel is a smart material made of hydrophilic polymers and swells in presence of water. Hydrogels have high physical integrity due to the presence of crosslinks within their structure, which makes them insoluble in nature (Nicholas A Peppas, Wood, and J. O. Blanchette 2004). Some hydrogels respond to the change in their surroundings. They are called physiologically-responsive hydrogels. They can change their structures in response to salt concentration, pH and temperature (N. Peppas et al. 2000; Ichikawa and N. Peppas 2001). Hydrogels are highly biocompatible, which makes them promising candidates for numerous clinical applications, such as, drug delivery, contact lenses and scaffolds for tissue engineering. Hydrogels can retain large amounts of water making them similar to natural tissue and may contribute to their high biocompatibility (Nicholas A Peppas, Wood, and J. O. Blanchette 2004). In drug delivery, the hydrogel can release a bioactive agent at a controlled rate to the body tissue beneath (Jha, A. Kumar, et al. 2011). The hydrogel is called a carrier when it is loaded with a drug. The hydrophilic polymers and the drug are

complexed together in presence of crosslinkers, such as, $NaCl$ salt and water, to form the hydrogel carrier loaded with drug (Figure-6.1). These carriers can interact with the mucosa lining in the gastrointestinal (GI) tract, colon, vagina, nose and other parts of the body due to their ability to prolong their residence time at the delivery location (N. Peppas et al. 2000; Y. Huang et al. 2000). These interactions mostly occur due to hydrogen bonding between the monomers in the hydrogel networks and glycoproteins in mucosa. Hydrogels containing a high density of carboxyl and hydroxy groups appear to be promising for this type of applications.

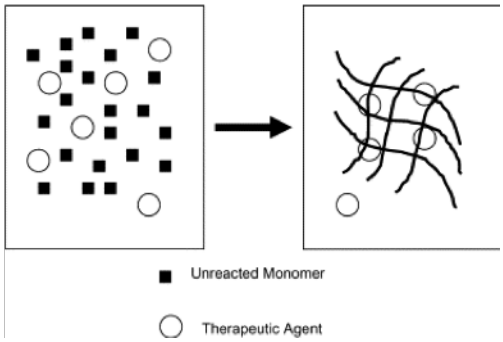

Figure 6.1 As the polymerization takes place, the free therapeutic agent becomes trapped within the hydrogel network with its diffusion controlled by the state of the network (collapsed vs. swollen). Figure adopted from J. Blanchette, Kavimandan, and Nicholas A Peppas 2004.

Physiologically responsive hydrogels may show a swelling behavior, where polymer complexes can be broken or the network can be swollen as a result of the changing external environment (N. Peppas et al. 2000; Nikolaos A Peppas 1991). Swelling of the physiologically-responsive hydrogels can be resulted from the change in pH, ionic strength, temperature and electromagnetic radiation in their surrounding environment (Nikolaos A Peppas 1991). When the hydrogel is used as a drug carrier, as the swelling increases, the chains of the cross-linked network move further apart and the drug can diffuse more quickly through the hydrogel to the tissue.

Hydrogel networks can be made of homopolymers or copolymers, where their prop-

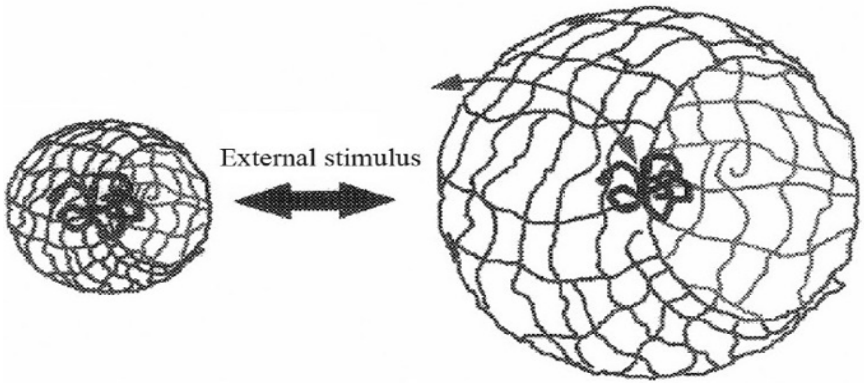

Figure 6.2 Hydrogel swelling at external stimulus (Jha, A. Kumar, et al. 2011).

erties are determined by the chemical structure of the polymers. Some of the most common monomers used to form hydrogels for protein delivery are 2-hydroxyethyl methacrylate, ethylene glycol dimethacrylate, N-isopropyl acrylamide, acrylic acid and methacrylic acid. Poly (ethylene glycol) (PEG) and poly(vinyl alcohol) are two other polymers that have been used to form hydrogels (Nicholas A Peppas, Wood, and J. O. Blanchette 2004).

A widely used hydrogel in biomedical applications is Hyaluronic Acid (HA) hydrogel (Luo, Kirker, and Prestwich 2000; Gerecht et al. 2007; Burdick and Prestwich 2011; H. Tan et al. 2009). Hyaluronic acid (HA) is recently being used as a drug carrier for controlled and targeted release of drugs in the tissues. HA is a naturally occurring linear polysaccharide consisting β-1, 4- linked D-glucuronic acid (β-1, 3) N-acetyl-D-glucosamine disaccharide units and it is the only non-sulfated glycosaminoglycan (GAG) in the extracellular matrix (ECM) of higher animals (Luo, Kirker, and Prestwich 2000). It has unique physicochemical properties and distinctive biological properties. This biocompatible material crosslinks and gels in minutes, and the dried film swells and rehydrates to a flexible hydrogel in seconds. HA also binds specifically to proteins in the ECM, on the cell surface, and within the cell cytosol (Saettone, Monti, and Torracca 1994). Hence, it can play an effective role in cartilage matrix

stabilization, cell motility, growth factor action, morphogenesis and embryonic development, and inflammation. For their multifunctional nature, HA is used as an adjuvant for ophthalmic drug delivery. It is also found to enhance the absorption of drugs and proteins via mucosal tissues. HA also has important applications in viscosurgery, viscosupplementation and wound healing (Luo, Kirker, and Prestwich 2000). Injecting hydrogels into MI infarcted heart increases the mechanical stability of the vulnerable heart to a significant extent (Hasan et al. 2015; Purcell et al. 2014). HA hydrogels have also been used as a mediator for local delivery of rTIMP for effective MMP inhibition for a prolonged period of time (Eckhouse et al. 2014; Purcell et al. 2014).

The adaptation of hydrogel as a drug dcarrier and its efficacy in different applications largely depends on the bulk structure (Fasano and Uzzau 1997; Berger et al. 2004; Donini et al. 2002).

6.1.2 Kinetics of drug release from hydrogels

Drug release from hydrogels can follow either of three mechanisms, which are, diffusion-controlled, chemically-controlled and swelling-controlled (Cohen et al. 1997; Nicholas A Peppas, Wood, and J. O. Blanchette 2004).

- *Diffusion-controlled* drug release from hydrogel depends on a physical phenomena of the movement of the drug through the bulk of the polymer, known as diffusion. The diffusion of drugs from the hydrogel structure can be microscopically described by Fick's law (Crank 1975), which is mathematically expressed as follows for transport in one dimension,

$$j_i = -D_{ip}\frac{dc_i}{dx} \tag{6.1}$$

$$\frac{\delta c_i}{\delta t} = D_{ip}\frac{\delta^2 c_i}{\delta x^2} \tag{6.2}$$

Here, c_i is the concentration and j_i is the mass flux of species, i, respectively; D_{ip} is the diffusion coefficient of species, i in the polymer matrix, and x and t stand for the independent variables of position and time, respectively. Analysis of drug release from these systems using the above mentioned equations shows that the release rate is independent of time, irrespective of whether the system is planar, spherical or cylindrical . The amount of drug release can be controlled by the thickness of the membrane, concentration difference of the drug across the membrane, the thermodynamic characteristics of the system , and the structure of the polymer through the solute diffusion coefficient (N. Peppas et al. 2000).

- *Swelling-controlled* release of drugs in hydrogels is controlled by the inward flux of solvent molecules and consequent swelling of the polymer matrix (N. Peppas et al. 2000; S. W. Kim, Bae, and Okano 1992; Colombo 1993). They usually contain hydrophilic matrixes and the drugs are initially dissolved or dispersed in the glassy polymers. When this structure comes in contact with biological fluids, the polymer matrix swells and two distinct phases can be observed in the polymer; the inner glassy phase and the swollen rubbery phase. The drug molecules are able to diffuse out of the rubbery phase of the polymer and the drug release is controlled by the velocity and position of the glass-rubbery interface (N. Peppas et al. 2000). The degree of swelling of ionic polymers is significantly influenced by several factors, such as, the properties of the polymer (charge, concentration and pK_a of the ionizable group, degree of ionization, cross-link density and hydrophilicity or hydrophobicity) and properties of the swelling medium (pH, ionic strength and the counterion and its valency) (Gupta, Vermani, and Garg 2002). The hydrogel swelling behavior was found to increase significantly above pH 7.0, thus correlating with the maximal transit time of the drug delivery system through the intestines (Shalaby and K. Park 1990).

- *Chemically-controlled* release of drugs from hydrogels can follow two distinct mechanisms: erosion and pendant chain degradation (N. Peppas et al. 2000) . The drug release rate is controlled by degradation or dissolution of the polymer by ordinary diffusion in the erodible systems. The rate limiting step in this mechanism is the trade-off between diffusion and erosion. In pendent chain systems, the drug is attached to the polymer via a hydrolytically or enzymatically labile bond, and the drug release is controlled by the rate of degradation of the bond (N. Peppas et al. 2000).

6.2 Hydrogel mediated delivery of polyelectrolyte-drug conjugate

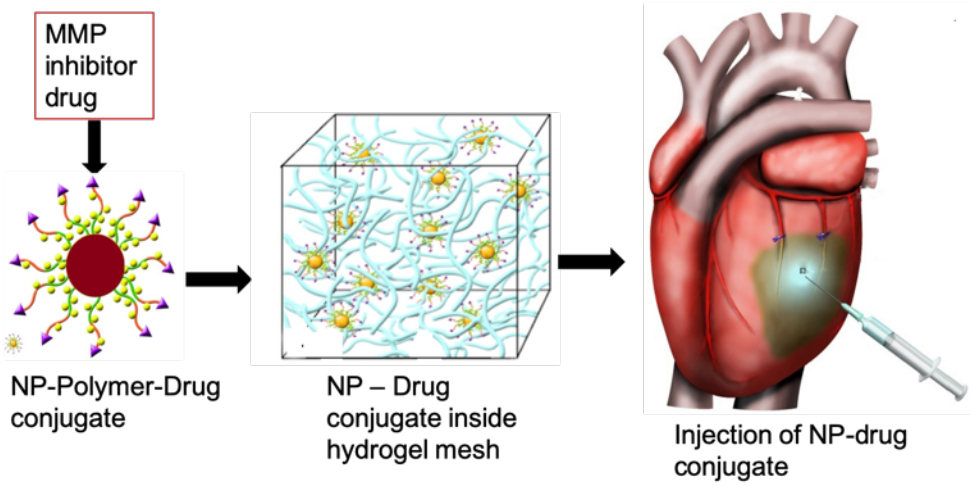

Figure 6.3 Schematic representation of a hydrogel conjugated delivery of a polymer-drug complex. *Acknowledgement : Adam Hartstone-Rose (Former researcher at the School of Medicine, University of South Carolina)*

The localized and controlled drug delivery system discussed in Chapter 4 can be further improved by using hyaluronic acid (HA) hydrogel to contain the polymer-drug complex (figure-6.3). The idea is to inject the hyaluronic acid (HA) in its soluble form along with nanoparticle-polymer-drug conjugate and crosslinkers (salt and water), directly to the MI infarcted heart. After injection, HA instantly forms a gel structure

that traps the drug conjugate. As the gel stays at the myocardium, it gradually degrades due to hydrolysis reaction with water from it's surrounding environment. This degradation will incite chemically-controlled release of the nanoparticle carrier containing drug for an extended period of time, ensuring high concentration of MMP inhibitor drug at the infarct for as long as needed.

Previous theoretical study on grafted weak-polyacid hydrogel have reported a complex swelling-deswelling transition due to varying pH and salt concentration (Longo, Olvera de la Cruz, and Igal Szleifer 2014; Longo, Olvera de La Cruz, and Szleifer 2010). Interplay between chemical free energy and electrostatic interactions play major role in this regard. These theoretical modeling of the hydrogel networks provide the molecular details of their structure, mesh size and charge scenario, which is beneficial to design targeted applications, such as, controlled drug delivery.

As part of the future work, we will develop a molecular theory for a hydrogel network that contains nanoparticle-polymer-drug conjugate using the similar approach that we used for other applications in this dissertation. While previous studies mentioned earlier have reported structural and chemical property changes of hydrogel in varying pH and ionic strength, their behavior when complexed with a small-molecule drug is yet to be uncovered. Hence, our study for nanoparticle-polymer-drug conjugate would be extremely beneficial to design suitable hydrogel network for controlled drug delivery. Molecular level understanding of the hydrogel mediated controlled delivery system would help us to tune the system properties to achieve highest efficiency in MMP inhibition.

Bibliography

Agewall, Stefan et al. (2016). "ESC working group position paper on myocardial infarction with non-obstructive coronary arteries". In: *European heart journal* 38.3, pp. 143–153.

Alvarez-Lorenzo, Carmen and Angel Concheiro (2008). "Intelligent drug delivery systems: polymeric micelles and hydrogels". In: *Mini reviews in medicinal chemistry* 8.11, pp. 1065–1074.

Anastassopoulou, J and T Theophanides (2002). "Magnesium–DNA interactions and the possible relation of magnesium to carcinogenesis. Irradiation and free radicals". In: *Critical reviews in oncology/hematology* 42.1, pp. 79–91.

Andersson, Jakob and Wolfgang Knoll (2019). "Tethered Lipid Membranes as Platforms for Biophysical Studies and Advanced Biosensors". In: *Biomimetic Lipid Membranes: Fundamentals, Applications, and Commercialization*. Springer, 183 –191.

Badeau, Barry A and Cole A DeForest (2019). "Programming Stimuli-Responsive Behavior into Biomaterials". In: *Annual review of biomedical engineering* 21, pp. 241–265.

Badoux, Michael, Mark Billing, and Harm-Anton Klok (2019). "Polymer brush interfaces for protein biosensing prepared by surface-initiated controlled radical polymerization". In: *Polymer Chemistry*.

Bai, Yu et al. (2007). "Quantitative and comprehensive decomposition of the ion atmosphere around nucleic acids". In: *Journal of the American Chemical Society* 129.48, pp. 14981–14988.

Banerjee, Jayeeta (2010). "Antibodies are challenged". In: *Indian journal of medical sciences* 64.3, pp. 144–144.

Banerjee, Jayeeta and Marit Nilsen-Hamilton (2013). "Aptamers: multifunctional molecules for biomedical research". In: *Journal of molecular medicine* 91.12, 1333–1342.

Berger, Jerome et al. (2004). "Structure and interactions in chitosan hydrogels formed by complexation or aggregation for biomedical applications". In: *European Journal of Pharmaceutics and Biopharmaceutics* 57.1, pp. 35–52.

Blanchette, James, Nikhil Kavimandan, and Nicholas A Peppas (2004). "Principles of transmucosal delivery of therapeutic agents". In: *Biomedicine & pharmacotherapy* 58.3, pp. 142–151.

Bloomfield, Victor and Donald M Crothers (2000). *Nucleic acids: structures, properties and functions*. 574.192 B52.

Borisov, OV, TM Birshtein, and EB Zhulina (1991). "Collapse of grafted polyelectrolyte layer". In: *Journal de Physique II* 1.5, pp. 521–526.

Borisov, OV and EB Zhulina (1998). "Effects of ionic strength and charge annealing in star-branched polyelectrolytes". In: *The European Physical Journal B-Condensed Matter and Complex Systems* 4.2, pp. 205–217.

Bouchard, PR, RM Hutabarat, and KM Thompson (2010). "Discovery and development of therapeutic aptamers". In: *Annual review of pharmacology and toxicology* 50, pp. 237–257.

Brannon-Peppas, Lisa (2000). "Poly (ethylene glycol): Chemistry and Biological Applications - JM Harris and S. Zalipsky, editors, American Chemical Society, Washington DC, 1997, 489 pp." In: *Journal of Controlled Release* 2.66, p. 321.

Brettmann, Blair Kathryn et al. (2016). "Bridging contributions to polyelectrolyte brush collapse in multivalent salt solutions". In: *Journal of Polymer Science Part A: Polymer Chemistry* 54.2, pp. 284–291.

Bunka, David HJ and Peter G Stockley (2006). "Aptamers come of age-at last". In: *Nature Reviews Microbiology* 4.8, p. 588.

Burdick, Jason A and Glenn D Prestwich (2011). "Hyaluronic acid hydrogels for biomedical applications". In: *Advanced materials* 23.12, H41–H56.

Carlson, Bob (2007). "Aptamers: the new frontier in drug development?" In: *Biotechnology healthcare* 4.2, p. 31.

Chen, Kai et al. (2019). "Stimuli-responsive polymer-doxorubicin conjugate: Anti-tumor mechanism and potential as nano-prodrug". In: *Acta biomaterialia* 84, pp. 339–355.

Cho, Eun Jeong, Joo-Woon Lee, and Andrew D Ellington (2009). "Applications of aptamers as sensors". In: *Annual Review of Analytical Chemistry* 2, pp. 241–264.

Cohen, Smadar et al. (1997). "A novel in situ-forming ophthalmic drug delivery system from alginates undergoing gelation in the eye". In: *Journal of Controlled Release* 44.2-3, pp. 201–208.

Cohn, Jay N, Roberto Ferrari, Norman Sharpe, et al. (2000). "Cardiac remodeling concepts and clinical implications: a consensus paper from an international forum on cardiac remodeling". In: *Journal of the American College of Cardiology* 35.3, pp. 569–582.

Colombo, Paolo (1993). "Swelling-controlled release in hydrogel matrices for oral route". In: *Advanced Drug Delivery Reviews* 11.1-2, pp. 37–57.

Complications of myocardial infarction Kernel Description. `http://medical-helpful-info.blogspot.com/2013/04/complications-of-myocardial-infarction.html`. Accessed: 2019-08-16.

Crank, J (1975). "The mathematics of diffusion 2nd Edition". In: *Oxford Science Publications,* p. 32.

Creemers, Esther EJM et al. (2001). "Matrix metalloproteinase inhibition after myocardial infarction: a new approach to prevent heart failure." In: *Circulation research* 89.3, pp. 201–210.

Dixon, Jennifer A and Francis G Spinale (2011). "Myocardial remodeling: cellular and extracellular events and targets". In: *Annual review of physiology* 73, pp. 47–68.

Dolan, AK and Samuel Frederick Edwards (1974). "Theory of the stabilization of colloids by adsorbed polymer". In: *Proceedings of the Royal Society of London. A. Mathematical and Physical Sciences* 337.1611, pp. 509–516.

Donini, C et al. (2002). "Preparation of poly (methacrylic acid-g-poly (ethylene glycol)) nanospheres from methacrylic monomers for pharmaceutical applications". In: *International Journal of Pharmaceutics* 245.1-2, pp. 83–91.

Dormán, György et al. (2010). "Matrix metalloproteinase inhibitors". In: *Drugs* 70.8, pp. 949–964.

Dua, Pooja et al. (2018). "Cell-SELEX-Based Identification of a Human and Mouse Cross-Reactive Endothelial Cell-Internalizing Aptamer". In: *Nucleic acid therapeutics*.

Dunlap, John H et al. (2018). "Multiply-Binding Polymeric Imidazole Ligands: Influence of Molecular Weight and Monomer Sequence on Colloidal Quantum Dot Stability". In: *The Journal of Physical Chemistry C* 122.46, pp. 26756–26763.

Eckhouse, Shaina R et al. (2014). "Local hydrogel release of recombinant TIMP-3 attenuates adverse left ventricular remodeling after experimental myocardial infarction". In: *Science translational medicine* 6.223, 223ra21–223ra21.

Edwards, Sam F (1965). "The statistical mechanics of polymers with excluded volume". In: *Proceedings of the Physical Society* 85.4, p. 613.

Famulok, M and G Mayer (1999). "Aptamers as tools in molecular biology and immunology". In: *Combinatorial Chemistry in Biology*. Springer, pp. 123–136.

Fasano, Alessio and Sergio Uzzau (1997). "Modulation of intestinal tight junctions by Zonula occludens toxin permits enteral administration of insulin and other macromolecules in an animal model." In: *The Journal of clinical investigation* 99.6, pp. 1158–1164.

Fichthorn, Kristen A and W Hh Weinberg (1991). "Theoretical foundations of dynamical Monte Carlo simulations". In: *The Journal of chemical physics* 95.2, pp. 1090–1096.

Fingleton, Barbara (2007). "Matrix metalloproteinases as valid clinical target". In: *Current pharmaceutical design* 13.3, pp. 333–346.

— (2008). "MMPs as therapeutic targets - still a viable option?" In: *Seminars in cell & developmental biology*. Vol. 19. 1. Elsevier, pp. 61–68.

Flory, Paul J and M Volkenstein (1969). *Statistical mechanics of chain molecules*.

Flory, PJ (1974). "Foundations of rotational isomeric state theory and general methods for generating configurational averages". In: *Macromolecules* 7.3, pp. 381–392.

Foster, Amanda and Maria C DeRosa (2014). "Development of a biocompatible layer-by-layer film system using aptamer technology for smart material applications". In: *Polymers* 6.5, pp. 1631–1654.

Foy, Jeffrey W-D et al. (2007). "Local tolerance and systemic safety of pegaptanib sodium in the dog and rabbit". In: *Journal of Ocular Pharmacology and Therapeutics* 23.5, pp. 452–466.

Fredrickson, Glenn et al. (2006). *The equilibrium theory of inhomogeneous polymers*. Vol. 134. Oxford University Press on Demand.

Fredrickson, Glenn H, Venkat Ganesan, and François Drolet (2002). "Field-theoretic computer simulation methods for polymers and complex fluids". In: *Macromolecules* 35.1, pp. 16–39.

Gao, Shuting et al. (2019). "Stimuli-responsive bio-based polymeric systems and their applications". In: *Journal of Materials Chemistry B* 7.5, pp. 709–729.

Gebala, Magdalena et al. (2015). "Cation–anion interactions within the nucleic acid ion atmosphere revealed by ion counting". In: *Journal of the American Chemical Society* 137.46, pp. 14705–14715.

Gebala, Magdalena et al. (2016). "Does cation size affect occupancy and electrostatic screening of the nucleic acid ion atmosphere?" In: *Journal of the American Chemical Society* 138.34, pp. 10925–10934.

Gerecht, Sharon et al. (2007). "Hyaluronic acid hydrogel for controlled self-renewal and differentiation of human embryonic stem cells". In: *Proceedings of the National Academy of Sciences* 104.27, pp. 11298–11303.

Gong, Peng et al. (2007). "Behavior of surface-anchored poly (acrylic acid) brushes with grafting density gradients on solid substrates: 2. Theory". In: *Macromolecules* 40.24, pp. 8765–8773.

Gonzalez Solveyra, Estefania and Igal Szleifer (2016). "What is the role of curvature on the properties of nanomaterials for biomedical applications?" In: *Wiley Interdisciplinary Reviews: Nanomedicine and Nanobiotechnology* 8.3, pp. 334–354.

Gupta, Piyush, Kavita Vermani, and Sanjay Garg (2002). "Hydrogels: from controlled release to pH-responsive drug delivery". In: *Drug discovery today* 7.10, pp. 569–579.

Hara, Masanori (1992). *Polyelectrolytes: science and technology*. CRC Press.

Harris, Audray K et al. (2013). "Structure and accessibility of HA trimers on intact 2009 H1N1 pandemic influenza virus to stem region-specific neutralizing antibodies". In: *Proceedings of the National Academy of Sciences* 110.12, pp. 4592–4597.

Hasan, Anwarul et al. (2015). "Injectable hydrogels for cardiac tissue repair after myocardial infarction". In: *Advanced Science* 2.11, p. 1500122.

Hayes, Ryan L et al. (2014). "Reduced model captures Mg2+-RNA interaction free energy of riboswitches". In: *Biophysical journal* 106.7, pp. 1508–1519.

Hidalgo, Manuel and S Gail Eckhardt (2001). "Development of matrix metalloproteinase inhibitors in cancer therapy". In: *Journal of the National Cancer Institute* 93.3, pp. 178–193.

Holland, Joseph G, David S Jordan, and Franz M Geiger (2011). "Divalent metal cation speciation and binding to surface-bound oligonucleotide single strands stud-

ied by second harmonic generation". In: *The Journal of Physical Chemistry B* 115.25, pp. 8338–8345.

Holland, Joseph G et al. (2011). "Specific and Nonspecific Metal Ion- Nucleotide Interactions at Aqueous/Solid Interfaces Functionalized with Adenine, Thymine, Guanine, and Cytosine Oligomers". In: *Journal of the American Chemical Society* 133.8, pp. 2567–2570.

Howard, Jesse J, Gillian C Lynch, and B Montgomery Pettitt (2010). "Ion and solvent density distributions around canonical B-DNA from integral equations". In: *The Journal of Physical Chemistry B* 115.3, pp. 547–556.

Hu, Qiong et al. (2019). "Electrochemically Controlled RAFT Polymerization for Highly Sensitive Electrochemical Biosensing of Protein Kinase Activity". In: *Analytical chemistry* 91.3, pp. 1936–1943.

Huang, Chaobo et al. (2011). "Stimuli-responsive electrospun fibers and their applications". In: *Chemical Society Reviews* 40.5, pp. 2417–2434.

Huang, Yanbin et al. (2000). "Molecular aspects of muco-and bioadhesion:: Tethered structures and site-specific surfaces". In: *Journal of controlled release* 65.1-2, pp. 63–71.

Ichikawa, H and NA Peppas (2001). "Synthesis and characterization of pH-responsive nanosized hydrogels of poly (methacrylic acid-g-ethylene glycol) for oral peptide delivery". In: *New trends in polymers for oral and parenteral administration: from design to receptors. Paris: Editions de Santé*, pp. 261–264.

Jacobson, David R and Omar A Saleh (2016). "Counting the ions surrounding nucleic acids". In: *Nucleic acids research* 45.4, pp. 1596–1605.

Jahan, Merina and Mark Uline (2018). "Quantifying Mg^{2+} Binding to ssDNA Oligomers: A Self-Consistent Field Theory Study at Varying Ionic Strengths and Grafting Densities". In: *Polymers* 10.12, p. 1403.

Jahan, Merina and Mark J Uline (2015). "Design of a Theoretical Model to Identify Specific SSDNA Aptamers for Biosensing Applications". In: *Biophysical Journal* 108.2, 327a.

— (2018). "Study of Polyelectrolyte-Small Molecule Drug Binding with Wormlike Chain Model". In: *Biophysical Journal* 114.3, 345a.

Jahan, Merina et al. (2017). "Molecular Design of a Nanoparticle-Polymer Conjugated Drug Delivery System for PD-166793 in Cardiovascular Repair". In: *Biophysical Journal* 112.3, 46a.

Jha, Gourishanker, Amit Kumar, et al. (2011). "Drug delivery through soft contact lenses: An introduction". In: *Chronicles of young Scientists* 2.1, p. 3.

Ji, Jinkai et al. (2019). "Light-Controlled in Vitro Gene Delivery Using Polymer-Tethered Spiropyran as a Photoswitchable Photosensitizer". In: *ACS Applied Materials & Interfaces* 11.17, pp. 15222–15232.

Jiang, Ying (2013). "Applications of the Wormlike Chain Model in Polymer Physics: Self-consistent Field Theory". In:

Kaludercic, Nina et al. (2008). "Inhibiting metalloproteases with PD 166793 in heart failure:impact on cardiac remodeling and beyond". In: *Cardiovascular Drug Reviews* 26.1, pp. 24–37.

Keefe, Anthony D, Supriya Pai, and Andrew Ellington (2010). "Aptamers as therapeutics". In: *Nature reviews Drug discovery* 9.7, p. 537.

Khati, Makobetsa (2010). "The future of aptamers in medicine". In: *Journal of Clinical Pathology* 63.6, pp. 480–487.

Kim, Julia S et al. (2019). "Protein—Polymer Conjugates Synthesized Using Water-Soluble Azlactone—Functionalized Polymers Enable Receptor—Specific Cellular Uptake toward Targeted Drug Delivery". In: *Bioconjugate chemistry* 30.4, pp. 1220–1231.

Kim, Sung Wan, You Han Bae, and Teruo Okano (1992). "Hydrogels: swelling, drug loading, and release". In: *Pharmaceutical research* 9.3, pp. 283–290.

Kremer, Kurt and Florian Müller-Plathe (2001). "Multiscale problems in polymer science: simulation approaches". In: *MRS bulletin* 26.3, pp. 205–210.

Kumar, Bipul et al. (2017). "Recent advances in nanoparticle-mediated drug delivery". In: *Journal of Drug Delivery Science and Technology* 41, pp. 260–268.

Kumar, Rajeev, Bobby G Sumpter, and S Michael Kilbey (2012). "Charge regulation and local dielectric function in planar polyelectrolyte brushes". In: *The Journal of chemical physics* 136.23, p. 234901.

Kutty, Ramesh S, Nicola Jones, and Narain Moorjani (2013). "Mechanical complications of acute myocardial infarction". In: *Cardiology clinics* 31.4, pp. 519–531.

Lee, Jae-Seung, Min Su Han, and Chad A Mirkin (2007). "Colorimetric detection of mercuric ion (Hg2+) in aqueous media using DNA-functionalized gold nanoparticles". In: *Angewandte Chemie International Edition* 46.22, pp. 4093–4096.

Lee, Yuno, Dave Thirumalai, and Changbong Hyeon (2017). "Ultrasensitivity of water exchange kinetics to the size of metal ion". In: *Journal of the American Chemical Society* 139.36, pp. 12334–12337.

Lewis, Thomas et al. (2013). "Complexation between weakly basic dendrimers and linear polyelectrolytes: effects of grafts, chain stiffness, and pOH". In: *Soft Matter* 9.29, pp. 6955–6969.

Li, Weifeng, Lars Nordenskiöld, and Yuguang Mu (2011). "Sequence-specific Mg^{2+}-DNA interactions: a molecular dynamics simulation study". In: *The Journal of Physical Chemistry B* 115.49, pp. 14713–14720.

Lindorff-Larsen, Kresten et al. (2012). "Systematic validation of protein force fields against experimental data". In: *PloS one* 7.2, e32131.

Lindsey, Merry L (2004). "MMP induction and inhibition in myocardial infarction". In: *Heart failure reviews* 9.1, pp. 7–19.

Lindsey, Merry L et al. (2006). "Matrix metalloproteinase-9 gene deletion facilitates angiogenesis after myocardial infarction". In: *American Journal of Physiology-Heart and Circulatory Physiology* 290.1, H232–H239.

Liu, Jian et al. (2003). "Mechanism of inhibition of matrix metalloproteinase-2 expression by doxycycline in human aortic smooth muscle cells". In: *Journal of vascular surgery* 38.6, pp. 1376–1383.

Liu, Juewen, Zehui Cao, and Yi Lu (2009). "Functional nucleic acid sensors". In: *Chemical reviews* 109.5, pp. 1948–1998.

Liu, Rui et al. (2018). "TiO2 Nanolayer-Enhanced Fluorescence for Simultaneous Multiplex Mycotoxin Detection by Aptamer Microarrays on a Porous Silicon Surface". In: *ACS applied materials & interfaces* 10.17, pp. 14447–14453.

Longo, Gabriel S, Monica Olvera de La Cruz, and I Szleifer (2010). "Molecular theory of weak polyelectrolyte gels: the role of pH and salt concentration". In: *Macromolecules* 44.1, pp. 147–158.

Longo, Gabriel S, Monica Olvera de la Cruz, and Igal Szleifer (2014). "Non-monotonic swelling of surface grafted hydrogels induced by pH and/or salt concentration". In: *The Journal of chemical physics* 141.12, p. 124909.

Luo, Yi, Kelly R Kirker, and Glenn D Prestwich (2000). "Cross-linked hyaluronic acid hydrogel films: new biomaterials for drug delivery". In: *Journal of controlled release* 69.1, pp. 169–184.

Matsen, Mark W (2006). “Self-consistent field theory and its applications”. In: *Soft Matter* 1.

Mayer, Günter (2009). “The chemical biology of aptamers”. In: *Angewandte Chemie International Edition* 48.15, pp. 2672–2689.

Members, Authors-Task Force et al. (2008). “Management of acute myocardial infarction in patients presenting with persistent ST-segment elevation: the Task Force on the Management of ST-Segment Elevation Acute Myocardial Infarction of the European Society of Cardiology”. In: *European heart journal* 29.23, pp. 2909–2945.

Mills, Pamela, Charles F Anderson, and M Thomas Record Jr (1985). “Monte Carlo studies of counterion-DNA interactions. Comparison of the radial distribution of counterions with predictions of other polyelectrolyte theories”. In: *The Journal of Physical Chemistry* 89.19, pp. 3984–3994.

Mocci, Francesca and Aatto Laaksonen (2012). “Insight into nucleic acid counterion interactions from inside molecular dynamics simulations is ‘worth its salt’”. In: *Soft Matter* 8.36, pp. 9268–9284.

Munnik, Nicholas P van der et al. (2018). “Determining the Potential of Mean Force for Amyloid-β Dimerization: Combining Self-Consistent Field Theory with Molecular Dynamics Simulation”. In: *Journal of chemical theory and computation* 14.5, pp. 2696–2704.

Nakatsuka, Nako et al. (2018). “Aptamer–field-effect transistors overcome Debye length limitations for small-molecule sensing”. In: *Science* 362.6412, pp. 319–324.

Nap, Rikkert J, Sung Hyun Park, and Igal Szleifer (2018). “Competitive calcium ion binding to end-tethered weak polyelectrolytes”. In: *Soft matter* 14.12, pp. 2365–2378.

Nap, Rikkert J, Estefania Gonzalez Solveyra, and Igal Szleifer (2018). “The interplay of nanointerface curvature and calcium binding in weak polyelectrolyte-coated nanoparticles”. In: *Biomaterials science* 6.5, pp. 1048–1058.

Nap, Rikkert J and Igal Szleifer (2018). “Effect of calcium ions on the interactions between surfaces end-grafted with weak polyelectrolytes”. In: *The Journal of chemical physics* 149.16, p. 163309.

Nap, Rikkert, Peng Gong, and Igal Szleifer (2006). “Weak polyelectrolytes tethered to surfaces: effect of geometry, acid-base equilibrium and electrical permittivity”. In: *Journal of Polymer Science Part B: Polymer Physics* 44.18, pp. 2638–2662.

Napper, Donald H (1983). *Polymeric stabilization of colloidal dispersions*. Vol. 3. Academic Press London.

Ng, Eugene WM et al. (2006). "Pegaptanib, a targeted anti-VEGF aptamer for ocular vascular disease". In: *Nature reviews drug discovery* 5.2, p. 123.

Nucara, Luca et al. (2017). "Ionic strength responsive sulfonated polystyrene opals". In: *ACS applied materials & interfaces* 9.5, pp. 4818–4827.

Ono, Akira et al. (2011). "Binding of metal ions by pyrimidine base pairs in DNA duplexes". In: *Chemical Society Reviews* 40.12, pp. 5855–5866.

Paolocci, Nazareno et al. (2006). "Metalloproteinase inhibitor counters high-energy phosphate depletion and AMP deaminase activity enhancing ventricular diastolic compliance in subacute heart failure". In: *Journal of Pharmacology and Experimental Therapeutics* 317.2, pp. 506–513.

Paquet, Eric and Herna L Viktor (2015). "Molecular dynamics, monte carlo simulations, and langevin dynamics: a computational review". In: *BioMed research international* 2015.

Park, Yoonjee et al. (2012). "Stability of superparamagnetic iron oxide nanoparticles at different pH values: experimental and theoretical analysis". In: *Langmuir* 28.15, pp. 6246–6255.

Pascal, Auffinger, Neena Grover, and Eric Westhof (Jan. 2011). "Metal ion binding to RNA". In: *Metal ions in life sciences* 9, pp. 1–35. DOI: 10.1039/9781849732512-00001.

Pendergrast, P Shannon et al. (2005). "Nucleic acid aptamers for target validation and therapeutic applications". In: *Journal of biomolecular techniques: JBT* 16.3, p. 224.

Peppas, NA et al. (2000). "Hydrogels in pharmaceutical formulations". In: *European journal of pharmaceutics and biopharmaceutics* 50.1, pp. 27–46.

Peppas, Nicholas A, Kristy M Wood, and James O Blanchette (2004). "Hydrogels for oral delivery of therapeutic proteins". In: *Expert Opin. Biol. Ther* 4.6.

Peppas, Nikolaos A (1991). "Physiologically responsive hydrogels". In: *Journal of bioactive and compatible polymers* 6.3, pp. 241–246.

Peterson, J Thomas (2004). "Matrix metalloproteinase inhibitor development and the remodeling of drug discovery". In: *Heart failure reviews* 9.1, pp. 63–79.

Peterson, J Thomas (2006). "The importance of estimating the therapeutic index in the development of matrix metalloproteinase inhibitors". In: *Cardiovascular research* 69.3, pp. 677–687.

Pfeffer, Marc A and Eugene Braunwald (1990). "Ventricular remodeling after myocardial infarction. Experimental observations and clinical implications." In: *Circulation* 81.4, pp. 1161–1172.

Pincus, Philip (1991). "Colloid stabilization with grafted polyelectrolytes". In: *Macromolecules* 24.10, pp. 2912–2919.

Purcell, Brendan P et al. (2014). "Injectable and bioresponsive hydrogels for on-demand matrix metalloproteinase inhibition". In: *Nature materials* 13.6, p. 653.

Pütz, Mathias, John G Curro, and Gary S Grest (2001). "Self-consistent integral equation theory for polyolefins: Comparison to molecular dynamics simulations and x-ray scattering". In: *The Journal of Chemical Physics* 114.6, pp. 2847–2860.

Radom, Filip et al. (2013). "Aptamers: molecules of great potential". In: *Biotechnology advances* 31.8, pp. 1260–1274.

Rao, B Govinda (2005). "Recent developments in the design of specific matrix metalloproteinase inhibitors aided by structural and computational studies". In: *Current pharmaceutical design* 11.3, pp. 295–322.

Ren, Chun-lai, RJ Nap, and I Szleifer (2008). "The role of hydrogen bonding in tethered polymer layers". In: *The Journal of Physical Chemistry B* 112.50, pp. 16238–16248.

Reshetnikov, Roman V et al. (2011). "Cation binding to 15-TBA quadruplex DNA is a multiple-pathway cation-dependent process". In: *Nucleic acids research* 39.22, pp. 9789–9802.

Rimmele, Martina (2003). "Nucleic acid aptamers as tools and drugs: recent developments". In: *Chembiochem* 4.10, pp. 963–971.

Romero-Perez, Diego et al. (2009). "Effects of Novel Semiselective Matrix Metalloproteinase Inhibitors on Ex Vivo Cardiac Structure–Function". In: *Journal of cardiovascular pharmacology* 53.6, p. 452.

Saenger, Wolfram (1984). "Metal ion binding to nucleic acids". In: *Principles of nucleic acid structure*. Springer, pp. 201–219.

Saettone, M Fabrizio, Daniela Monti, and Patrizia Torracca Maria Tildeand Chetoni (1994). "Mucoadhesive ophthalmic vehicles: evaluation of polymeric low-viscosity

formulations". In: *Journal of Ocular Pharmacology and Therapeutics* 10.1, pp. 83–92.

Savelyev, Alexey and Alexander D MacKerell Jr (2015). "Competition among Li^+, Na^+, K^+, and Rb^+ monovalent ions for DNA in molecular dynamics simulations using the additive CHARMM36 and Drude polarizable force fields". In: *The Journal of Physical Chemistry B* 119.12, pp. 4428–4440.

Scranton, Alec B, B Rangarajan, and J Klier (1995). "Biomedical applications of polyelectrolytes". In: *Biopolymers Ii*. Springer, pp. 1–54.

Sefah, Kwame et al. (2009). "Nucleic acid aptamers for biosensors and bio-analytical applications". In: *Analyst* 134.9, pp. 1765–1775.

Sefah, Kwame et al. (2010). "Development of DNA aptamers using Cell-SELEX". In: *Nature protocols* 5.6, p. 1169.

Shalaby, Waleed SW and Kinam Park (1990). "Biochemical and mechanical characterization of enzyme-digestible hydrogels". In: *Pharmaceutical research* 7.8, pp. 816–823.

Shvartzman-Cohen, Rina et al. (2004). "Selective dispersion of single-walled carbon nanotubes in the presence of polymers: the role of molecular and colloidal length scales". In: *Journal of the American Chemical Society* 126.45, pp. 14850–14857.

Song, Shiping et al. (2008). "Aptamer-based biosensors". In: *TrAC Trends in Analytical Chemistry* 27.2, pp. 108–117.

Spinale, Francis G (2007). "Myocardial matrix remodeling and the matrix metalloproteinases: influence on cardiac form and function". In: *Physiological reviews* 87.4, pp. 1285–1342.

Spinale, Francis G et al. (1999). "Matrix metalloproteinase inhibition during the development of congestive heart failure: effects on left ventricular dimensions and function". In: *Circulation research* 85.4, pp. 364–376.

Stuart, Martien A Cohen et al. (2010). "Emerging applications of stimuli-responsive polymer materials". In: *Nature materials* 9.2, p. 101.

Sundaram, Padma et al. (2013). "Therapeutic RNA aptamers in clinical trials". In: *European Journal of Pharmaceutical Sciences* 48.1-2, pp. 259–271.

Sutton, Martin G St John and Norman Sharpe (2000). "Left ventricular remodeling after myocardial infarction: pathophysiology and therapy". In: *Circulation* 101.25, pp. 2981–2988.

Szleifer, I and MA Carignano (1996). "Tethered polymer layers". In: *Advances in Chemical Physics: Polymeric Systems* 94, pp. 165–260.

— (2000). "Tethered polymer layers: phase transitions and reduction of protein adsorption". In: *Macromolecular rapid communications* 21.8, pp. 423–448.

Tan, Huaping et al. (2009). "Thermosensitive injectable hyaluronic acid hydrogel for adipose tissue engineering". In: *Biomaterials* 30.36, pp. 6844–6853.

Tan, Weihong et al. (2011). "Molecular aptamers for drug delivery". In: *Trends in biotechnology* 29.12, pp. 634–640.

Thygesen, Kristian, Joseph S Alpert, Harvey D White, et al. (2007). "Universal definition of myocardial infarction". In: *Journal of the American College of Cardiology* 50.22, pp. 2173–2195.

Torchilin, Vladimir P et al. (1994). "Poly (ethylene glycol) on the liposome surface: on the mechanism of polymer-coated liposome longevity". In: *Biochimica et Biophysica Acta (BBA)-Biomembranes* 1195.1, pp. 11–20.

Trombly, David M, Victor Pryamitsyn, and Venkat Ganesan (2011). "Self-Assembly of Diblock Copolymer on Substrates Modified by Random Copolymer Brushes". In: DOI: 10.1021/ma202075d. URL: http://pubs.acs.org/doi/pdf/10.1021/ma202075d.

Uline, Mark J, Shihong Meng, and Igal Szleifer (2010). "Surfactant driven surface anchoring transitions in liquid crystal thin films". In: *Soft Matter* 6.21, pp. 5482–5490.

Uline, Mark J, Yitzhak Rabin, and Igal Szleifer (2011). "Effects of the salt concentration on charge regulation in tethered polyacid monolayers". In: *Langmuir* 27.8, pp. 4679–4689.

Verma, Rajeshwar P and Corwin Hansch (2007). "Matrix metalloproteinases (MMPs): chemical–biological functions and (Q) SARs". In: *Bioorganic & medicinal chemistry* 15.6, pp. 2223–2268.

Visse, Robert and Hideaki Nagase (2003). "Matrix metalloproteinases and tissue inhibitors of metalloproteinases: structure, function, and biochemistry". In: *Circulation research* 92.8, pp. 827–839.

Wang, Lei et al. (2015). "Polymer grafted recyclable magnetic nanoparticles". In: *Polymer Chemistry* 6.2, pp. 248–255.

Wei, Menglian et al. (2017). “Stimuli-responsive polymers and their applications”. In: *Polymer Chemistry* 8.1, pp. 127–143.

Wiggins, Kelly M, Johnathan N Brantley, and Christopher W Bielawski (2013). “Methods for activating and characterizing mechanically responsive polymers”. In: *Chemical Society Reviews* 42.17, pp. 7130–7147.

Wolter, Olga and Günter Mayer (2017). “Aptamers as valuable molecular tools in neurosciences”. In: *Journal of Neuroscience* 37.10, pp. 2517–2523.

Wu, Tao et al. (2007). “Behavior of surface-anchored poly (acrylic acid) brushes with grafting density gradients on solid substrates: 1. Experiment”. In: *Macromolecules* 40.24, pp. 8756–8764.

Yu, Jing et al. (2016). “Structure of polyelectrolyte brushes in the presence of multivalent counterions”. In: *Macromolecules* 49.15, pp. 5609–5617.

Zamilpa, Rogelio and Merry L Lindsey (2010). “Extracellular matrix turnover and signaling during cardiac remodeling following MI: causes and consequences”. In: *Journal of molecular and cellular cardiology* 48.3, pp. 558–563.

Zheng, Yang et al. (2017). “pH and thermal dual-responsive nanoparticles for controlled drug delivery with high loading content”. In: *Acs Omega* 2.7, pp. 3399–3405.

Zhou, Gang et al. (2018). “Aptamers as targeting ligands and therapeutic molecules for overcoming drug resistance in cancers”. In: *Advanced drug delivery reviews*.

Zhou, Wenhu et al. (2014). “Aptamer-based biosensors for biomedical diagnostics”. In: *Analyst* 139.11, pp. 2627–2640.

Zhulina, EB and OV Borisov (1997). “Structure and interaction of weakly charged polyelectrolyte brushes: Self-consistent field theory”. In: *The Journal of chemical physics* 107.15, pp. 5952–5967.

Zhulina, EB, OV Borisov, and TM Birshtein (1992). “Structure of grafted polyelectrolyte layer”. In: *Journal de Physique II* 2.1, pp. 63–74.

Zwanikken, Jos W et al. (2011). “Local ionic environment around polyvalent nucleic acid-functionalized nanoparticles”. In: *The Journal of Physical Chemistry C* 115.33, pp. 16368–16373.